From Dynamical Decoupling

to

Dynamical Amplification

by

Ankit Tiwari

A Thesis Presented in Partial Fulfillment
of the Requirements for the Degree
Master of Science

Approved July 2023 by the
Graduate Supervisory Committee:

Christian Arenz, Chair
Kanu Sinha
Michael Goryll

ARIZONA STATE UNIVERSITY

August 2023

ABSTRACT

Dynamical decoupling (DD) is a promising approach to mitigate the detrimental effects that interactions with the environment have on a quantum system. In DD, the finite-dimensional system is rotated about specified axes using strong and fast controls that eliminate system-environment interactions and protect the system from decoherence. In this thesis, the framework of DD is theoretically studied, and later it discusses how this framework can be implemented on an infinite-dimensional system that amplifies system components rather than suppressing them through quadrature squeezing operations. It begins by studying the impact of system-environment interactions on a quantum system, and then it analyzes how DD suppresses these interactions. The conditions for protecting a finite-dimensional system through DD are reviewed, and a numerical analysis of the DD conditions for simple systems is conducted. Using bang-bang controls, a framework for decoupling decoherence-inducing components from a general finite-dimensional system is studied. Later, following an overview of schemes that amplify the strength of a quantum signal through reversible squeezing, a theoretical study of Hamiltonian Amplification (HA) for quantum harmonic oscillators is presented. By implementing the DD framework with squeezing operations, HA achieves speed-up in the dynamics of quantum harmonic oscillators, which translates into the strengthening of interactions between harmonic oscillators. Finally, the application of HA in amplifying the third-order nonlinearity in a Kerr medium is proposed to obtain a speed-up in the implementation of controlled phase gates for optical quantum computations. Numerically simulated results show that large amplification in nonlinearity is feasible with sufficient squeezing resources, completing the set of universal quantum gates in optical quantum computing.

DEDICATION

I dedicate this thesis to my late grandmother Mrs. Kusum Tiwari.

ACKNOWLEDGMENTS

I must begin by acknowledging my heartfelt gratitude to my supervisor Christian Arenz. His guidance throughout the completion of this thesis is immensely invaluable. Despite being fairly occupied, he had always made time to address my questions, no matter how mundane they were. I would especially acknowledge Chrsitian's research proposal and suggestions from Saikat Guha, which have served as the basis for the original work in this thesis. I also extend my abundant thanks to the members of my research group, especially to Arefur with whom I nurtured my fundamentals of dynamical decoupling. Mahum greatly helped me during my time writing this thesis. Her inputs on my manuscripts greatly enhanced the quality and clarity of my work. Prakriti, who is my comrade on this journey of quantum enlightenment, has been a constant source of zeel and sincerity during this period.

I appreciate the help that I have received from my committee members, Kanu Sinha and Michael Goryll. I have learned a great deal about quantum optics from my discussions with Kanu, which is surely to be found in these pages. I am thankful to Michael, whose excellent class laid the groundwork for my basic concepts of mathematics and physics ingrained in quantum mechanics. Finally, I want to thank my family and friends who have encouraged me in all of my endeavors and inspired me to follow my dreams. I am forever grateful for the continued love and support shown by my parents, Ashutosh and Vinay, and for the strong belief shown by my dear sister, Srashti. Without them, this day would not have been possible.

A desire of knowledge is the natural feeling of mankind;
and every human being whose mind is not debauched
will be willing to give all that he has to get
knowledge.

- Samuel Johnson

TABLE OF CONTENTS

Page

CHAPTER Page

LIST OF FIGURES

Figure Page

Chapter 1

INTRODUCTION

Quantum mechanics is the mathematical theory that predicts the behavior of microscopic particles or, at least, outlines a framework that describes the tools we use to examine this behavior. Although perhaps not complete [1], it has been immensely successful in describing the nature of the microscopic universe up to the present day.

It began as "quantum theory", which was initially a set of hypotheses to explain a variety of mysterious phenomena: the wave-particle nature of quantum particles, the quantization of energy, the probabilistic nature of the quantum particles in space and time, and so on [2]. The laws governing quantum mechanics were formulated in the early 20th century with a series of novel contributions from physicists, chemists, and mathematicians. In the present day, the laws of quantum mechanics are fundamentals in physics, chemistry, biology, engineering, and information technology. Perhaps the most well-known application of quantum mechanics is to solve a computational problem through a "quantum computer" [3]. Inarguably, there has been tremendous progress in the area of experimental implementation of devices that exploit the properties of quantum particles; however, there are still significant challenges involved in constructing a continual, error-free quantum computer [4].

One common challenge in realizing these devices is the unwanted interaction of the quantum particles with the macroscopic world. Quantum mechanical systems, in general, are extremely sensitive to the noise induced by the environment [5]. The noise plagues the system in such a way that it loses its "quantumness" and behaves like a classical system. At this point, the notions of quantum and classical may be confusing, and to understand the difference between the two, we will consider the

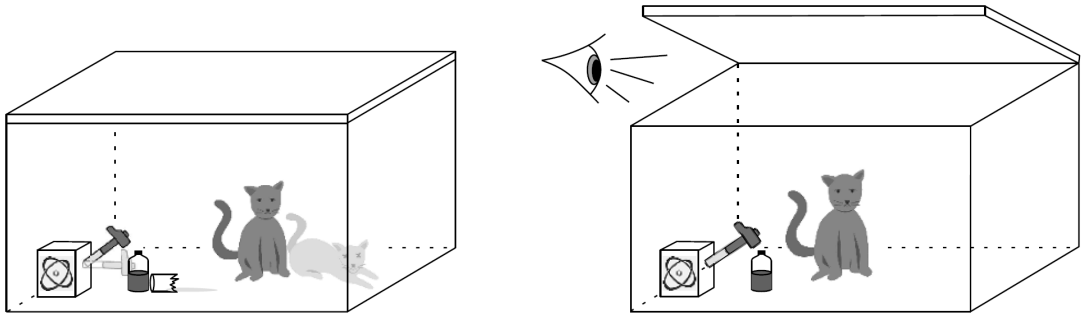

(a) (b)

Figure 1.1: (a) According to the postulates of quantum mechanics, the atom, the hammer, the poison, and the cat exist in a superposition of two mutually incompatible states, one of which describes the cat as alive and dead in the other. In the closed box, the cat is, fictitiously, both dead and alive simultaneously. (b) By the laws of quantum mechanics, when an observer opens the box, the superposition of the dead and alive states is collapsed to either one of the two states (in this case, the cat is found alive). Figure adopted from Schlosshauer, "Decoherence: and the quantum-to-classical transition.", 2007, pg. 2.

infamous thought experiment of Schrödinger's cat [6].

For the experiment, imagine a cat trapped in a box, as shown in Fig 1.1(a). Within the box, a two-level atom serves as a trigger for the hammer to break the flask containing poison. The atom is connected to the hammer in such a way that if the atom is excited to a high energy level, the hammer will fall on the flask and release the poison, which will kill the cat. But if the atom is in the ground state, the hammer is untriggered, and the cat is alive. This entire setup corresponds the excited and ground states of an atom to the dead and alive states of the cat.

According to the laws of quantum mechanics, the atom is characterized by the superposition of excited and ground states. Since the atom is in the excited and

ground states at the same time, the cat is both dead and alive at the same time! This property of the atom to exist in a superposition of classically mutually exclusive states describes the "quantumness" of microscopic particles, called "quantum coherence" or simply "quantum superposition" [6].

In the second part of the experiment (see Fig 1.1(b)) imagine we are allowed to open the box and check the state of the cat. One of the postulates of quantum mechanics predicts that when an observation is made on a quantum system, the superposition state collapses into one of its component states. Thus, if we open the box and find the cat alive, the atom's superposition of the ground and excited states must have collapsed to the ground state. Similarly, if the poor animal is found dead, then the atom must have collapsed to its excited state. It is the observer who decides the fate of the animal by simply opening the box. This is essentially a classical case where a system exists in any one of the states but not in the superposition of all of them.

Obviously, the thought experiment by Schrödinger is based on certain assumptions. One of them is that the box within which the cat is confined is assumed to be isolated from the rest of the universe. Experience shows that a quantum mechanical system cannot be kept completely insulated from the effects of the environment around it [5, 7]. Thus, for an accurate description of the system's dynamics, the quantum system must be considered "open," and the effect of the surroundings around it must be taken into account. The effect of the openness of the system could be understood with the same Schrödinger's cat experiment. Let's assume a similar setup as shown in Fig 1.1(a), but this time an electromagnetic field from an unknown source is interacting with the atom inside the box. The result of the interaction is that the atom loses its coherence over the course of time and collapses into one of the states. Now if the box is opened by an external observer, the cat will be found in either dead

or alive state; however, this time it's not the observer who enforces classicality on the system but it is due to the uncontrollable interaction between the atom and the field.

The uniqueness of quantum systems lies in their ability to exist in a superposition of their component states. The rapid development of quantum technologies heavily relies on how long we can preserve this superposition state before it decays to a mixture of classical probabilities. In addition, the larger a quantum system is, the more strongly it interacts with its environment, and the faster the system loses its coherence or undergoes "decoherence" [5]. The effect of decoherence could be observed as a source of error in quantum computation, which depends on large-scale superpositions. To achieve a longer coherence time, we tend to combat the detrimental effects of the environment using quantum error correction techniques. We will study the challenges involved in developing these techniques and briefly review some of them in Chapter 3. Our primary focus in this thesis is to thoroughly study "dynamical decoupling" (DD) [8], which suppresses the system-environment interaction by rotating the system about a set of axes such that the average deviation of the system from the desired state is zero. By using this technique, the system's state is preserved, and larger computations can be performed.

We aspire to address the fundamentals of DD in a simplified manner; however, we do not limit ourselves to it. Instead, we switch ourselves from finite-dimensional systems to infinite-dimensional systems with the purpose of identifying schemes, in the same vein as DD, that may enhance the properties of the system instead of suppressing them. Such a scheme has been shown to amplify desired interactions between system components, which is crucial for maintaining quantum effects in a quantum device [9]. In this thesis, we propose that through the "Hamiltonian amplification" (HA) [9] protocol, weak nonlinear interaction between photonic qubits can be enhanced by squeezing the photonic states along two quadratures. We numerically show that

with the nonlinearity amplified, a speed-up in the implementation of controlled phase gates can be achieved for media with weak nonlinear interactions in optical quantum computing.

The narrative of the thesis as a whole can be divided into two parts. The first part provides an outline of how a quantum system is affected by system-environment interactions and how DD suppresses these interactions. Throughout the overview, we try to represent the decoherence and the dynamics involved with mathematical models previously proposed by Lidar and Brun [5], and Viola and Lloyd [8]. We review the necessary conditions derived in [5] for decoupling a general open quantum system from an environment and numerically examine these conditions by evaluating the dynamics of a simple qubit system driven with specifically tailored controls. Finally, we derive "bang-bang controls" [8] from a continuous-time control drive and obtain a framework of transformations that eliminates the system-environment interaction in a general finite-dimensional system.

The second part takes nearly the opposite turn. In this context, our narrative shifts to infinite-dimensional systems that describe harmonic motion, for example, a quantum harmonic oscillator. We briefly discuss how quantum harmonic oscillators are described in the sense of quantum mechanics and then we go through the squeezed coherent states in Chapter 4. With the knowledge of squeezed states, we review recently proposed amplification schemes that amplify the magnitude of a quantum signal with reversible squeezing. Then, we meticulously discuss Hamiltonian amplification (HA) [9], or what we preferably call "dynamical amplification" (DA), which aims to speed-up the dynamics of harmonic oscillators via quadrature squeezing. Consequently, this speed-up translates into the amplification of interactions when the harmonic oscillator is coupled with another system. We look into the systems where this scheme provides an additional advantage in the system dynamics,

and finally, we review the emerging field of optical quantum computing and propose the application of DA for fast implementation of controlled phase gates by enhancing the nonlinear photon-photon interactions.

Chapter 2

BACKGROUND

2.1 Quantum Superposition

The idea of superposition is intrinsically based on the wave-like nature of quantum particles. Classically, two coherent waves may interfere with each other to form a wave with a waveform defined by the superposition of the two waves. If the wave associated with a quantum particle is split into two, defining the two states of a quantum particle, then these waves might interfere with each other to generate another state described by the superposition of the two states. The peculiarity of quantum superposition becomes evident when the two states are "mutually exclusive", which corresponds to Schrödinger cat's dead and alive states, which we earlier discussed. But how can an animal be dead and alive at the same time?

To accurately explain the characteristics of quantum superposition in a classical scenario is extremely challenging. This property is exclusively observed for quantum particles like silver atoms in the Stern-Gerlach experiment [10] and for photons in Young's double slit experiment [11]. In fact, the ability of a quantum particle to exist in a superposition state is the cornerstone of every advantage provided by quantum systems over their classical counterparts. From quantum computation [3, 12–14], nanoscale thermodynamics [15, 16], quantum sensing [17], metrology [18, 19] to biology [19–21] and condensed matter [22, 23] are some of the fields where quantum superposition is a precious resource. Quantum algorithms [24], which became popular after the introduction of Shor's algorithm [25], are based on the superposition of inputs, which results in parallel computations also known as "quantum parallelism".

In a mathematical setting, the two mutually exclusive states of a quantum particle can be represented in Dirac notation by orthonormal vectors $|u_1\rangle$ and $|u_2\rangle$ in a complex Hilbert space. A superposition of the orthogonal states is represented as

$$|\psi\rangle = c_1 |u_1\rangle + c_2 |u_2\rangle , \tag{2.1}$$

where c_1, $c_2 \in \mathbb{C}$ and the states are normalized such that the inner product $\langle\psi|\psi\rangle = |c_1|^2 + |c_2|^2 = 1$. The absolute square of c_1 and c_2 provides the probability to find state $|\psi\rangle$ in one of the two orthonormal states. And the interference between $|u_1\rangle$ and $|u_2\rangle$ is due to the constant phase difference between complex numbers c_1 and c_2. Moreover, the vectors $|u_1\rangle$ and $|u_2\rangle$ form the basis of the Hilbert space in which any arbitrary superposition of the two states exists. In general, a state in a n dimensional Hilbert space is given by

$$|\psi\rangle = \sum_{i=1}^{n} c_i |u_i\rangle , \tag{2.2}$$

where c_i is the complex scalar associated with $|u_i\rangle$, which forms a complete and orthonormal basis spanning the Hilbert space. At this point, it may be appropriate to consider the famous double-slit experiment to physically realize the phenomenon of quantum superposition.

In the experiment [11] (see Fig 2.1) single photons are sent through a barrier with two slits, which are then detected by a photon detector. The number of photons detected in the vertical direction is a function of the horizontal position on the screen. In Fig 2.2(a) the detector is exposed to a small number of single photons coming out of the two slits, and we observe the random distribution of photons on the screen. However, when the detector is exposed to a large population of single photons in Fig 2.2(b), we notice a pattern starts to emerge. And in Fig 2.2(c), for sufficiently large photon counts, we clearly observe the interference fringes similar to the one obtained in Young's double-slit interference pattern for a beam of light [27].

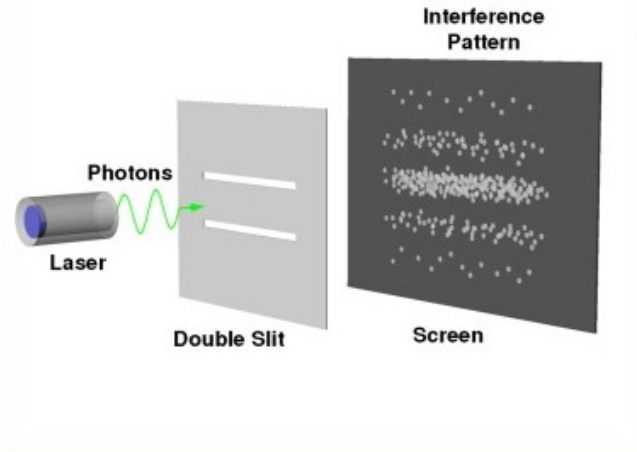

Figure 2.1: Illustration of the experimental setup of a single photon double-slit experiment which exhibits the interference fringes formed by single photons. Figure taken from Tang and Hu, "Analysis of single-photon self-interference in young's double-slit experiments.", 2022.

But, given that a single photon arrives at the slits, the interference pattern is only possible if a photon coexists in both of the slits at the same moment. This is explained by the wave nature of the photon, which is split into two at the slits. Now if we denote the two possible trajectories of a photon through the slits by states $|\psi_1\rangle$ and $|\psi_2\rangle$, the photon will be in the superposition state given by

$$|\Psi\rangle = \frac{1}{\sqrt{2}}(|\psi_1\rangle + |\psi_2\rangle). \tag{2.3}$$

Note that the superposition state cannot be described by a classical statistical distribution. For a classical case, we expect that the particle will go through either of the two slits and yield the standard Gaussian distribution centered behind each slit [28]. Therefore, the interference pattern confirms the existence of a superposition of states, which is a non-classical case.

We also note that to observe quantum superposition, one has to study a large number of identical quantum systems. This collection of identical systems is referred

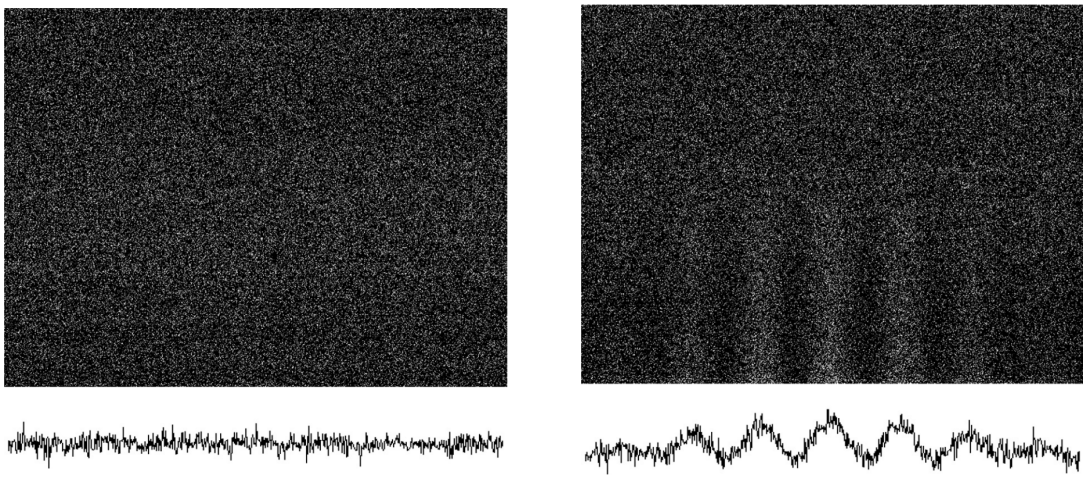

(a) (b)

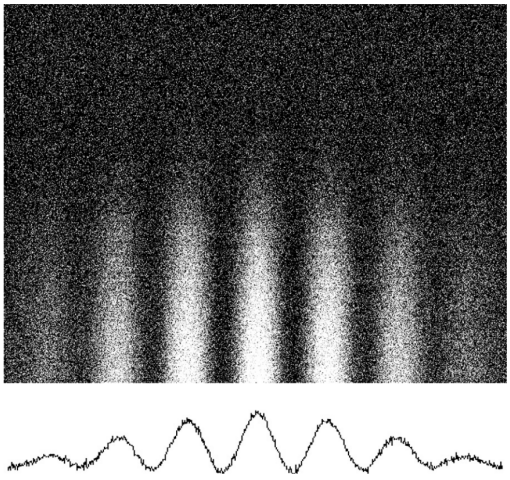

(c)

Figure 2.2: (a) Pattern obtained on photon detector for 0.1 s exposure time. The grayscale represents a range of 0–20 pixel counts. The graph on the bottom shows the number of counts detected in the vertical direction as a function of horizontal position. (b) Pattern for 1 s exposure time; the graph and image grayscale is 0–20 counts. (c) Pattern for 120 s exposure time: the graph and image grayscale is 0–500 counts. Clearly, for longer exposure time we obtain the interference fringe characterized by the superposition of photons. Figures taken from Rueckner and Peidle, "Young's double-slit experiment with single photons and quantum eraser.", 2013.

to as an ensemble. If we consider all the systems in the ensemble to be in a state $|\psi\rangle$, the entire ensemble can be represented by $|\psi\rangle$ which we call a "pure state". However, for an ensemble where not all the systems are in the same state or are in a "mixed state", we represent it with a density operator [29]

$$\rho = \sum_j p_j \left|\psi_j\right\rangle \left\langle\psi_j\right|, \tag{2.4}$$

where p_j describes the fraction of ensemble in state $|\psi_j\rangle$. Note that ρ describes a pure state when $p_j = 1$. Hence, the density operator is a general representation of the state of an ensemble. A thorough discussion about the density operators can be found in the book by Sakurai and Napolitano [10]. For this work, we require only the fundamental properties of the density operator, which are described in Appendix A.3.

We now consider an ensemble of pure states $|\psi\rangle = \sum_i c_i |u_i\rangle$ which can also be written as

$$\rho = \sum_i \sum_j c_i c_j^* \left|u_i\right\rangle \left\langle u_j\right|. \tag{2.5}$$

The diagonal elements $|c_i|^2$ in (2.5) represent the probabilities of finding a system in the corresponding state $|u_i\rangle$ whereas the off-diagonal elements $c_i c_j^*$ represent the interference between the "coexisting" states $|u_i\rangle$ and $|u_j\rangle$. These off-diagonal elements describe the coherence present in the system. However, we must be careful with our choice of basis for the states. Just because the density matrix is diagonal does not mean that the system is classical in nature. Whether off-diagonal elements appear or not will depend on our choice of basis.

Now consider a two-level closed system described by the Hamiltonian

$$H_S = \hbar\omega_0\sigma_z, \tag{2.6}$$

where σ_z is a Pauli-Z operator with eigenvalues {1, -1} corresponding to eigenstates $\{|0\rangle, |1\rangle\}$ and ω_0 describes the natural frequency at which the system oscillates be-

tween the basis states. This system is preferably called a single qubit system (see Fig 2.3), and we will extensively use it throughout this work. Moreover, for simplicity, we assume $\hbar = 1$ whenever we describe the dynamics of a system in the thesis. Let's consider that the qubit is initially in a pure state represented in basis states $\{|0\rangle, |1\rangle\}$ such that

$$|\psi(t_0)\rangle = \frac{1}{\sqrt{2}}(|0\rangle + |1\rangle). \tag{2.7}$$

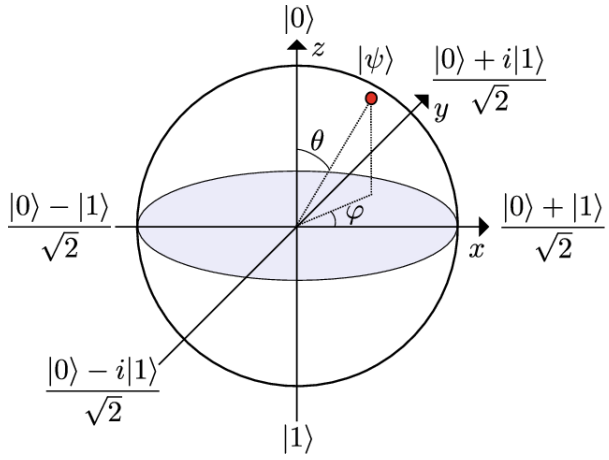

Figure 2.3: Bloch sphere representation of a qubit state. The north pole is $|0\rangle$ and the south pole is $|1\rangle$. Any arbitrary superposition of $|0\rangle$ and $|1\rangle$ is $|\psi\rangle = \cos\left(\frac{\theta}{2}\right)|0\rangle + e^{i\varphi}\sin\left(\frac{\theta}{2}\right)|1\rangle$ where θ is polar angle from positive z axis and φ is the azimuth angle from positive x axis. Figure adopted from Wendin and Shumeiko, "Quantum bits with josephson junctions.", 2007.

The matrix representation of the density operator for $|\psi(t_0)\rangle$ is given by

$$\rho(t_0) = \begin{pmatrix} \frac{1}{2} & \frac{1}{2} \\ \frac{1}{2} & \frac{1}{2} \end{pmatrix}, \tag{2.8}$$

where the off-diagonal elements resemble the superposition state between the basis states $|0\rangle$ and $|1\rangle$. If we look into the dynamics of the density operator, which is given

by the solution of Liou-ville–von Neumann equation [7], we get

$$\rho(t) = e^{-iH_S(t-t_0)}\rho(t_0)e^{iH_S(t-t_0)}, \tag{2.9}$$

where the matrix representation of $\rho(t)$ is

$$\rho(t) = \begin{pmatrix} \frac{1}{2} & \frac{1}{2}e^{-i\omega_0 2(t-t_0)} \\ \frac{1}{2}e^{i\omega_0 2(t-t_0)} & \frac{1}{2} \end{pmatrix}. \tag{2.10}$$

Note that the off-diagonal elements oscillate with frequency $2\omega_0$ in opposite directions to each other. This is due to the dynamics induced in the relative phase between the basis states $|0\rangle$ and $|1\rangle$ which itself evolve with respect to the unitary operator $e^{-iH_S(t-t_0)}$.

In the framework of closed systems, quantum mechanics can be understood in the most simple and fundamental way. In a quantum mechanical setting, a closed system is an isolated system that doesn't exchange any energy with its surroundings. The entropy of a closed system is preserved, and transformations in the state of these systems are unitary in nature. However, in realistic scenarios, there are no truly closed systems. Only for certain time scales could the dynamics of practical systems be defined by those of closed quantum systems. These time scales are called coherence times since, beyond this time, the quantum system loses its coherence and is then reduced to a mixture of classical probabilities. For example, the coherence time for a spin qubit in silicon is experimentally observed to be ≈ 200 µs [31]. For superconducting qubits, coherence times exceeding 0.30 ms have been demonstrated [32, 33]. Thus, to obtain a more accurate description of the dynamics of a quantum system, one must take the effects of its surroundings into account.

2.2 Open Quantum System

A quantum mechanical system is called an open system if it is partially or entirely coupled to an environment. The term environment here refers to an external system whose coupling with the system of our interest results in the loss of information. By "environment", we do not mean only the macroscopic objects like detectors or lasers, but we refer to everything in the universe that can couple with the closed system. This includes interaction with other qubits in a multi-qubit system, interaction with an electromagnetic field, or the noise induced by air particles, sound waves, or even the cosmic wave background. This coupling with the environment, no matter how weak it is, induces features that result in the inclusion of decoherence in the system. Decoherence can be simply introduced as the loss of a density matrix's off-diagonal elements during its evolution; however, one should not confuse decoherence with effects like dissipation and dephasing, which also result in the decay of off-diagonals in a density matrix of a system.

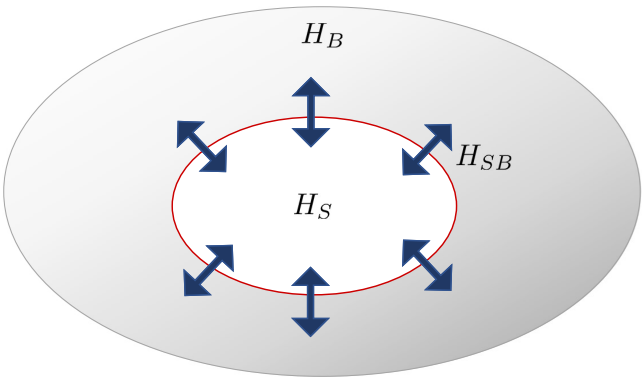

Figure 2.4: An illustration of a quantum system coupled to an environment. The Hamiltonians H_S and H_B describe system and environment respectively. The system-environment interaction is shown by H_{SB}.

Dissipation in quantum mechanics occurs when the energy in the system is ir-

reversibly lost to the environment. In general, dissipation is a quantum analog of the dissipation of energy in classical mechanics. The energy from the system is distributed over many degrees of freedom in the environment, and over time, the energy is entirely lost to the environment. For example, consider an excited two-level atom interacting with an electromagnetic field in a cavity resonator [34]. The coupling between the field and atoms causes an energy exchange, and if the system is perfectly insulated, the energy exchange inside the cavity remains unperturbed. However, in practical scenarios, the atom interacts with an external bath of fields such that energy exchange between the atom and modes in the bath takes place in a nonunitary fashion. Since the energy of the bath is (i) not well defined and (ii) distributed over many modes of field, the atom-bath interaction results in the complete removal of energy from the cavity resonator, and the atom collapses in its ground state. For dissipation, the loss of energy over time corresponds to the decay of diagonal elements $\rho_{ii}(t)$ of the density operator, which resemble the energy eigenstates of the system. To preserve the positivity of $\rho(t)$ (see Appendix A.7) the off-diagonals elements should also decay, which intrinsically causes decoherence.

An ensemble is subjected to dephasing when due to a classical noise the average over the relative phase factor of its systems, in which each individual system is described by a pure state, results in zero [6]. This corresponds to the disappearance of off-diagonal elements in the density operator of the ensemble. Let us consider the example by Schlosshauer in [6]. Suppose an ensemble of N identical systems is characterized by a pure state such that the kth system is given by

$$|\psi_k\rangle = \frac{1}{\sqrt{2}}(|0\rangle + e^{i\phi}\,|1\rangle), \tag{2.11}$$

where ϕ is a relative phase factor. Let's assume due to some external disturbances the relative phase factor in each system is perturbed by a factor δ_k such that $|\psi_k\rangle$ is

now

$$|\psi_k\rangle = \frac{1}{\sqrt{2}}(|0\rangle + e^{i(\phi\pm\delta_k)}\,|1\rangle). \tag{2.12}$$

Now if we take an average over the ensemble with the ensemble density operator, we obtain

$$\begin{aligned}\rho = & \frac{1}{N}\sum_{k=1}^{N}|\psi_k\rangle\langle\psi_k| \\ = & \frac{1}{2}|0\rangle\langle 0| + \frac{1}{2}|1\rangle\langle 1| + \left(\frac{1}{2N}\sum_{k=1}^{N}e^{-i(\phi\pm\delta_k)}\right)|0\rangle\langle 1| + \left(\frac{1}{2N}\sum_{k=1}^{N}e^{i(\phi\pm\delta_k)}\right)|1\rangle\langle 0|,\end{aligned} \tag{2.13}$$

where for $N \to \infty$, the average over the phase factors $e^{\pm i(\phi\pm\delta_i)}$ results in zero and we get the diagonal density matrix,

$$\rho = \frac{1}{\sqrt{2}}|0\rangle\langle 0| + \frac{1}{\sqrt{2}}|1\rangle\langle 1|. \tag{2.14}$$

It is important to point out that the loss of off-diagonal elements does not mean that dephasing and decoherence are the same phenomena [35]. Dephasing occurs due to inaccuracy on the classical level and may contribute to decoherence in spin systems, but the noise information about the cause of dephasing can be obtained in advance and possibly rectified [35]. However, knowledge about decoherence cannot be perceived earlier to undo its effect. This point will become more clear when we look into decoherence.

2.3 Decoherence

In the simplest terms, decoherence is the loss of the ability of a quantum system to exhibit superposition between its basis states. For example, consider the superposition state $\frac{1}{\sqrt{2}}(|0\rangle+|1\rangle)$ for the system described in (2.6). If the system is coupled to an environment, then the effect is that after a certain time the superposition state decays into either $|0\rangle$ or $|1\rangle$. It can be interpreted as the environment taking measurements of the system, which collapses the superposition state into logical states associated with

the observables monitored by the environment, which in the above example coincides with the basis we (the observer) considered. This environment's selection of certain states from the system's Hilbert space is called "einselection", and states onto which the system collapses are called "pointer states" or simply einselected states [35].

The mechanism of decoherence is governed by the system-environment interaction, which results in the entanglement of system and environment states. Entanglement implies the irreversible transfer of information from the system to the environment. In general, the time scale at which the system is entangled with the environment is extremely small [36]. As observers, we seem to compete with the environment for system information. But because of the continuous and unperturbed interaction and its large size, the environment wins the competition, obtaining information faster than the observer [35].

In terms of the density operator, decoherence corresponds to the decay of the off-diagonal elements. This is also evident from the example of decoherence of state $\frac{1}{\sqrt{2}}(|0\rangle+|1\rangle)$ to $|0\rangle$ or $|1\rangle$ we above considered. The density operator for the einselected states in the example is simply $\rho(t) = \frac{1}{2}|0\rangle\langle 0| + \frac{1}{2}|1\rangle\langle 1|$ or

$$\rho(t) = \begin{pmatrix} \frac{1}{2} & 0 \\ 0 & \frac{1}{2} \end{pmatrix}. \tag{2.15}$$

Recall from (2.14) that for dephasing in an ensemble density operator, we obtained a similar density matrix. It should be emphasized that in the case of dephasing, there is no entanglement between the system and environment, and subsequently, there is no transfer of information. However, due to dephasing, the states lose phase coherence, which randomizes the phases of states in a system interacting with the environment. This is a factor that contributes to the decoherence of the system [37, 38]. Thus, we note that both dissipation and dephasing, collectively and individually, could be

contributing factors in decoherence.

2.4 Decoherence of a Single Qubit

To examine the mechanism behind environment-induced decoherence, we consider a single qubit given in (2.6) interacting with an environment such that the interaction Hamiltonian is given by

$$H_{SB} = \hbar\omega_0\sigma_z \otimes B, \tag{2.16}$$

where B is Hermitian and describes an arbitrary environment operator. The dynamics of states in the open system are described by combined density operator $\rho_{tot}(t)$ s.t.

$$\rho_{tot}(t) = e^{-iH_{SB}(t-t_0)}\rho_S(t_0) \otimes \rho_B(t_0)e^{iH_{SB}(t-t_0)}, \tag{2.17}$$

where $\rho_S(t_0)$ and $\rho_B(t_0)$ represent the initial system and environment states. Here we considered a standard assumption that qubit and the environment are initially uncorrelated. Now, we wish to observe only the system's dynamics in the overall system-environment interaction. This is accomplished using the operation "partial trace" (see Appendix A.4) which averages over the degrees of freedom of the environment to obtain the reduced density operator $\rho_S(t)$ s.t.

$$\begin{aligned}\rho_S(t) =& \mathrm{Tr}_B\{\rho_{tot}(t)\} \\ =& \mathrm{Tr}_B\{e^{-iH_{SB}(t-t_0)}\rho_S(t_0) \otimes \rho_B(t_0)e^{iH_{SB}(t-t_0)}\}.\end{aligned} \tag{2.18}$$

At this point, we may assume that the environment's Hilbert space is spanned by the orthonormal basis $\{|\phi_r\rangle\}$. We further assume that $\{|\phi_r\rangle\}$ are eigenstates for B with eigenvalues $\{\lambda_r\}$. Now, for any time t the elements of the reduced density matrix $\rho_S(t)$ are simply given by

$$\begin{aligned}\langle i|\,\rho_S(t)\,|j\rangle &= \langle i| \sum_r \langle\phi_r|\,\{e^{-ig\lambda_r\omega_0\sigma_z(t-t_0)}\rho_S(t_0) \otimes \rho_B(t_0)e^{ig\lambda_r\omega_0\sigma_z(t-t_0)}\}\,|\phi_r\rangle\,|j\rangle \\ &= \rho_{ij}(t),\end{aligned} \tag{2.19}$$

where $|i\rangle, |j\rangle \in \{|0\rangle, |1\rangle\}$. For the diagonal elements we obtain

$$\begin{aligned}\rho_{00}(t) &= \langle i| \rho_S(t_0) |i\rangle \sum_r \langle \phi_r| \rho_B(t_0) |\phi_r\rangle \\ &= \rho_{00}(t_0).\end{aligned} \tag{2.20}$$

Similarly, $\rho_{11}(t) = \rho_{11}(t_0)$. On the other hand, the off-diagonal elements are

$$\rho_{01}(t) = \langle 0| \rho_S(t_0) |1\rangle \sum_r e^{-i2g\lambda_r\omega_0(t-t_0)} \langle \phi_r| \rho_B(t_0) |\phi_r\rangle, \tag{2.21}$$

and $\rho_{10}(t) = (\rho_{01}(t))^*$. If we assume that $\rho_S(t_0) = |+\rangle\langle+|$ and the environment is initially in pure state $|\psi_B\rangle$ then, from (2.8) we know

$$\rho_{00}(t_0) = \rho_{11}(t_0) = \frac{1}{2}, \tag{2.22}$$

and,

$$\begin{aligned}\rho_{01}(t) &= \frac{1}{2} \sum_r e^{-i2g\lambda_r\omega_0(t-t_0)} \langle \phi_r|\psi_B\rangle \langle \psi_B|\phi_r\rangle \\ &= \frac{1}{2} \langle \psi_B| \Big(\sum_r e^{-ig\lambda_r\omega_0(t-t_0)} |\phi_r\rangle \langle \phi_r| e^{-ig\lambda_r\omega_0(t-t_0)} \Big) |\psi_B\rangle \\ &= \frac{1}{2} v_B(t, t_0),\end{aligned} \tag{2.23}$$

where $v_B(t, t_0) = \langle \psi_B| e^{-i2gB\omega_0(t-t_0)} |\psi_B\rangle$. Thus, the reduced density matrix $\rho_S(t)$ is given by

$$\rho_S(t) = \begin{pmatrix} \frac{1}{2} & \frac{1}{2} v_B(t, t_0) \\ \frac{1}{2} v_B^*(t, t_0) & \frac{1}{2} \end{pmatrix}. \tag{2.24}$$

Suppose that for a time t' the value $v_B(t', t_0)$ and $v_B^*(t', t_0)$ becomes zero then, the matrix $\rho_S(t')$ decays to

$$\rho_S(t') = \begin{pmatrix} \frac{1}{2} & 0 \\ 0 & \frac{1}{2} \end{pmatrix}. \tag{2.25}$$

The off-diagonal elements disappear over time due to the unavoidable system-environment interaction, and eventually, the quantum system exhibits the behavior of a classical system with two logical states.

We can explicitly describe the environment by a bath of continuum of harmonic oscillators to interpret the impact of environment-induced decoherence on the system, as described in the single qubit dephasing mechanism by Viola and Llyod in [8]. For the qubit system described in (2.6) interacting with a bath of harmonic oscillators, the overall system plus bath Hamiltonian can be written as

$$\begin{aligned} H_0 = &\ H_S + H_B + H_{SB} \\ = &\ \hbar\omega_0\sigma_z + \sum_k \hbar\omega_k b_k^\dagger b_k + \sum_k \hbar\sigma_z(g_k b_k^\dagger + g_k^* b_k), \end{aligned} \tag{2.26}$$

where H_S and H_B are the system and bath Hamiltonians respectively and H_{SB} describes a bilinear interaction between the system and bath. The bath operators b_k and $b_k^\dagger$ are bosonic operators, ω_k is the frequency, and g_k is the complex coupling parameter of kth field mode. In the joint Hamiltonian, the tensor product of two different modes and the tensor product of the system and bath are shown by simple multiplication. Note the commutator relation $[H_S, H_{SB}] = 0$, which implies that the system and interaction Hamiltonian share common eigenbases. Indeed, these eigenbases are the preferred state in which the system collapses after decoherence.

In this model, decoherence is assumed to occur purely through the dephasing mechanism with no energy dissipation. With the detailed derivation in Appendix B, we can show that the time evolution of H_0 in the interaction picture $\widetilde{U}_{tot}(t, t_0)$ induces entanglement between the qubit and bath state. This entanglement is precisely responsible for the decoherence of the system. If we consider an example where initially the system is in state $|\psi(0)\rangle = |+\rangle = \frac{1}{\sqrt{2}}(|0\rangle + |1\rangle)$ and the kth mode of bath is in the vacuum state, then the states are evolved through $\widetilde{U}_{tot}(t)$ to generate the entangled state [39]

$$\left(\frac{1}{\sqrt{2}}(|0\rangle + |1\rangle)\right)|0\rangle_k \xrightarrow{\widetilde{U}_{tot}(t)} \frac{1}{\sqrt{2}}\left(|0\rangle\left|\frac{1}{2}\xi_k(t)\right\rangle + |1\rangle\left|-\frac{1}{2}\xi_k(t)\right\rangle\right), \tag{2.27}$$

where the initial state is transformed into an entangled state correlated with the

orthogonal coherent state $\left|\pm\frac{1}{2}\xi_k(t)\right\rangle$, where $\xi_k(t)$ is

$$\xi_k(t) = \frac{2g_k}{\omega_k}(1 - e^{i\omega_k t}). \tag{2.28}$$

The entanglement in (2.27) consequently destroys the purity of the quantum state and enforces the transition from a pure state to the classical mixture of basis states. This can be seen for the elements in the system's reduced density matrix $\widetilde{\rho}_S(t)$, where the diagonal elements $\widetilde{\rho}_{00}(t) = \rho_{00}(t_0)$ and $\widetilde{\rho}_{11}(t) = \rho_{11}(t_0)$, whereas for the off-diagonal elements we obtain

$$\widetilde{\rho}_{01}(t) = \rho_{01}(t_0)e^{-\Gamma(t-t_0)}, \tag{2.29}$$

where $\Gamma(t - t_0)$ is a real time-dependent function, called "decoherence function" [7]. Following the result in [40] we obtain

$$\Gamma(t - t_0) = \Gamma(\Delta t) = \sum_k \frac{|\xi_k(\Delta t)|^2}{2} \coth\left(\frac{\omega_k}{2T}\right), \tag{2.30}$$

where T is the temperature of the bath. Clearly, $\Gamma(\Delta t)$ corresponds to the decay of off-diagonal elements in the reduced density matrix and enforces classicality in the system. If the qubit's initial state is given by (2.7) then, we can write the reduced density matrix $\rho_S(t)$ in Schrödinger picture as

$$\rho_S(t) = \begin{pmatrix} \frac{1}{2} & \frac{1}{2}e^{-i\omega 2\Delta t}e^{-\Gamma(\Delta t)} \\ \frac{1}{2}e^{i\omega 2\Delta t}e^{-\Gamma(\Delta t)} & \frac{1}{2} \end{pmatrix}, \tag{2.31}$$

which after a certain time t decays into

$$\rho_S(t) = \begin{pmatrix} \frac{1}{2} & 0 \\ 0 & \frac{1}{2} \end{pmatrix}. \tag{2.32}$$

The decoherence function $\Gamma(\Delta t)$ depends upon various parameters like the size of the system under consideration, the nature of the environment, and the strength of system-environment coupling [7]. It describes the spectral density of the bath, the spectrum over which the energy from the system is distributed as a function of modes, which in turn determines the time scales of decoherence.

Small-scale experiments that can be conducted within the coherence time of a quantum system have been demonstrated in recent times [41–43]. However, large-scale quantum systems are required for classically intractable calculations to achieve quantum superiority over the classical approach of computations [44, 45]. In general, as the scale of components in a quantum system grows, its interactions with the environment get stronger, and the coherence time decreases [5]. Techniques that apply external controls can be used to increase the coherence time of systems by suppressing the errors due to system-environment interaction or removing the components that induce these errors. In the next Chapter, we will investigate techniques that can suppress decoherence due to system-environment interactions or, ideally, eliminate the effect completely.

Chapter 3

DYNAMICAL DECOUPLING

3.1 Introduction

Eliminating the effect of decoherence is the most critical and universal requirement for achieving longer coherence times in a quantum system. Development of such a framework is a prerequisite for systems which rely on the capability of maintaining extended coherence times for large-scale computations. These applications include quantum computations [3, 5] and quantum information processing [46], as well as in experiments with photonic qubits [47], trapped ions [48], quantum dots [49] and optomechanics [50]. In classical error correction, the error generators are identified through repeated measurements, and then the error is suppressed via a feedback mechanism [51]. However, one will quickly realize that the exact scheme won't work for a quantum system. Firstly, any measurement will change the state of a quantum system, and error correction through direct feedback is impossible. Secondly, since cloning is not possible for quantum states, one cannot make copies of the state and calculate errors by measuring the copied states.

For scenarios where the error rates are below a threshold, these challenges can be overcome by developing quantum error correction techniques [52]. In recent years, many efficient tools have been introduced in the field of quantum error correction to mitigate the impact of environment-induced decoherence [5, 53]. Error correction codes [5, 52, 53] have been shown to effectively realize improvements in state fidelity [54–56]. Lidar et al. [57] suggested using decoherence-free subspaces to encode information that is intrinsically unaffected by noise. Topological quantum computing

[58, 59] makes use of anyonic systems, which are naturally robust to computational errors.

Dynamical decoupling (DD) is an effective quantum error correction technique, especially in cases where the knowledge of the system-environment interaction is unknown. It originates from NMR spectroscopy [60–62] where we strongly need precise spectroscopy of complex molecules. In the context of quantum computing, DD was introduced to suppress dephasing in spin systems by the application of a periodic sequence of strong instantaneous pulses that flip the qubit in such a manner that the net dephasing in the qubit is averaged to zero [5, 8, 63]. Later, the technique was used to achieve noise-tolerant controls for a general open quantum system [64]. Lately, in addition to increasing coherence time in various physical systems [48, 65–67], DD has been demonstrated as an efficient method to create high-fidelity gates [68–70] and for noise spectroscopy in various systems [71–74]. In order to establish a strong understanding of DD, let us begin with the famous Hahn's "spin echo" experiment [75, 76].

3.2 Spin Echo

In the spin echo experiment, we have an ensemble of spins with magnetic moments along the direction of a strong applied magnetic field (along $|0\rangle$ in Fig 3.1). These spins are now rotated about x axis with $\pi/2$ pulse along the equator of the Bloch sphere. At this point, we notice that due to local inhomogeneities in the magnetic field, certain spins rotate with higher frequencies (due to higher field strength) and certain spins rotate with lower frequencies (due to lower field strength). This causes dephasing in the spin ensemble, where higher-frequency spins are rotating faster than the lower frequencies. Due to the strong magnetic field, the dissipation is minimized, and the spins decohere only via dephasing [77].

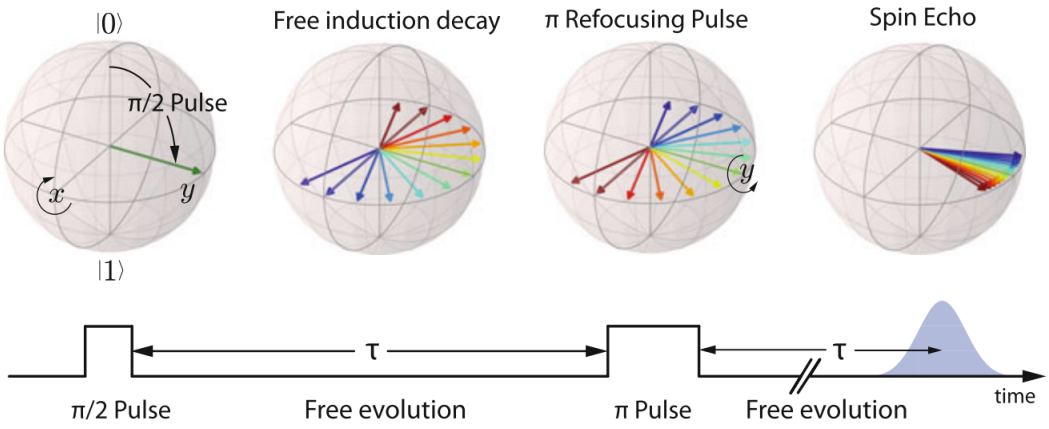

Figure 3.1: Bloch sphere representation of pulse sequences used in spin echo experiment. On applying $\pi/2$ pulse the spin ensemble rotates in xy plane and dephases due to an inhomogeneous magnetic field. After waiting for time τ the ensemble is rotated by π pulse about y axis and the spins refocus after time 2τ. Figure adopted from Putz, "Circuit cavity QED with macroscopic solid-state spin ensembles.", 2017, pg. 114.

After allowing the dephasing for time τ, if the spins are rotated 180° about y axis with π pulse (see in Fig 3.1) we notice that the dephasing has now been reversed. Hence, the spins rotating with lower frequencies catch up with the ones with higher frequencies, and spins get back into phase after time τ. With this scheme of pulses, we momentarily evade dephasing. If we keep repeating the scheme for any arbitrary time t, with the ideal pulses, the dephasing can be effectively eliminated.

Viola and Llyod extended this method of refocusing of spins to a general quantum system setting with bang-bang controls [8, 63] after realizing that, similar to dephasing in NMR, in an open quantum system the decoherence process never takes place instantaneously. And if the dynamics of the system are altered faster than the shortest time scales at which the system-environment interaction induces decoherence, these

effects can be suppressed over the course of time.

3.3 The Concept of Dynamical Decoupling

To better understand the underlying concept let's invoke the single-qubit model from (2.16) where the system-environment interaction is given by

$$H_{SB} = \hbar\omega_0\sigma_z \otimes B. \tag{3.1}$$

This interaction induces decoherence in the system and we aim to suppress the dynamics driven by H_{SB}. For simplicity, we assume $\omega_0 = 1$. Further assume that we can apply instantaneous π pulses to rotate the qubit by 180° about x axis, with the operator

$$R_x(\pi) = \exp\left(-i\frac{\pi}{2}\sigma_x\right) \otimes \mathbb{1}_B, \tag{3.2}$$

where σ_x is the Pauli-X operator and $\mathbb{1}_B$ is the identity matrix of the same dimensions as operator B. In a similar way, using $R_x^\dagger(\pi)$ we can rotate the system in the opposite direction i.e. in counter-clockwise direction if $R_x(\pi)$ rotates the system in clockwise direction and vice versa. Now if we switch on and off these pulses in the intervals of Δt in the order:

$$U(2\Delta t) = e^{-iH_{SB}\Delta t}R_x^\dagger(\pi)e^{-iH_{SB}\Delta t}R_x(\pi), \tag{3.3}$$

where upto a global phase, unitary operator $R_x(\pi) = R_x^\dagger(\pi) = \sigma_x \otimes \mathbb{1}_B$. As a result

$$\left(e^{-i\sigma_z\Delta t}\sigma_x e^{-i\sigma_z\Delta t}\sigma_x\right) \otimes \mathbb{1}_B = \left(e^{-i\sigma_z\Delta t}e^{-i\sigma_x\sigma_z\sigma_x\Delta t}\right) \otimes \mathbb{1}_B. \tag{3.4}$$

Since $\sigma_x\sigma_z\sigma_x = -\sigma_z$, then (3.3) can be simplified to

$$U(2\Delta t) = \left(e^{-i\sigma_z\Delta t}e^{i\sigma_z\Delta t}\right) \otimes \mathbb{1}_B = \mathbb{1}. \tag{3.5}$$

Thus, after time $2\Delta t$ the qubit returns to its initial state, and the net evolution of the system is zero. Note that $[\sigma_x\sigma_z\sigma_x, H_{SB}] = 0$, hence in this case, decoupling can be achieved for an arbitrary time interval $2\Delta t$ [79]. Moreover, since we have complete

knowledge of system-environment interaction, we can easily define a decoupling set for the given interaction Hamiltonian. However, in general, we have zero or partial knowledge of system operators which interact with the environment. In the following section, we will show that DD can be implemented for a general open quantum system under minimal assumptions about the system-environment interactions.

3.4 Dynamical Decoupling in a Continuous-Time Framework

In a general control-theoretic framework, we can analyze DD by considering a finite-dimensional open quantum system as described in [5, 63]. In this framework, we consider a finite time-independent quantum system S coupled to an uncontrollable bath B defined on the Hilbert space $\mathscr{H} = \mathscr{H}_S \otimes \mathscr{H}_B$, where $\mathscr{H}_S$ and $\mathscr{H}_B$ are system and bath Hilbert spaces, respectively. The combined Hamiltonian is given by

$$H_0 = H_S + H_B + H_{SB}, \quad H_{SB} = \sum_a S_a \otimes B_a, \tag{3.6}$$

where H_S and H_B are system and bath Hamiltonians, respectively, and the interaction H_{SB} is the term that induces decoherence in the system. Both H_S and S_a are chosen to be traceless. Furthermore, it is essential that S_a and H_{SB} are assumed to be finite in order to define a finite set of decoupling operations [5]. We will see later why these assumptions are critical for the effective decoupling of the system.

We begin with a standard assumption: the system and environment are initially uncorrelated, i.e., $\rho_{SB}(0) = \rho_S(0) \otimes \rho_B(0)$, and the reduced density operator for the system at time t is given by $\rho_S(t) = \mathrm{Tr}_B\{\rho_{SB}(t)\}$. To achieve control over the dynamics of the system, we adjoin the Hamiltonian H_0 with a controllable time-dependent Hamiltonian $H_c(t)$ which selectively acts on the system. The joint Hamiltonian is then modified to

$$H(t) \longrightarrow H_0 + H_c(t) \otimes \mathbb{1}_B, \quad H_c(t) = \sum_i u_i(t) H_i, \tag{3.7}$$

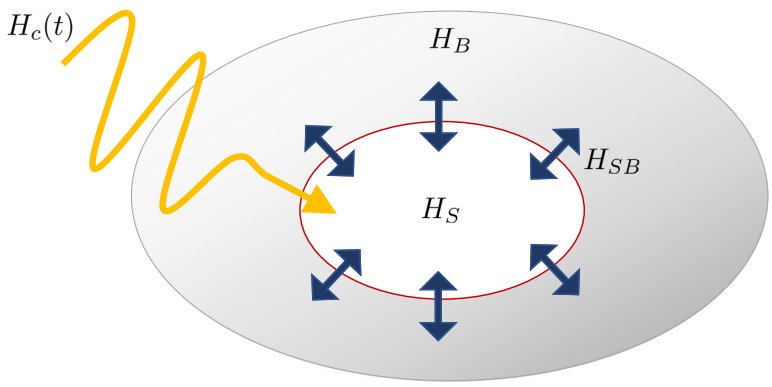

Figure 3.2: An illustration of controls applied to an open quantum system through the time-dependent controller $H_c(t)$.

where $u_i(t)$ are control inputs corresponding to the primary control Hamiltonian H_i. The desired control action can be produced by applying any linear combination of local controls $u_i(t)H_i$ to the system. The control propagator governed by $H_c(t)$ is given by

$$U_c(t) = \mathcal{T} \exp\left(-i \int_0^t ds H_c(s)\right), \tag{3.8}$$

where $\mathcal{T}$ is time ordering operator. If the decoupling is achieved at time $t = T_c$, then to realize a decoherence-free system for an arbitrarily long time t such that $t = NT_c$, where $N \in \mathbb{N}$, the controls are designed to be cyclic over T_c i.e.

$$U_c(t) = U_c(t + T_c). \tag{3.9}$$

In order to identify the conditions where the interaction Hamiltonian is suppressed, we examine the dynamics of the combined system. In open quantum systems, the dynamics of states are given by the density operator, which in this case is

$$\rho_{SB}(t) = U(t)[\rho_S(0) \otimes \rho_B(0)]U^\dagger(t), \tag{3.10}$$

where $U(t)$ is evolution of joint Hamiltonian $H(t)$. At this point, it is convenient to switch to a reference frame rotating about the control propagator in order to "unwind" $U(t)$ into different components. A technical overview of the consistency

of rotating frames in quantum mechanics is well explained in [80]. Moreover, the equation of motion in the rotating frame can be found in Appendix A.5. Thus the revised dynamics with reference to the rotating frame is

$$\rho_{SB}(t) = U_c(t)\widetilde{\rho}_{SB}(t)U_c^{\dagger}(t), \tag{3.11}$$

where $\widetilde{\rho}_{SB}(t)$ is the density operator in rotating frame. If the evolution of the combined system in a rotating frame is given by $\widetilde{U}(t)$, then

$$\widetilde{\rho_{SB}}(t) = \widetilde{U}(t)[\rho_S(0) \otimes \rho_B(0)]\widetilde{U}^{\dagger}(t), \tag{3.12}$$

where $\widetilde{U}(t)$ is the time evolution of Hamiltonian $\widetilde{H}(t)$ such that

$$\widetilde{H}(t) = U_c^{\dagger}(t)H_0U_c(t). \tag{3.13}$$

From equations (3.10), (3.11) and (3.12) we get

$$U(t) = U_c(t)\widetilde{U}(t). \tag{3.14}$$

If we choose to design the control field such that $U_c(T_c) = \mathbb{1}$, then for time $t = NT_c$, the total evolution of the combined system is given by

$$U(NT_c) = \widetilde{U}(NT_c). \tag{3.15}$$

From average Hamiltonian theory, $\widetilde{U}(NT_c)$ can be expressed as an exponential of the form $\exp\left(-i\bar{H}NT_c\right)$ where the time-independent "effective Hamiltonian" or average Hamiltonian $\bar{H}$ describes exactly the evolution of the time-dependent Hamiltonian $\widetilde{H}(t)$ over the time period T_c [5]. The effective Hamiltonian can be expanded in a series called the Magnus expansion [81] as

$$\bar{H} = \bar{H}^{(0)} + \bar{H}^{(1)} + \bar{H}^{(2)} + \bar{H}^{(3)} \ldots, \tag{3.16}$$

where the term $\bar{H}^{(n)}$ is referred as the nth order average Hamiltonian. The first two terms of the Magnus expansion are given by

$$\bar{H}^{(0)} = \frac{1}{T_c}\int_0^{T_c} dt'\widetilde{H}(t'), \tag{3.17}$$

$$\bar{H}^{(1)} = \frac{-i}{2T_c}\int_0^{T_c} dt'' \int_0^{t''} dt'[\widetilde{H}(t''), \widetilde{H}(t')]. \tag{3.18}$$

With the assumption that H_0 is bounded such that the spectral norm $\|H_0\| \leq \kappa$, the spectral norm for the nth term of Magnus expansion is given by [5]

$$\|\bar{H}^{(n)}\| = \mathscr{O}[\kappa(\kappa T_c)^n], \tag{3.19}$$

where $\kappa > 0$, has units of frequency associated with the energy greater than or equal to the largest eigenvalue of H_0. Note that the Magnus series rapidly converges when

$$\kappa T_c \ll 1, \tag{3.20}$$

which gives a loose upper bound on T_c. From (3.19) and (3.20), it is clear that for sufficiently fast control, i.e., in the limit $T_c \to 0$, the contributions from higher orders ($\bar{H}^{(n)}, n \geq 1$) in (3.16) are negligible. Since $T_c = T/N$, alternatively, we can state that convergence is achieved for sufficiently large N such that $\lim N \to \infty$. Consequently, under convergence conditions, the DD problem is simply reduced to devising a unitary operator $U_c(t)$ such that evolution described by the first order term of the Magnus series $\bar{H}^{(0)}$ is successfully eliminated, i.e.

$$\lim_{T_c \to 0} U(NT_c) = \exp\Big(-i\bar{H}^{(0)}NT_c\Big) = \mathbb{1}. \tag{3.21}$$

In particular, we see that achieving effective decoupling doesn't require specific knowledge of the system operators interacting with the environment. Instead, the unwanted dynamics induced by the interaction Hamiltonian can always be suppressed by

(i) choosing a proper set of decoupling operations, and

(ii) implementing these operations faster than the time scales at which decoherence completely destroys the superposition states in the system's Hilbert space.

We now numerically simulate the DD scheme discussed above to investigate how effectively the time evolution of a target Hamiltonian is suppressed in the $\lim T_c \to 0$. Let us consider a time-independent Hamiltonian

$$H_0 = \hbar\omega_0\sigma_y, \tag{3.22}$$

where σ_y is Pauli-Y operator. This system is assumed to be completely coupled with the environment such that $H_0 \rightarrow H_0 \otimes B$, where B is an environment operator. For simplicity lets assume $\omega_0 = 1$. We use $H_c(t)$ as the control Hamiltonian which continuously rotates the system about the x axis in the Bloch sphere. Now the control propagator $U_c(t)$ is designed such that

$$\int_0^{T_c} dt' U_c^\dagger(t') H_0 U_c(t') = 0. \tag{3.23}$$

Let us say,

$$U_c(t) = \exp(-if(t)\sigma_x), \tag{3.24}$$

then the decoupling in H_0 is obtained when

$$\int_0^{T_c} dt' e^{\pm i2f(t')} = 0. \tag{3.25}$$

This is accomplished by using Hansen-Bessel formula [82] so that $f(t)$ is chosen in such a way that

$$f(t) = \frac{z}{2}\sin\left(\frac{2\pi t}{T_c}\right) = \frac{z}{2}\sin(\omega_c t), \tag{3.26}$$

where z is the zeros of zeroth order Bessel functions of the first kind [83] and ω_c is the control frequency. The time t is determined such that the sampling frequency for the discretization of $U_c(t)$ satisfies the Nyquist–Shannon sampling theorem [84]. We calculate the expectation value of Pauli-Z operator where dynamics of the states are described by unitary operator $U(t)$ (see (3.14)) where initially $|\psi(0)\rangle = |0\rangle$. From (3.19) and (3.20) we know that for this case the Magnus series converges when spectral norm $\|\sigma_y\| \leq \kappa$, where $\|\sigma_y\| = 1$. Thus the convergence condition in this case is

$$T_c \ll 1. \tag{3.27}$$

Note in Fig (3.3) that when T_c satisfy the above condition, the dynamics from the

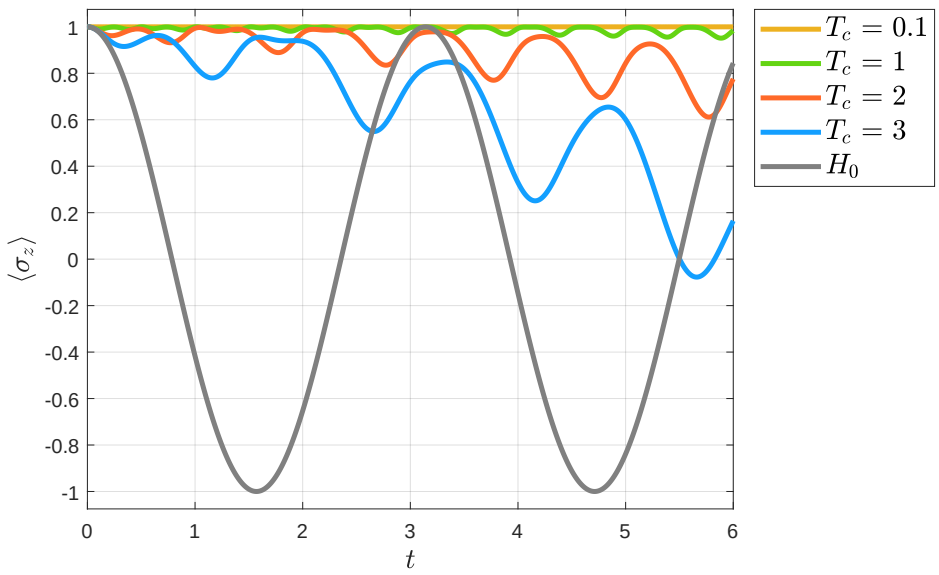

Figure 3.3: Expectation value of Pauli-Z as a function of time for Hamiltonian $H_0 + H_c(t)$. For simulation, we used total time $t = 6$ and number of data points $n = 10^4$. Note that in the absence of control, the system evolves with free dynamics, as shown by the gray line. When the system is perturbed by $H_c(t)$ with $T_c = 3$, $T_c = 2$, and $T_c = 1$, the expectation value is "up-shifted" closer to 1 and oscillates away as time progresses. For $T_c = 0.1$, the states approximately remain in their initial state at all times.

interaction Hamiltonian H_0 are effectively eliminated, i.e., $U(t) \approx \mathbb{1}$ and the system remains in its initial state $|0\rangle$. Now, if we instill time dependence on the H_0 such that ω_0 is a time-dependent angular frequency and the Hamiltonian is modified to

$$H_1 = \hbar(\cos(4t) + \cos(2t))\sigma_y. \tag{3.28}$$

We use same $U_c(t)$ from (3.24) to suppress the system-environment interaction. In Fig (3.4) and Fig (3.5), DD is achieved when T_c is less then the smallest time scale present in H_1 or ω_c is larger than any frequency component present in H_1.

The shown results can be generalized for any time-dependent Hamiltonian, i.e. in

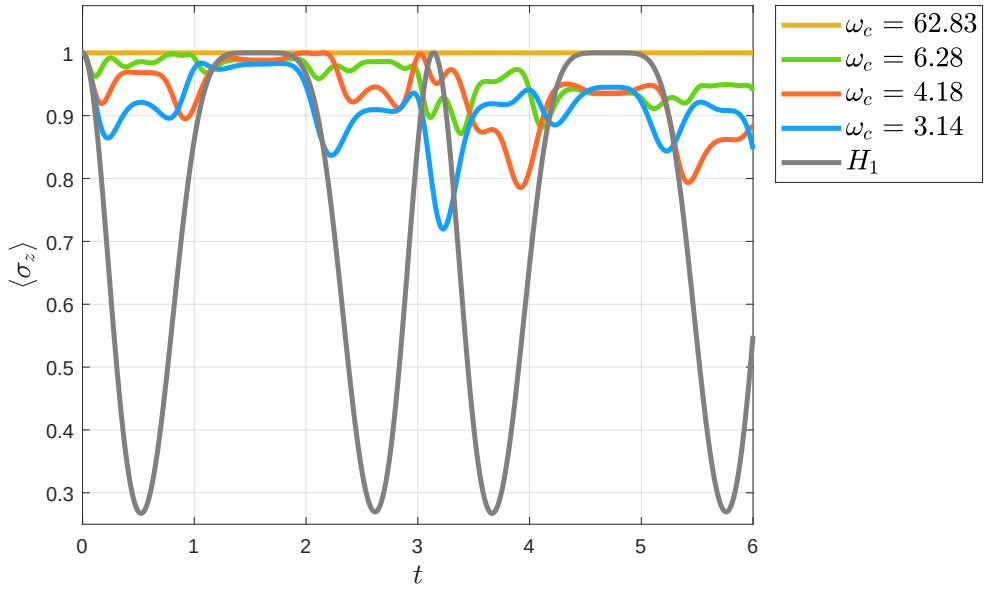

Figure 3.4: Expectation value of Pauli-Z as a function of time for Hamiltonian $H_1 + H_c(t)$. We used similar parameters from Fig 3.3. Similar to the previous case, for larger values of ω_c the expectation value is shifted upwards towards 1. For $\omega_c = 62.83$ or $T_c = 0.1$, the evolution of the system is effectively suppressed.

the limiting condition $\omega_c \to \infty$, any finite time-dependent Hamiltonian can be treated like time-independent in the period T_c. Thus no matter how fast the time scale for the evolution of interaction Hamiltonian is, for a short duration, the system drifts slowly into some fixed direction, and these control operations quickly rotate it such that the net movement in the direction is close to zero.

3.5 Bang-Bang Dynamical Decoupling

In the previous section, we numerically demonstrated DD, which is applied continuously along with the system dynamics to suppress decoherence. The alternative to continuous controls is the originally proposed bang-bang decoupling [8], which is closer to the spirit of the scheme of pulses used in Hahn's spin echo experiment. To

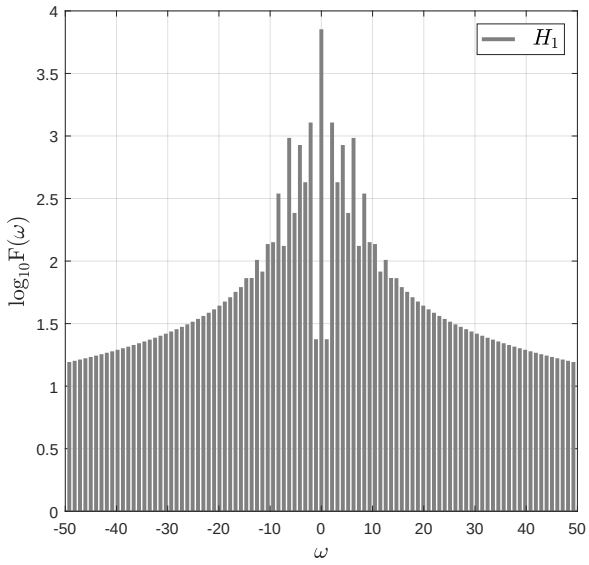

(a)

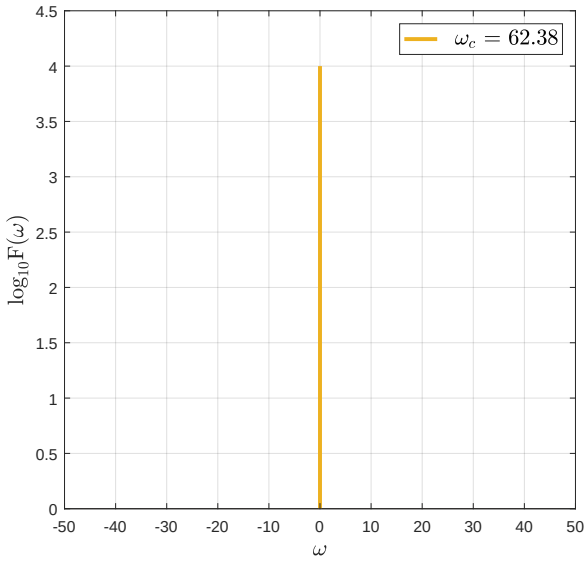

(b)

Figure 3.5: Frequency spectrums of the expectation values for the dynamics governed by (a) H_1 and (b) $H_1 + H_c(t)$. The logarithmic value of the Fourier transform is plotted on the y-axis where we neglected the values for $F(\omega) < 1$. The frequency range is $-50 \leq \omega \leq 50$. For sufficiently large controls $\omega_c = 62.83$, we see that all frequencies other than 0 are completely suppressed in (b).

derive bang-bang controls for an open quantum system, we recall the general system-environment model controlled by $H_c(t)$ in (3.6). From (3.20) we know that in the limit of fast control, the goal of DD is simplified to suppress the dynamics from the first term of Magnus expansion. Now consider that we can design the control field as a sequence of pulses given by

$$H_c(t) = \begin{cases} H_1 & 0 < t \leq t_{P_1} \\ H_2 & t_{P_1} < t \leq t_{P_2} \\ \vdots & \\ H_{n_p} & t_{P_{n_p-1}} < t \leq t_{P_{n_p}}, \end{cases} \tag{3.29}$$

where H_k is the time-independent Hamiltonian describing the pulse at time t, where $t \in (t_{P_{k-1}}, t_{P_k}]$ and $t_{P_0} = 0$. The number of pulses subjected to the system in one cycle T_c is denoted by n_p. The sequence of pulses is uniformly distributed over time, i.e.,

$$\Delta t = t_{P_{n_p}} - t_{P_{n_p-1}} = \ldots = t_{P_2} - t_{P_1} = t_{P_1} - 0, \tag{3.30}$$

where $t_{P_{n_p}} = T_c$ and $\Delta t = T_c/n_p$. From (3.8), the evolutions of control Hamiltonian described in (3.29) for time $t \in (t_{P_{k-1}}, t_{P_k}]$ is given by

$$U_c(t, t_{P_{k-1}}) = \mathcal{T} \exp\left(-i \int_{t_{P_{k-1}}}^{t} dt' H_k\right). \tag{3.31}$$

If we invoke the composition property of unitary operators [85] i.e. for a unitary operator V,

$$\begin{aligned} V(t_n, t_0) &= V(t_n, t_{n-1}) \ldots V(t_2, t_1) V(t_1, t_0) \\ &= \prod_{k=1}^{n} V(t_k, t_{k-1}). \end{aligned} \tag{3.32}$$

Then, in similar fashion the evolution of $\bar{H}^{(0)}$ over T_c is given by

$$\exp\left(-i\bar{H}^{(0)} T_c\right) = \prod_{k=1}^{n_p} \exp\left(-i \int_{t_{P_{k-1}}}^{t_{P_k}} dt U_c^{\dagger}(t, t_{P_{k-1}}) H_0 U_c(t, t_{P_{k-1}})\right). \tag{3.33}$$

To ensure that the time scale at which pulses are applied is smaller than the decoherence time, we ideally want that the pulses are

(i) an unit impulse (given by Dirac delta distribution) [86];

$$H_c(t) = \sum_k^{n_p} H_k \delta(t - t_{P_k}). \tag{3.34}$$

(ii) strong pulses or parity "kicks" [87], i.e., the open system does not evolve within each pulse. For control fields given by (3.34) the unitary operator $U_c(t, t_{P_{k-1}})$ is given by

$$\begin{aligned} U_c(t, t_{P_{k-1}}) &= \mathcal{T} \exp\left(-i \int_{t_{P_{k-1}}}^{t} dt' H_k \delta(t' - t_{P_{k-1}}) \right) \\ &= \exp(-iH_k). \end{aligned} \tag{3.35}$$

Note that the time ordering operator is omitted in the second step since H_k commutes with itself in the duration of the pulse. We also note that $U_c(t, t_{P_{k-1}})$ is now a time-independent operator, and for convenience, let's say $U_c(t, t_{P_{k-1}}) = g_k$. Then (3.33) is further simplified to

$$\exp\Big(-i\bar{H}^{(0)}T_c\Big) = \prod_{k=1}^{n_p} \exp\Big(-ig_k^\dagger H_0 g_k \Delta t\Big). \tag{3.36}$$

Now we wish to calculate the evolution of total system Hamiltonian $H(t)$ for an arbitrary long time t, where $t = mT_c$, $m \in \mathbb{N}$, which is described by the unitary operator

$$\begin{aligned} U(t) &= \left[\exp\Big(-i\bar{H}^{(0)}T_c\Big)\right]^m \\ &= \left[\prod_{k=1}^{n_p} \exp\Big(-ig_k^\dagger H_0 g_k \Delta t\Big)\right]^m. \end{aligned} \tag{3.37}$$

From (3.20) we know that the simultaneous condition for the convergence of Magnus expansion is $\lim m \to \infty$. Moreover, Δt can be rewritten for time t as

$$\Delta t = \frac{mT_c}{mn_p} = \frac{t}{mn_p}. \tag{3.38}$$

It is immediately seen that under above conditions, $U(t)$ is given by the Trotter product formula [88]

$$U(t) = \lim_{m\to\infty}\Big[\prod_{k=1}^{n_p}\exp\Big(-ig_k^\dagger H_0 g_k \Delta t\Big)\Big]^m \tag{3.39}$$
$$= \exp\left(-i\left[\frac{1}{n_p}\sum_{k=1}^{n_p} g_k^\dagger H_0 g_k\right]t\right)$$
$$= \exp(-i\mathcal{M}_{DD}(H_0)t),$$

where $\mathcal{M}_{DD}$ is a linear Hermitian map that applies decoupling operators g taken from a finite decoupling set $\mathcal{G}$, such that

$$\mathcal{M}_{DD}(H_0) = \frac{1}{|\mathcal{G}|}\sum_{g_k\in\mathcal{G}} g_k^\dagger H_0 g_k, \tag{3.40}$$

where $|\mathcal{G}|$ denotes the number of elements in the set $\mathcal{G}$. From (3.39) and (3.6) we can calculate $\mathcal{M}_{DD}(H_0)$ while taking into account that decoupling operations are applied only to the system, as

$$\mathcal{M}_{DD}(H_0) = \mathcal{M}_{DD}(H_S) + H_B + \sum_a \mathcal{M}_{DD}(S_a)\otimes B_a. \tag{3.41}$$

We recall the presumption that H_S and S_a are trace-less. Thus, for a single qubit, the system operator S_a can be written as a linear combination of Pauli operators such that

$$S_a = \lambda^x\sigma_x + \lambda^y\sigma_y + \lambda^z\sigma_z, \tag{3.42}$$

which is averaged out to zero with decoupling set $\mathcal{G} = \{\sigma_x, \sigma_y, \sigma_z, \mathbb{1}\}$ (see Appendix C). Similarly, for K qubits system decoupling can be achieved with $\mathcal{G} = \{\sigma_\alpha^{(i)}, \mathbb{1}\}^{\otimes K}$, where $\alpha = x, y, z$ and $i = 1, 2, \ldots K$ [63]. Similar inferences can be made for H_S. Hence, on applying an appropriate decoupling set, we follow the result:

$$\mathcal{M}_{DD}(H_0) = 0 + H_B + \sum_a 0\otimes B_a = H_B. \tag{3.43}$$

Thus, the dynamics of joint system $U(t)$ is simply given by

$$U(t) = \exp(-iH_B t), \tag{3.44}$$

where under this transformation, the states in the system remain invariant to the environment-induced decoherence.

To analyze bang-bang decoupling in the qubit-boson model we earlier discussed in section 2.4, we implement infinitely strong π pulses that rotate the qubit system described in (2.26) about x axis, i.e., from pointing up to down in the Bloch sphere or vice versa with the controls

$$H_c(t) = \sum_{k=1}^{n_p} \frac{\pi}{2} \sigma_x \delta(t - t_{P_k}). \tag{3.45}$$

In the interaction picture, the control propagator at time $t = t_{P_k}$, is given by (see Appendix D)

$$\begin{aligned} \widetilde{U}_c(t_{P_k}) &= \exp\left(-i\frac{\pi}{2} e^{i\omega_0 \sigma_z t_{P_k}} \sigma_x e^{-i\omega_0 \sigma_z t_{P_k}}\right) \\ &= P_k. \end{aligned} \tag{3.46}$$

Similar to the pulse sequence defined in (3.3), we implement the sequence for $n_p = 2$ in the order as schematically shown in Fig 3.6. Firstly, the system evolves under $\widetilde{H}_{SB}(t)$ during $t_0 \leq t < t_{P_1}$; at t_{P_1} pulse P_1 is applied; then the system evolves freely during $t_{P_1} \leq t < t_{P_2}$; pulse P_2 is applied at t_{P_2} [8]. For the sake of ease, we keep the pulses equally spaced in time,

$$\Delta t = t_{P_1} - t_0 = t_{P_2} - t_{P_1}. \tag{3.47}$$

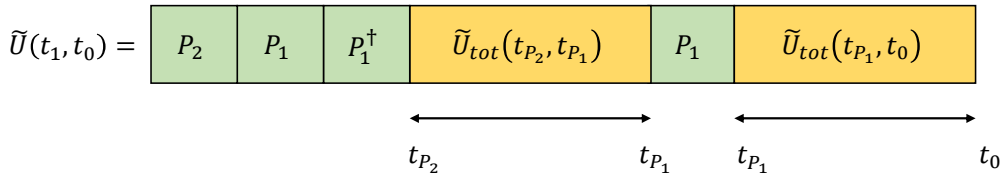

Figure 3.6: Pulse sequence for bang-bang controls used for DD in [8] for a single cycle with number of pulses $n_p = 2$. The combined unitary operator for the application of one cycle of control pulses is given by $\widetilde{U}(t_1, t_0)$.

With detailed derivation in Appendix D, the total evolution after N cycles is determined by the time-ordered product of the evolutions for each cycle, s.t.

$$\widetilde{U}(t_N, t_0) = \widetilde{U}(t_N, t_{N-1}) \dots \widetilde{U}(t_2, t_1)\widetilde{U}(t_1, t_0). \tag{3.48}$$

We now proceed to compute the off-diagonal elements of the reduced density matrix for the system. The diagonal elements in $\widetilde{\rho}_S(t)$ remains invariant, however the off-diagonal elements are

$$\widetilde{\rho}_{01}(t_N) = e^{i2\omega_0(t_N - t_0)}\rho_{01}(t_0)e^{-\Gamma_P(N,\Delta t)}, \tag{3.49}$$

where $\Gamma_P(N, \Delta t)$ is similar to (2.30), a decoherence function which can be written as

$$\Gamma_P(N, \Delta t) = \sum_k \frac{|\mu_k(N, \Delta t)|^2}{2} \coth\left(\frac{\omega_k}{2T}\right). \tag{3.50}$$

We invoke the evolution of off-diagonal elements in the absence of pulses from (2.29) and notice two key differences: (i) a phase contribution from eigenbases of σ_z (ii) a modified decoherence function proportional to $|\mu_k(N, \Delta t)|^2$ [8]. We will see in a moment what effect the added phase factor has on the elements, but first, let us analyze the decoherence function. By considering a single mode of frequency ω, we can compute the ratio

$$\frac{|\mu(N, \Delta t)|^2}{|\xi(t_N - t_0)|^2} = \tan^2\left(\frac{\omega \Delta t}{2}\right). \tag{3.51}$$

The above relation shows that for a given mode of frequency ω, there exists a finite region $\omega\Delta t \leq \pi/2$ where

$$|\mu(N, \Delta t)|^2 \leq |\xi(t_N - t_0)|^2. \tag{3.52}$$

Thus, in this particular region, the contribution from decoherence is relatively smaller when the system is subjected to pulses [8]. Notice that this condition can be met for appropriate smaller values of Δt which consequently means rapid execution of pulses. Unsurprisingly, this is in accordance with the convergence condition from (3.20) which we obtained for a general finite-dimensional open quantum system. Similar to the

limiting case numerics we simulated for (3.22) and (3.28), in this case, we can check an idealized situation by considering the following limits:

$$\lim_{\substack{\Delta t\to 0,\\ N\to\infty}} \Gamma_P(N,\Delta t) = \lim_{\Delta t\to 0}\sum_k \frac{|\mu_k(N,\Delta t)|^2}{2}\coth\left(\frac{\omega_k}{2T}\right). \tag{3.53}$$

With the assumption that Δt is sufficiently small so that for any arbitrary field mode $\omega_k\Delta t \to 0$, we obtain the limit (see Appendix D),

$$\lim_{\substack{\Delta t\to 0\\ N\to\infty}} \mu_k(N,\Delta t) = 0. \tag{3.54}$$

Thus, in an idealistic scenario, the decoherence function

$$\lim_{\Delta t\to 0} \Gamma_P(N,\Delta t) = 0, \tag{3.55}$$

which suggests that the complete and accurate removal of decoherence is achieved when the qubit is flipped in a continuously fast manner, irrespective of the temperature of the bath. However, there exists a cut-off frequency ω_l beyond which the spectral density of the bath is negligible [5]. For this reason, a lower bound proportional to ω_l^{-1} can be assumed for pulse intervals. Thus, a sufficient condition to reach the ideal case (3.55) is [8]

$$\omega_l\Delta t \lesssim 1. \tag{3.56}$$

The final step is to calculate the reduced density matrix $\rho(t_N)$ of the qubit, in a similar manner to (2.31). In Schrödinger picture, we obtain

$$\begin{pmatrix} \frac{1}{2} & \frac{1}{2}e^{-i\omega_0 2t_0} \\ \frac{1}{2}e^{i\omega_0 2t_0} & \frac{1}{2} \end{pmatrix} \xrightarrow{t_N} \begin{pmatrix} \frac{1}{2} & \frac{1}{2}e^{-\Gamma_P(N,\Delta t)} \\ \frac{1}{2}e^{-\Gamma_P(N,\Delta t)} & \frac{1}{2} \end{pmatrix}. \tag{3.57}$$

Note that the off-diagonal elements no longer have a phase factor when compared with (2.31). This is due to the reversal of the state of the qubit from the pulses applied to the system. Since the qubit is flipped in the opposite direction to its oscillations with the exact same frequency, the oscillations of the qubit are refocused, and when we move to Schrödinger picture, the net movement is zero. If the condition in (3.56)

is met, the density matrix is simply

$$\rho_S(t_N) = \begin{pmatrix} \frac{1}{2} & \frac{1}{2} \\ \frac{1}{2} & \frac{1}{2} \end{pmatrix}. \tag{3.58}$$

Numerous adaptations of DD have been proposed in recent times to achieve the elimination of high-order terms in the Magnus expansion for non-zero cyclic time T_c. In general, bang-bang pulses applied periodically (PDD) [5] in the sequence described in (3.3) achieves the elimination of the first-order term $\bar{H}^{(0)}$. Removal of up to the second-order term is obtained if the pulses are applied in a time-symmetric sequence so that the PDD is applied for the first half of a cycle and in reverse sequence for the second half [66, 89]. With concatenated dynamical decoupling (CDD), terms up to any arbitrary order N can be eliminated with the application of a number of pulses of order $\mathscr{O}(4^N)$ for every cycle, whereas with Uhrig dynamical decoupling (UDD), any single kind of error is removed up to Nth order with pulses of order $\mathscr{O}(N)$ [89]. Quadratic dynamical decoupling (QDD) [90] improvised on UDD with the removal of any arbitrary error to N order with $\mathscr{O}(N^2)$ pulses every cycle [89]. Randomized dynamical decoupling (RDD) [91] was introduced for large quantum systems, where instead of following a deterministic sequence, decoupling operations are selected randomly from a given decoupling set [79]. Other novel adaptations include fault-tolerant dynamical decoupling [92], mixed dynamical decoupling [93], adaptive dynamical decoupling (ADAPT) [94] and optimal dynamical decoupling [95].

Although our discussions were limited to the decoupling of finite systems, in a recent work, Arenz et al. [96] analyzed cases of infinite-dimensional Hamiltonians to which DD may be applicable. This provides an opportunity for describing a dimension-independent DD scheme, which will be investigated in our future work.

Chapter 4

DYNAMICAL AMPLIFICATION

4.1 Introduction

Earlier, we showed that DD can suppress the decoherence-causing components of a system with appropriately designed controls. Now, one may wonder whether a similar kind of scheme can be used to amplify the dynamics of desired system components. Since the effective implementation of such a scheme will have twofold advantages: (i) enhanced coupling strength amongst the components of a quantum system; and (ii) speeding up the dynamics of the system, such a framework is strongly desired for the advancement of quantum devices. For example, in optomechanics [97–99], in quantum sensors [100, 101], in trapped-ion systems [102, 103] and in general any multi-qubit system [3, 104] require strong interactions to maintain their quantum effects.

The goal of such a scheme would be to modify the natural unitary evolution of time-independent Hamiltonian H_0 into an amplified evolution such that [9]

$$\exp(-iH_0t) \to \exp(-i\lambda H_0t), \quad \text{where } \lambda > 1. \tag{4.1}$$

In the case where we have complete knowledge of the Hamiltonian and total control over the system, the amplification factor λ can be easily achieved by perturbing the system with a suitable control Hamiltonian $H' = (\lambda - 1)H_0$ i.e.

$$H_0 + H' = \lambda H_0. \tag{4.2}$$

However, acquiring full knowledge of even small systems, in general, is very hard [105, 106]. In practical cases, mostly we have limited knowledge about the system, or the set of control parameters that drive the systems are restricted. It is interesting to

note in (4.2) that if we have resources to construct Hamiltonian H' then, we already have an amplified system!

In a realistic scenario, we wish to achieve speed-up with local controls without having any prior knowledge about the details of the system. Consider that a sequence of bang-bang controls V, as described in (3.39), is implemented on the dynamics of Hamiltonian H_0 which transforms into an amplification of scalar λ, i.e.

$$\frac{1}{|V|}\sum_{v\in V} v^\dagger H_0 v = \lambda H_0. \tag{4.3}$$

Now, we take the Frobenius norm of the operators on both sides to obtain

$$\left\| \frac{1}{|V|}\sum_{v\in V} v^\dagger H_0 v \right\| = |\lambda| \left\| H_0 \right\|. \tag{4.4}$$

If we recall the triangle inequality for the norm of summation of operators [107] we get

$$\left\| \frac{1}{|V|}\sum_{v\in V} v^\dagger H_0 v \right\| \leq \frac{1}{|V|}\sum_{v\in V} \left\| v^\dagger H_0 v \right\|, \tag{4.5}$$

where we know that the Frobenius norm is unitarily invariant. Then, from (4.4) and (4.5) we obtain the inequality

$$|\lambda| \left\| H_0 \right\| \leq \left\| H_0 \right\|, \quad \text{where } \lambda > 1. \tag{4.6}$$

which is obviously not true if H_0 is finite. A general proof to show that finite-dimensional Hamiltonians cannot be amplified can be found in Appendix E.1. However, such a constraint does not exist for infinite-dimensional systems. For example, a quantum harmonic oscillator is an optimal system to implement amplification owing to the fact that the largest energy associated with an eigenstate of a quantum harmonic oscillator is infinite [108].

A quantum harmonic oscillator is central to concepts in quantum optics [108], molecular physics [109], quantum field theory [110], and any physical system that involves a quantum degree of freedom. For systems described by quantum harmonic oscillators, squeezing has been proven to be an effective technique to enhance the

system's characteristics [111, 112]. Protocols to achieve amplification with squeezing have been proposed to enhance cavity-qubit coupling in cavity quantum electrodynamics (CQED) [113–115], interactions in optomechanical systems [116, 117], speed of quantum gates [118], metrology in microwave cavities [119, 120], interactions in quantum hybrid systems [121], the sensitivity of mechanical oscillators [122] and the coupling in electron-phonon superconductivity [123]. In a recent proposal, Arenz et al. [9] introduced the scheme of Hamiltonian amplification (HA) to amplify the dynamics of a quantum harmonic oscillator by squeezing at two different angles. We aspire to thoroughly study the concept of HA by starting off with similar but simple protocols that aim to amplify coherent displacement in a harmonic oscillator. Then we generalize the ideas to speed-up the dynamics of a quantum harmonic oscillator by gradually moving toward more complex cases. But first, let us comprehend the idea of squeezing.

4.2 Squeezed States and Squeezing Operations

We proceed by providing a brief introduction to quantum optics relevant to understand squeezing. For a general introduction to quantum optics, we highly recommend the excellent book by Gerry and Knight [108]. Unsurprisingly the majority of this introduction overlaps with that book. To begin with, consider a single mode of light with frequency ω which quantum mechanically is represented by the Hamiltonian

$$H = \hbar\omega\left[a^\dagger a + \frac{1}{2}\right] = \hbar\omega\Big[X^2 + P^2\Big], \tag{4.7}$$

where $a^\dagger$ and a are annihilation and creation operators which obey the commutation relation $[a,\, a^\dagger] = \mathbb{1}$. The operator product $a^\dagger a$ is called the number operator denoted by n. The eigenstate of the number operator $|n\rangle$ describes the energy eigenvalue E_n of the field such that

$$H\left|n\right\rangle = \hbar\omega\left[a^{\dagger}a + \frac{1}{2}\right]\left|n\right\rangle = E_n\left|n\right\rangle, \tag{4.8}$$

where the number states $|n\rangle$ are orthonormal i.e. $\langle n'|n\rangle = \delta_{nn'}$. We can describe an electric field of single mode propagating along z coordinate and polarized along x coordinate in terms of a and $a^{\dagger}$ as

$$E_x = \frac{i}{\sqrt{2}}\,\mathcal{E}_0[ae^{i(kz-\omega t)} - a^{\dagger}e^{-i(kz-\omega t)}], \tag{4.9}$$

where $\mathcal{E}_0$ represents electric fields per photon and k is the wavenumber of the field.

One can also represent a single mode of light by the Hermitian operators X and P, which describe the field amplitudes oscillating out of phase with each other by 90° or one-quarter of a cycle. Therefore, they are called quadrature operators, and they are related to a and $a^{\dagger}$ as

$$X = \frac{1}{2}(a + a^{\dagger}) \quad \text{and} \quad P = \frac{1}{2i}(a - a^{\dagger}), \tag{4.10}$$

which essentially describes position $x = \sqrt{\frac{\hbar}{2m\omega}}(a+a^{\dagger})$ and momentum $p = \frac{1}{i}\sqrt{\frac{\hbar m\omega}{2}}(a-a^{\dagger})$ operator of a quantum harmonic oscillator, scaled to be dimensionless [108]. In terms of the quadrature operator, the electric field of a single mode is

$$E_x = -2\,\xi_0[X\sin(kz-\omega t) + P\cos(kz-\omega t)]. \tag{4.11}$$

The quadrature operator also satisfies the uncertainty relation as

$$\langle(\Delta X)^2\rangle\langle(\Delta P)^2\rangle \geq \frac{1}{16}. \tag{4.12}$$

The fluctuations of the field in both quadratures can be calculated by the variance for the number state $|n\rangle$. The expected value of quadrature operators is zero, but the expected value of the square of quadrature operators is given by

$$\left\langle n\right|X^2\left|n\right\rangle = \left\langle n\right|P^2\left|n\right\rangle = \frac{1}{4}(2n+1). \tag{4.13}$$

Then, we can write the variance as

$$\langle(\Delta X)^2\rangle = \langle(\Delta P)^2\rangle = \frac{1}{4}(2n+1), \tag{4.14}$$

where n represents the number of photons in state $|n\rangle$. When $n = 0$, i.e., for a vacuum state, the uncertainties in both quadratures still exist; however, in this case, the uncertainties are minimal

$$\langle(\Delta X)^2\rangle = \langle(\Delta P)^2\rangle = \frac{1}{4}. \tag{4.15}$$

It is now appropriate to introduce the coherent state of light, which in practice describes the light in a laser [124]. It is represented by $|\alpha\rangle$ which is the eigenstate of the annihilation operator a, such that

$$a\,|\alpha\rangle = \alpha\,|\alpha\rangle\,, \tag{4.16}$$

where $\alpha = |\alpha|e^{i\theta}$ is a complex number and $|\alpha\rangle$ is the superposition of infinite photons with normalized coefficients given by

$$|\alpha\rangle = e^{-\frac{1}{2}|\alpha|^2} \sum_{n=0}^{\infty} \frac{\alpha^n}{\sqrt{n!}}\,|n\rangle\,. \tag{4.17}$$

The number state $|n\rangle$ defines the energy of the field, but it's not a state of a well-defined field [108]. But a coherent state closely resembles a classical state of light because

(i) For a coherent state the mean value of the field is very similar to a classical field;

$$\langle\alpha|\,E_x\,|\alpha\rangle = \sqrt{2}|\alpha|\mathcal{E}_0 \sin(\omega t - kz - \theta), \tag{4.18}$$

which is a field oscillating sinusoidally in time at a fixed point. On the other hand, for number state $\langle n|\,E_x\,|n\rangle = 0$, no matter how large the value of n is.

(ii) The fluctuations in the quadrature operator for coherent states are minimal;

$$\langle(\Delta X)^2\rangle_\alpha = \langle(\Delta P)^2\rangle_\alpha = \frac{1}{4}. \tag{4.19}$$

Thus, the uncertainty in two orthogonal quadrature operators is equal. From (4.10) we can compute the expectation value as: $\langle X\rangle_\alpha = (\alpha + \alpha^*)/2 = \mathrm{Re}(\alpha)$ and $\langle P\rangle_\alpha = (\alpha - \alpha^*)/2i = \mathrm{Im}(\alpha)$. Hence, we can represent a coherent state in a complex α plane, where real and imaginary parts depict the quadrature operators. Since the

uncertainty associated with a coherent state is minimal, we represent it in phase space as a circle in a frame rotating at the oscillator frequency, as shown in Fig 4.1 and Fig 4.2.

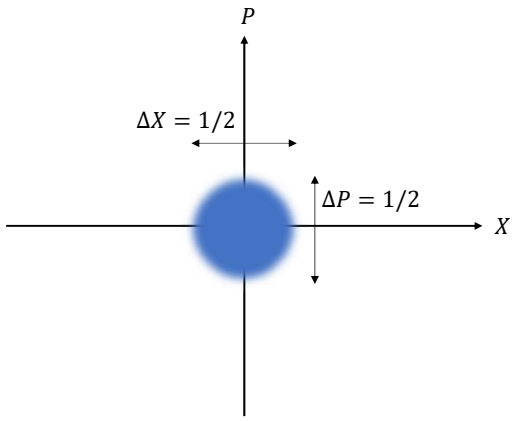

Figure 4.1: Phase space representation of a vacuum state.

We can create a coherent state from vacuum using the displacement operator $D(\alpha)$ defined by

$$D(\alpha) = \exp\Big(\alpha a^\dagger - \alpha^* a\Big). \tag{4.20}$$

The displacement operator displaces the vacuum state to coherent state given by

$$|\alpha\rangle = D(\alpha)\,|0\rangle\,. \tag{4.21}$$

We have shown a phase space representation of the displaced state in Fig 4.2, where the vacuum state is displaced by magnitude $|\alpha|$ at an angle θ from X quadrature. Recall the uncertainty relation from (4.12) which for a coherent state is minimized to

$$\langle(\Delta X)^2\rangle\langle(\Delta P)^2\rangle = \frac{1}{16}. \tag{4.22}$$

We call a coherent state a squeezed state when the uncertainty along a quadrature is lower than the uncertainty in a vacuum state, i.e.,

$$\langle(\Delta X)^2\rangle < \frac{1}{4} \quad \text{or} \quad \langle(\Delta P)^2\rangle < \frac{1}{4}. \tag{4.23}$$

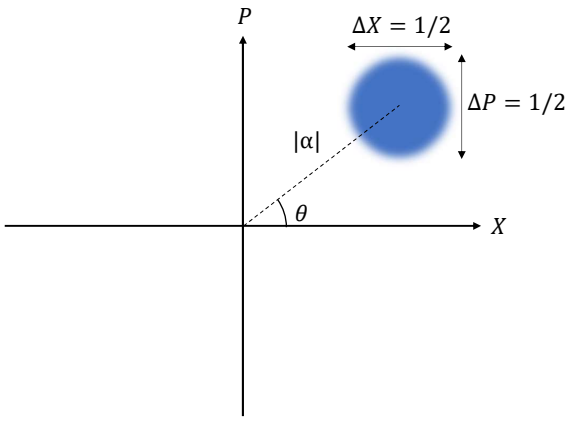

Figure 4.2: Phase space representation of a displaced vacuum state.

Obviously, squeezing in one quadrature will increase the fluctuations in other quadrature to satisfy the relation in (4.22). The squeezed states are obtained by the squeezing operator defined as

$$S(\xi) = \exp\left[\frac{1}{2}(\xi^* a^2 - \xi a^{\dagger 2})\right], \tag{4.24}$$

where $\xi = re^{i\beta}$. We define r as the squeezing parameter and $0 \leq r < \infty$, and β determines the angle of squeezing and $0 \leq \beta \leq 2\pi$. The parameter ξ defined here should not be confused with the one in (2.27), where it describes a totally different function. A squeezed vacuum state denoted by $|\xi\rangle$ is given by

$$|\xi\rangle = S(\xi)\,|0\rangle\,. \tag{4.25}$$

Now, if we wish to find the uncertainties in the X and P quadratures for squeezed states, we invoke the results derived from the Baker-Hausdorff lemma [108]:

$$\begin{aligned} S^\dagger(\xi) a S(\xi) &= a\cosh r - e^{i\beta} a^\dagger \sinh r \\ S^\dagger(\xi) a^\dagger S(\xi) &= a^\dagger \cosh r - e^{-i\beta} a \sinh r. \end{aligned} \tag{4.26}$$

Hence, the variances for the squeezed vacuum state are

$$\langle (\Delta X)^2 \rangle = \frac{1}{4} e^{-2r} \quad \text{and} \quad \langle (\Delta P)^2 \rangle = \frac{1}{4} e^{2r}. \tag{4.27}$$

We show the phase space representation of the squeezed state for $\beta = 0$ in Fig 4.3.

When $\beta = \pi$, squeezing exists in P quadrature, as shown in Fig 4.4. Note that the product of uncertainties satisfies the condition in (4.22). However, in general, the squeezed states do not equalize the uncertainty relation [108].

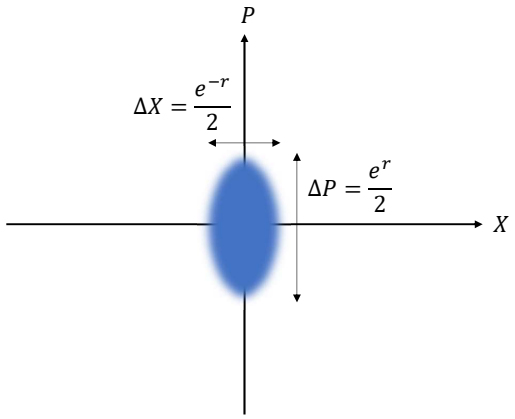

Figure 4.3: Phase space representation of a vacuum state squeezed along X quadrature.

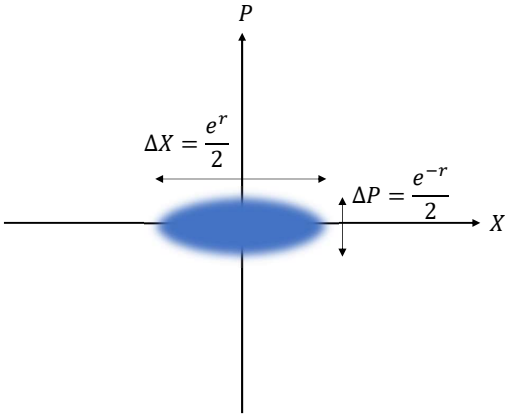

Figure 4.4: Phase space representation of a vacuum state squeezed along P quadrature.

For a general coherent state, squeezed states can be obtained using the displacement operator to get

$$|\alpha, \xi\rangle = D(\alpha)S(\xi)\,|0\rangle\,. \tag{4.28}$$

It is important to highlight that squeezing is a unitary operation, i.e. $S^{\dagger}(\xi)S(\xi) = \mathbb{1}$, where $S^{\dagger}(\xi) = S(-\xi)$, where $S^{\dagger}(\xi)$ executes the "anti-squeezing" operation. For example if $\beta = 0$, operation $S^{\dagger}(\xi)\,|0\rangle$ will increase fluctuations in X and squeezing appears in P quadrature.

4.3 Amplification of Coherent Displacement

For the detection of weak forces in nature, a mechanical oscillator is proven to be a strong tool [125, 126]. The forces to be measured can be coupled with a high - Q harmonic oscillator, and then the observables of the oscillator are monitored. However, the precision to which the forces can be measured is limited by the quantum fluctuations, which, as we earlier discussed, exist even in the vacuum state (or ground state) of an oscillator. By squeezing, one can enhance the precision of measurement of an observable; however, the noise added during detection must be smaller than the squeezed noise. In order to overcome the requirement of low-noise detection, Burd et al. [122] proposed the amplification of a coherent displacement of a mechanical oscillator to amplify the magnitude of the signal to be measured, ideally with no added noise.

According to the proposed protocol [122] (see Fig 4.5), first the vacuum state is squeezed along any direction in phase-space (along X in Fig 4.5) to suppress the quantum fluctuations. Then a small displacement α_i is applied along the squeezed axis. Finally, by applying an anti-squeezing operation, the oscillator returns to its vacuum state with a larger amplitude $\alpha_f = \lambda_1\alpha_i$, where λ_1 is the gain in the displacement. In particular, the scheme can be written in terms of operators as

$$D(\lambda_1\alpha_i) = S^{\dagger}(\xi)D(\alpha_i)S(\xi), \tag{4.29}$$

where,

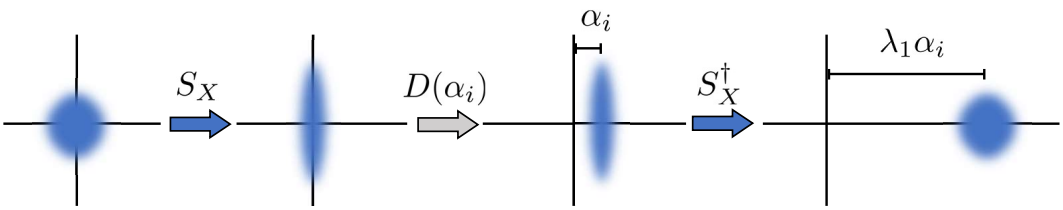

Figure 4.5: An illustration of the amplification of a vacuum state of a quantum harmonic oscillator. The vacuum state is squeezed along the X quadrature and then displaced along the squeezed axis. The displaced state is then anti-squeezed along X quadrature to obtain amplified displacement $\lambda_1\alpha_i$. The protocol is assumed to add no noise during the operations. Figure adapted from Burd et al., "Quantum amplification of mechanical oscillator motion.", 2019.

$$\lambda_1 = \cosh r + e^{i(\beta-2\theta)} \sinh r, \tag{4.30}$$

and, where θ is the angle of displacement and β is the squeezing angle. Notice that when displacement angle $\theta = \beta/2$ or $\beta - 2\theta = 2k\pi$ for integer k, the gain is maximum i.e., $\lambda_1 = e^r$. Thus, given that we have full knowledge of α_i then, with the application of two orthogonal squeezing operations before and after the small displacement, the displacement can be amplified to the factor e^r.

This technique is experimentally demonstrated in [122] using a single trapped ion as the mechanical oscillator. Since the gain is dependent on the phase relationship between displacement and squeezing angle, the final coherent displacement could become smaller than its initial value, i.e.,

$$e^{-r} \leq \lambda_1 \leq e^r. \tag{4.31}$$

Therefore, it may be difficult to stabilize θ and β with regard to the nature of the system considered [127].

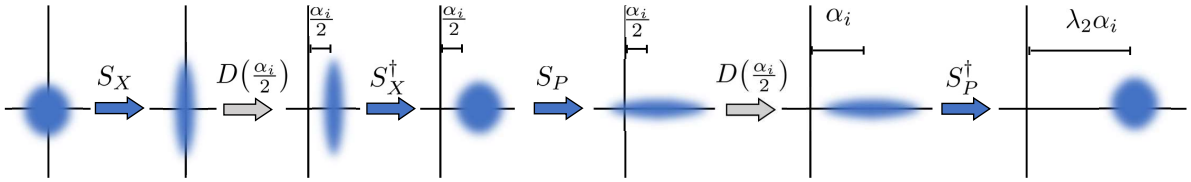

Figure 4.6: An illustration of the phase-insensitive amplification of a vacuum state of a quantum harmonic oscillator. The vacuum state is squeezed along the X quadrature, displaced by $\alpha_i/2$ and anti-squeezed along the X quadrature. The operations are then repeated in the P quadrature. As a result, the displaced state is amplified to factor $\lambda_2 = \cosh(r)$. Figure adapted from Burd et al., "Experimental speedup of quantum dynamics through squeezing.", 2023.

To avoid the phase-dependent amplification, Burd et al. [127] modified the protocol by dividing the displacement into two equal steps and amplifying each step with squeezing and anti-squeezing operators as shown in Fig 4.6. However, in this scheme of operations, the squeezing angle is predetermined. For the first displacement the angle of squeezing and anti-squeezing $\beta = 0$, and for the second displacement $\beta = \pi$. The sequence of operations required to achieve phase-independent amplification is given by

$$D(\lambda_2\alpha_i) = S_\pi^\dagger(r)D\Big(\frac{\alpha_i}{2}\Big)S_\pi(r)S_0^\dagger(r)D\Big(\frac{\alpha_i}{2}\Big)S_0(r), \tag{4.32}$$

By substituting $\beta = 0$ and $\beta = \pi$ in (4.26) we can divide the above expression into two terms as

$$\begin{aligned} S_0^\dagger(r)D\Big(\frac{\alpha_i}{2}\Big)S_0(r) &= \exp\Big\{\frac{\alpha_i}{2}(a^\dagger\cosh(r) - a\sinh(r)) - \frac{\alpha_i^*}{2}(a\cosh(r) - a^\dagger\sinh(r))\Big\}, \\ S_\pi^\dagger(r)D\Big(\frac{\alpha_i}{2}\Big)S_\pi(r) &= \exp\Big\{\frac{\alpha_i}{2}(a^\dagger\cosh(r) + a\sinh(r)) - \frac{\alpha_i^*}{2}(a\cosh(r) + a^\dagger\sinh(r))\Big\}. \end{aligned} \tag{4.33}$$

Using the Baker-Campbell-Hausdorff formula [5] the product of two terms, up to a global phase, is nothing but a displacement operator $D(\lambda_2\alpha_i)$ where $\lambda_2 = \cosh(r)$.

Thus, with the above sequence of predetermined squeezing, we amplify the displacement by gain λ_2 which is independent of phases θ and β. With this scheme of operations, no prior knowledge of α_i is required to amplify the displacement. Note that although we achieve phase insensitivity by orthogonal squeezing, in comparison to the previous scheme, the maximum gain in this case is reduced, i.e., $\lambda_2 < \lambda_1$ for $r > 0$.

4.4 Amplification of Interactions between Quantum Harmonic Oscillators

The protocols earlier discussed amplify the displacement of the vacuum state, which enhances the strength of the signal to be measured. We can generalize the idea of amplification by orthogonal squeezing to enhance interactions in a system described by the Hamiltonian of the form [127]

$$H = \hbar\Omega(\mu a^\dagger + \mu^\dagger a), \tag{4.34}$$

where a and $a^\dagger$ are annihilation and creation operators of a quantum harmonic oscillator, and Ω is the interaction strength between the oscillator and either a quantum system, in which case μ is an operator, or an external drive, where μ is a complex number. If a constant amplitude drive is applied to the harmonic oscillator for time t such that in the evolution $-i\Omega\mu t = \alpha$, then the unitary operator $\exp(-iHt) = D(\alpha)$ which will result in a coherent displacement of the oscillator. On the contrary, if $\mu = \sigma_-$, the lowering operator for a single qubit system, then (4.34) describes the interaction Hamiltonian in a Jaynes-Cummings model [108, 127].

In order to amplify the coupling strength between two interacting systems in a Jaynes-Cummings type interaction, we follow a similar sequence of operations as implemented in (4.32) to obtain [127]

$$U(t) = S_\pi^\dagger(r)U_H\left(\frac{t}{2}\right)S_\pi(r)S_0^\dagger(r)U_H\left(\frac{t}{2}\right)S_0(r), \tag{4.35}$$

where $U_H(t) = \exp(-iHt)$. As we did in (4.33), we divide the above expression into two terms:

$$S_\pi^\dagger(r)U_H\left(\frac{t}{2}\right)S_\pi(r) \times S_0^\dagger(r)U_H\left(\frac{t}{2}\right)S_0(r) = \exp\left(-iH_+\frac{t}{2}\right) \times \exp\left(-iH_-\frac{t}{2}\right), \quad (4.36)$$

where,

$$H_\pm = \Omega\cosh r(\mu a^\dagger + \mu^\dagger a) \pm \Omega(\mu^\dagger a^\dagger \sinh r + \mu a \cosh r)). \quad (4.37)$$

Now, if we invoke Baker–Campbell–Hausdorff formula,

$$e^{-iH_+\frac{t}{2}}\, e^{-iH_-\frac{t}{2}} = e^{-i(H_++H_-)\frac{t}{2} - \frac{1}{2}[H_+,H_-]\frac{t^2}{4} + \frac{i}{12}([H_+,[H_+,H_-]+[H_-,[H_-,H_+])\frac{t^3}{8}\cdots}, \quad (4.38)$$

we note that we do obtain an amplified Hamiltonian with this scheme, but with additional "error-causing" terms that grow exponentially for a sufficiently long period of time. To minimize the error, we divide the total time t into smaller intervals $\Delta t = t/2n$ and Trotterize the sequence in (4.35) for sufficiently large n (see Fig 4.7) such that

$$U(t) = \lim_{n\to\infty}\left[S_\pi^\dagger(r)U_H(\Delta t)S_\pi(r)S_0^\dagger(r)U_H(\Delta t)S_0(r)\right]^n. \quad (4.39)$$

Using (4.36) we simplify the above expression into

$$U(t) = \lim_{n\to\infty}\left[\exp(-iH_+\Delta t)\ \exp(-iH_-\Delta t)\right]^n \quad (4.40)$$

$$= \exp\left(-i(H_+ + H_-)\frac{t}{2}\right) \quad (4.41)$$

$$= \exp(-i\cosh(r)Ht).$$

Thus, when the squeezing operations are implemented instantaneously and switched

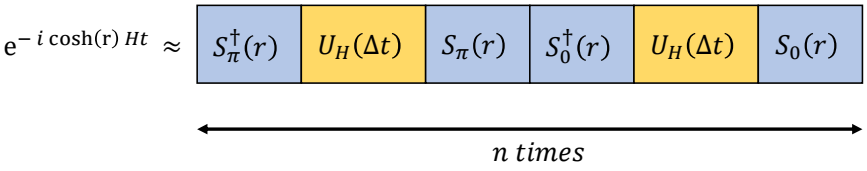

Figure 4.7: Bang-bang controls type squeezing operations used in [127] which are Trotterized for n times to achieve dynamical amplification of factor $\cosh(r)$.

infinitely fast between the two angles, the interaction strength in the Hamiltonian H is amplified by the factor λ which in this case $\lambda = \cosh(r)$. Similar to the scheme in (4.32), we do not require knowledge of interaction strength Ω for amplification. At this point, one can also note the similarity between DD and the amplification scheme we discussed above. As we defined a map in (3.40) which suppresses the system Hamiltonian H, in a similar fashion, for a set of squeezing operations defined by $V = \{S_\pi(r), S_0(r)\}$ implemented in a Trotter type sequence $\lim_{n\to\infty}\Big[\prod_{v\in V} v^\dagger \exp\Big(-iH\frac{t}{|V|n}\Big)v\Big]^n$, where $|V|$ is the cardinality of set V. We can define a linear map which amplifies a Hamiltonian H given by [9]

$$\begin{aligned}\mathcal{M}_{DA}(H) &= \frac{1}{|V|}\sum_{v\in V} v^\dagger H v \\ &= \lambda H, \quad \text{where } \lambda > 1.\end{aligned} \tag{4.42}$$

We will use this definition of amplification extensively throughout the remainder of this work.

Since the scheme's effect is that the system Hamiltonian is amplified, the protocol is introduced as Hamiltonian amplification (HA) in [9, 128]. However, as we can see, essentially it is the dynamics of the Hamiltonian that is amplified, and given its resemblance to DD, we call it "dynamical amplification" (DA) in this thesis.

The Hamiltonian (4.34) represents a quantum harmonic oscillator for a single mode if, $\mu = a$ and $\omega = 2\Omega$. We call this Hamiltonian as H_0 and

$$H_0 = \hbar\omega\left[a^\dagger a + \frac{1}{2}\right]. \tag{4.43}$$

On applying DA with squeezing operators $V = \{S_\pi(r), S_0(r)\}$ we obtain

$$\mathcal{M}_{DA}(H_0) = \frac{1}{2}\Big[S_\pi^\dagger H_0 S_\pi + S_0^\dagger H_0 S_0\Big]. \tag{4.44}$$

We know that $S^\dagger(\xi)S(\xi) = \mathbb{1}$ then, from (4.26) we solve the expression to obtain the amplified Hamiltonian,

$$\mathcal{M}_{DA}(H_0) = \cosh(2r)H_0. \tag{4.45}$$

Note that both, the harmonic oscillator and the interaction term in the Jaynes-Cummings model can be amplified with the exact set of operations. While taking into account that the DA works only for infinite dimensional Hamiltonians, this scheme can be used to amplify the qubit-qubit interaction strength in systems where the coupling between qubits is mediated via a quantum harmonic oscillator [9]. We will discuss the potential applications of the scheme in greater detail later, for now, let us examine DA for a case of interacting harmonic oscillators.

Consider N modes of interacting quantum harmonic oscillators described by quadratic Hamiltonian of the form

$$H_0 = \sum_{j=1}^{N} \omega_j a_j^\dagger a_j + \sum_{i=1}^{N} \omega_i a_i^\dagger a_i + \sum_{i,j=1}^{N} h_{ij}[a_i^\dagger a_j + a_i a_j^\dagger] + \sum_{i,j=1}^{N} g_{ij}[a_i^\dagger a_j^\dagger + a_i a_j], \qquad (4.46)$$

where ω_i, ω_j are the frequency of each mode of oscillators, h_{ij} and g_{ij} are coupling constants defined such that, matrix $\mathbf{h} = [h_{ij}]$ is Hermitian and matrix $\mathbf{g} = [g_{ij}]$ is symmetric [129]. Now, assume that multi-mode squeezing is implemented by the operations $V = \{\mathcal{S}_\pi, \mathcal{S}_0\}$ where $\mathcal{S}_\beta = \prod_{i=1}^{N} S_{(i)\beta}(r)$. On implementing DA with these operations we, once again, get $\mathcal{M}_{DA}(H_0) = \cosh(2r)H_0$, where the calculations can be found in Appendix E.2.

Thus, we find that without any knowledge of the frequencies ω_i, ω_j and coupling constants h_{ij}, g_{ij} in the system Hamiltonian of the form (4.46) we can amplify these terms simultaneously to factor $\lambda = \cosh(2r)$ through the exact local squeezing operations. In a similar vein, we now want to broaden this method to a general quadratic Hamiltonian.

In order to study amplification for a general case of quadratic Hamiltonians we now describe our system with canonical position x and momentum p operators. To begin with, consider N modes of quantum harmonic oscillator which corresponds to N pairs of position and momentum operators $\{x_i, p_j\}_{i,j=1}^{N}$. These operators can be

arranged in a vectorial operator $\mathbf{b}$, where $\mathbf{b} = (x_1, p_1, x_2, p_2, \ldots, x_N, p_N)^\mathsf{T}$, such that we can define a most general quadratic Hamiltonian operator H, as [130]

$$H = \frac{1}{2}\mathbf{b}^\mathsf{T}\mathbf{A}\mathbf{b} + \mathbf{b}^\mathsf{T}\mathbf{b}, \tag{4.47}$$

where $\mathbf{A}$ is a $2N \times 2N$ symmetric matrix. We can split H into two parts H_0 and H_1 such that; H_0 constitutes of terms

$$H_0 = \sum_{i,j=1}^{N} (c_{ij}^x x_i x_j + c_{ij}^p p_i p_j), \tag{4.48}$$

and H_1 comprises of

$$H_1 = \sum_{i,j=1}^{N} (c_{ij}^{xp} x_i p_j + c_{ij}^{px} p_i x_j), \tag{4.49}$$

where c is an appropriate coefficient computed from (4.47). It may be useful to recall the transformation in (4.26) for canonical momentum and position operators

$$\begin{aligned} S_\beta^\dagger(r) x S_\beta(r) &= x\cosh(r) - \frac{1}{2}\Big[x(e^{i\beta} + e^{-i\beta}) + i\frac{1}{m\omega}p(e^{-i\beta} - e^{i\beta})\Big]\sinh(r), \\ S_\beta^\dagger(r) p S_\beta(r) &= p\cosh(r) + i\frac{m\omega}{2}\Big[x(e^{i\beta} - e^{-i\beta}) - i\frac{1}{m\omega}p(e^{-i\beta} + e^{i\beta})\Big]\sinh(r). \end{aligned} \tag{4.50}$$

Under the amplification through the set $V = \{\mathcal{S}_\pi, \mathcal{S}_0\}$ the Hamiltonian H is amplified as $\mathcal{M}_{DA}(H) = \cosh(2r)H_0 + H_1$. The terms in H_0 are amplified through the transformation to factor $\cosh(2r)$ however, H_1 is invariant to DA [9]. This is because when squeezing is implemented along one quadrature for half a cycle in the sequence (4.39) the net squeezing in operators $x_i p_j$ and $p_i x_j$ is nullified. Equivalently, the terms are unaffected by squeezing along the other quadrature, i.e.,

$$\begin{aligned} \mathcal{S}_0^\dagger x_i p_j \mathcal{S}_0 &= x_i p_j, \\ \mathcal{S}_\pi^\dagger x_i p_j \mathcal{S}_\pi &= x_i p_j. \end{aligned} \tag{4.51}$$

One can draw similar conclusions for operators $p_i x_j$. Interestingly, if we implement squeezing by operations $V' = \{\mathcal{S}_{-\pi/2}, \mathcal{S}_{\pi/2}\}$ the terms in H_1 are amplified to $\lambda = \cosh(2r)$, however we don't achieve an amplification for H_0. Therefore, we conclude that the unitary transformations which amplify a general quadratic Hamiltonian H

have yet to be identified [9].

Apart from enhancing qubit-qubit interactions [9], DA has been proposed to be advantageous in the spectator-based recovery of quantum states [131], to amplify shortcuts-to-adiabatic (STA) dynamics in order to rapidly generate ground states of Rabi model [132] and to construct a quantum transducer by controlling the coupling strength in the swapped quantum non-demolition (QND) gate [133]. A perspective on DA to enhance coupling between photons or phonons with qubits or a bosonic mode is suggested in [134]. There are many different areas that we believe can benefit from such a strategy [135–137], and hereby we purpose another field where DA may be advantageous.

4.5 Amplification of Cross-Kerr Phase Shifts

4.5.1 Optical Quantum Computing

As of now, a number of physical implementations have been pursued to realize a quantum computing device that could meet these basic requirements: a physical and scalable two-state quantum system that can be initialized, measured, and interact in a controlled manner to implement a universal set of quantum logic gates, but in addition, it remains isolated from the effects of the environment. Some of these quantum technologies include trapped ion systems [138], nuclear magnetic resonance [139], quantum dots and dopants in solids solid state [140] and super-conducting systems [3, 141]. A recent addition to the list is "topological qubits", which store information using non-abelian quantum phases of matter [142, 143].

An attractive approach for building a quantum computer is using photons. They are famous in quantum information as "flying qubits" since they can be transferred over long distances with minimal loss in optical fibers. They are chargeless particles,

and their interaction with other particles and matter is very weak, which makes these systems relatively free of the decoherence that plagues other quantum systems [85].

In order to realize photons as qubits, we need a way to represent distinguishable states as binary numbers. These states could have some observable bipartite degree of freedom. One way of encoding information on photons is "single-rail representation". In this regime, the logical bases are any orthonormal states of a single optical mode, i.e. a physical system whose state space consists of superpositions of the number states $|n\rangle$. For example, a logical basis could be the vacuum and single-photon states of a single quantum mode, such that $|\mathbf{0}\rangle = |0\rangle$ and $|\mathbf{1}\rangle = |1\rangle$.

Another way to encode information in photons, and perhaps the most famous one, is using two distinct optical modes. If we consider two orthogonal optical modes represented by the annihilation operators a and b and their vacuum modes given by $|0\rangle_a$ and $|0\rangle_b$ respectively, then the logical basis for the qubits can be defined as $|\mathbf{0}\rangle = |1\rangle_a |0\rangle_b$ and $|\mathbf{1}\rangle = |0\rangle_a |1\rangle_b$, where $|\mathbf{0}\rangle$ signifies single photon in the first mode and zero photons in the second mode, and vice versa for $|\mathbf{1}\rangle$. Since we use two modes to represent a qubit, it is called "dual-rail representation" [85, 144].

Once we have an optical qubit, we need the capability to manipulate its state through gates. Any arbitrary single-qubit operation can be achieved using linear optical gates; mirrors, phase shifters, and beam splitters [145]. However, for implementing universal quantum computations, we need nonlinear optical gates. In this context, "nonlinearity" simply refers to the feature through which the relative phase difference between two photons changes according to the state of one of the photons. In general, this action is achieved through nonlinear gates [85]. A simple example of a nonlinear gate is a controlled-NOT (C-NOT) gate.

A CNOT gate is a two-qubit gate where one qubit acts as a control and the other qubit as the target. This is because when the control qubit is in state $|\mathbf{0}\rangle$ the target

qubit remains unaffected, but when the control qubit is in state $|\mathbf{1}\rangle$ the target qubit flips its state from $|\mathbf{0}\rangle \rightarrow |\mathbf{1}\rangle$ and vice versa. If we represent the control qubit in a superposition state, we realize that CNOT operation requires maximally entangled qubits [144]. These entangled states can be implemented only if the qubits interact in a nonlinear fashion. So then, how might this interaction between two photons be carried out?

One practical component to achieve such a nonlinear configuration is a "Kerr medium"; a material whose index of refraction n varies proportionally with the total intensity of light I going through it, as

$$n(I) = n_0 + n_2 I, \tag{4.52}$$

where n_0 is the linear index of refraction and n_2 is a nonlinearity coefficient. This is known as the optical Kerr effect. This occurs very weakly in liquids, gases, and crystals. Silica fibers has a nonlinearity coefficient n_2 of $\approx 2.52 \times 10^{-16}$ cm^2/W [146] and for semiconductor doped glasses, the observed n_2 is as high as $\approx 1.52 \times 10^{-4}$ cm^2/W [147]. When two modes of photons pass through such a medium, the atoms inside mediate "cross-phase modulation" between them [85]. Due to this effect, a phase difference is observed between the photons. This results in a phase shift in one of the photons, which is called "cross-Kerr phase shift" [144] and the Hamiltonian that describes this effect is

$$H_{ck} = -\chi a^\dagger a \otimes b^\dagger b, \tag{4.53}$$

where χ is third-order nonlinear susceptibility (usually written as $\chi^{(3)}$) and, a represents one optical mode and b another. χ is related to nonlinearity coefficient n_2 by [148]

$$n_2 = \frac{\chi}{n_0 \epsilon_0} \sqrt{\frac{\mu}{\epsilon}} \simeq \frac{\chi}{n_0^2 \epsilon_0^2 c}, \tag{4.54}$$

where μ is the magnetic permeability of the material, ϵ_0 and ϵ is the dielectric constant

of vacuum and the material respectively, n_2 is in cm^2/W and χ is given in units of esu. For a medium of length L, the time evolution governed by H_{ck} is given by

$$U_{ck}(t) = \exp\Big(i\chi L t\, a^\dagger a \otimes b^\dagger b\Big). \tag{4.55}$$

With this unitary operator, the controlled-Z (CZ) gate can be constructed for which all the qubit states are unchanged except $|\mathbf{11}\rangle \rightarrow -|\mathbf{11}\rangle$. To implement CZ gate with unitary operator $U_{ck}(t)$, we want the following configuration

$$\begin{aligned} U_{ck}(t)|\mathbf{00}\rangle =& |\mathbf{00}\rangle, \\ U_{ck}(t)|\mathbf{01}\rangle =& |\mathbf{01}\rangle, \\ U_{ck}(t)|\mathbf{10}\rangle =& |\mathbf{10}\rangle, \\ U_{ck}(t)|\mathbf{11}\rangle =& e^{i\chi L t}|\mathbf{11}\rangle, \end{aligned} \tag{4.56}$$

where we choose $\chi L t = \pi$ to flip the sign of the target qubit. A CNOT gate can be easily implemented with a CZ gate by using Hadamard gates before and after the CZ operation on the target qubit [144]. Thus, we have a complete set of universal quantum gates required to execute any arbitrary computation.

However, it has been experimentally shown that the value χ is far too small to practically realize a CZ gate [85, 144, 149]. This is also evident from values of n_2 earlier provided. To get around this issue, the primary focus in the field of optical quantum computing has been on using linear gates to construct nonlinearity between photons, referred to as Knill-Laflamme-Milburn (KLM) scheme [150, 151]. The major disadvantage of using KLM scheme is that it requires a large number of optical components to perform useful computations [150]. Measurement-based quantum computing [152, 153] has been suggested as an alternative to KLM scheme where prepared entangled states are used for nondeterministic measurements. In the last two decades, many schemes realizing CZ gate have been proposed using giant cross-Kerr nonlinearity [151, 154–158], here we show that using DA, a speed-up in the implementation

of CZ gate can be achieved even for a medium with weaker cross-Kerr nonlinearity.

4.5.2 Dynamcial Amplification of Cross-Kerr Phase Shifts

We implement the pulse sequence as shown in Fig 4.8 on a Kerr medium described by the Hamiltonian H_{ck} (4.53), where the pulses execute squeezing operation alternatively along X and P quadrature as described in (4.39). The pulses are selectively applied on the mode defined by annihilation operator a in the intervals of $\Delta t = t/2n$ s.t.

$$U(t) = \left[S^{\dagger}_{\pi,a}(r)U_{ck}(\Delta t)S_{\pi,a}(r)S^{\dagger}_{0,a}(r)U_{ck}(\Delta t)S_{0,a}(r)\right]^{n}. \tag{4.57}$$

From [9], we know that when the pulse sequence is repeated for a sufficient number

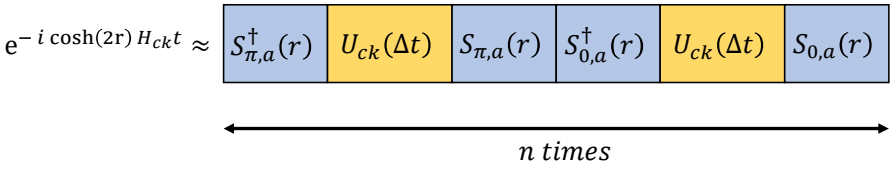

Figure 4.8: Bang-bang controls type squeezing operations applied on mode a of a Kerr medium which are Trotterized for n times to achieve dynamical amplification of factor $\cosh(2r)$.

of times, the harmonic oscillator $a^{\dagger}a$ is amplified by factor $\lambda = \cosh(2r)$ i.e.

$$\mathcal{M}_{DA}(H_{ck}) = \lambda H_{ck}. \tag{4.58}$$

As a result of the amplification of one mode, the Hamiltonian in the dynamics of the system is transformed to λH_{ck}. Hence, the time evolution of state $|\mathbf{11}\rangle$ is given as:

$$e^{-i\lambda H_{ck}t}|\mathbf{11}\rangle = e^{i\lambda\chi Lt}|\mathbf{11}\rangle. \tag{4.59}$$

To construct a CZ gate, we now require $\lambda\chi Lt = \pi$, where $\lambda > 1$ is a controllable parameter. Therefore, with a sufficiently large squeezing parameter implemented via rapid fast squeezing alternating instantaneously between the two quadratures, a

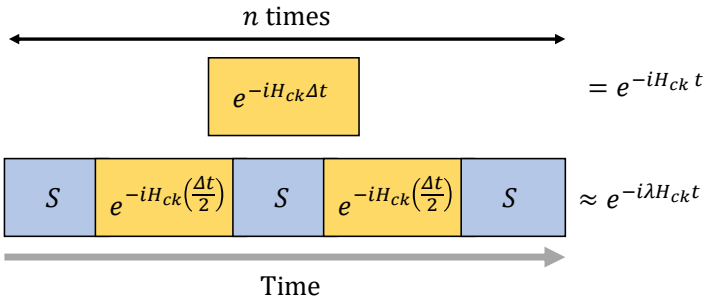

Figure 4.9: Schematic comparison between the non-amplified iterations and amplified cross-Kerr phase shifts via DA. The time interval $\Delta t = t/n$, and both of the evolutions are repeated for large n times. Note that the amplification via DA results in the downscaling of gate time by λ.

speed-up in the implementation of the CZ gate can be achieved even when a medium with weak third-order nonlinear susceptibility is taken into use (see Fig 4.9). For a finite interval between pulses Δt, the error can be upper-bounded with a state-dependent Trotter error bound [159]. The infinite-dimensional state space of quantum harmonic oscillators is projected into the computational range of the CZ gate with a projection matrix, and with the assumption that H_{ck} is bounded, we obtain the upper-bound on error as

$$\epsilon \leq \left(\frac{\chi^2 t \sinh^2(2r)}{4n}\right)\sqrt{6}(1+\sqrt{5}), \tag{4.60}$$

where the error is computed using operator norm and n is the number of times the sequence has been repeated in Trotter sequence or simply Trotter steps (for further details see Appendix E.3).

To examine numerically, we truncated the Hilbert space of H_{ck} to appropriate dimensions and evaluated the error for $n = 10$ in Fig 4.10. The amplification factor is chosen for assumed values of χ for 5 media whose parameters can be found in the caption of Fig 4.10. As expected, the gate error decreases for large Trotter steps

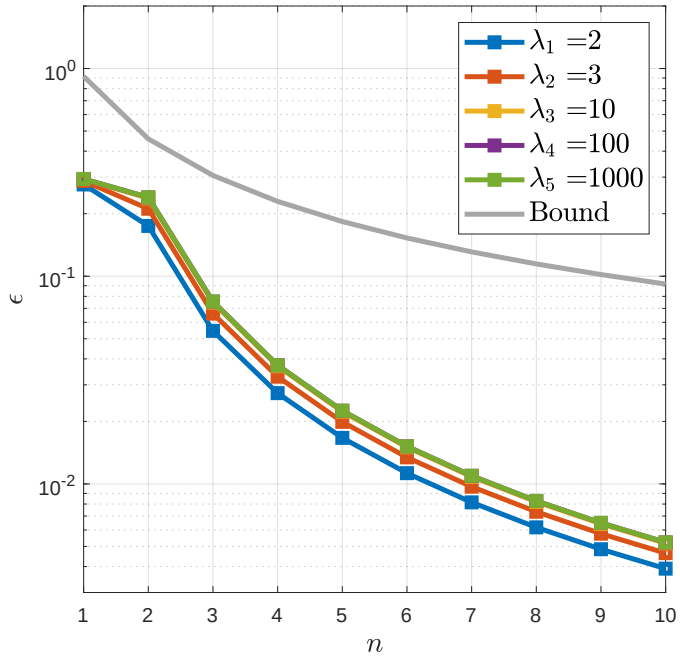

Figure 4.10: Gate error for amplifying the Hamiltonian of five Kerr media with the length of media $L = 1$ and time to implement gate $t = 1$ as a function of Trotter steps implemented for sequence schematically shown in Fig 4.8. The squeezing operations are applied in an idealized bang-bang sequence to amplify medium with nonlinear susceptibility (1) $\chi = \pi/2$ (blue squares) (2) $\chi = \pi/3$ (red squares) (3) $\chi = \pi/10$ (yellow squares) (4) $\chi = \pi/100$ (purple squares) (5) $\chi = \pi/1000$ (green squares) to the amplification factor λ in such a way that for every medium $\lambda\chi = \pi$. The solid gray line shows the upper bound given in (4.60) normalized to an appropriate factor. Clearly, for large Trotter steps the error decreases rapidly for each of the medium.

for large χ ($\lambda_{1,2}$ = 2,3). However, for smaller values of χ ($\lambda_{4,5} = 10^2, 10^3$) the error becomes indistinguishable for all Trotter steps (see Fig 4.11). It implies that the error doesn't increase with an increasing amplification factor when λ is sufficiently large. This is explained by recalling the Trotter terms $H_\pm$ from (4.40) which for this case is modified to

$$H_\pm = \chi\left[\cosh(2r)a^\dagger a \mp \frac{\sinh(2r)}{2}(a^\dagger a^\dagger + aa)\right] \otimes b^\dagger b, \tag{4.61}$$

where for large values of squeezing parameter r;

$$\cosh(2r) \approx \sinh(2r) \approx \frac{e^{2r}}{2}. \tag{4.62}$$

Since r is chosen such that $\cosh(2r)\chi = \pi$, then

$$H_\pm \approx \pi\left[a^\dagger a \mp \frac{(a^\dagger a^\dagger + aa)}{2}\right] \otimes b^\dagger b, \tag{4.63}$$

which is independent of r and, hence, λ. Therefore the Trotter product for n steps $(e^{-iH_+\frac{t}{2n}}e^{-iH_-\frac{t}{2n}})^n$ remains approximately constant for large amplification, and so does the gate error in Fig 4.10.

The scheme proposed here is for a simple case of single-mode fields. Shapiro [160] and Gea-Banacloche [161] earlier showed that single-mode analysis of Kerr media fails to address the multi-mode effect which prevents the large cross-phase modulation between the photons. Since the atoms mediate the phase shift in Kerr media, the photons are physically localized in space and not in frequency. This creates a difference between the spectral width and the response time of the Kerr medium, inducing negligible phase shift [151]. However, it has recently been demonstrated that in some cases, the multi-mode effects can be overcome with novel experimental setups [162–165].

Our approach of amplifying cross-Kerr phase shifts via DA is further supported by two positive outcomes. Firstly, it is not impractical to achieve strong squeezed states in the present day [166, 167]. For vacuum states, squeezing as strong as 15

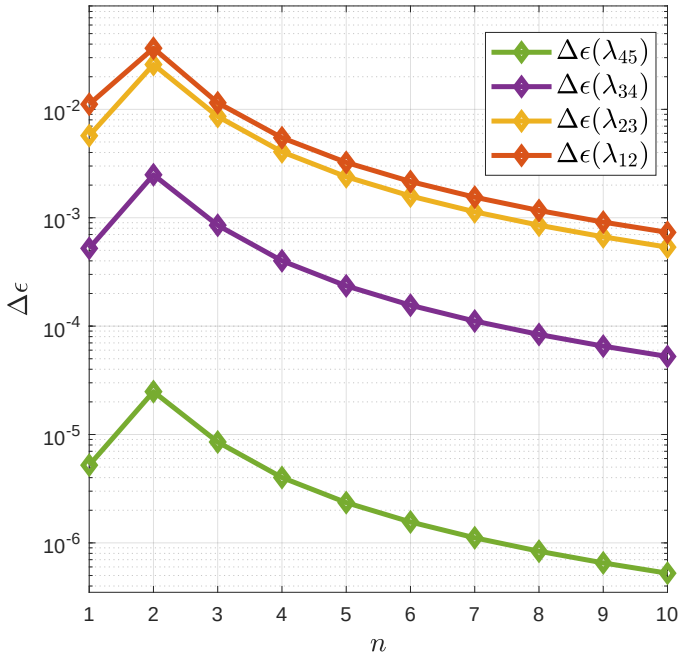

Figure 4.11: Difference in gate error (see Fig 4.10) between successive Kerr media with length $L = 1$ and gate time $t = 1$ as a function of Trotter steps. The label $\Delta\epsilon(\lambda_{ij}) = \epsilon(\lambda_j) - \epsilon(\lambda_i)$ implies the difference between errors to achieve amplification factor λ_j and λ_i. The graph depicts that errors in the amplification of Kerr medium become approximately identical for large values of λ.

dB ($r \approx 1.73$) in optical parametric amplifier [168] and 12.6 dB ($r \approx 1.45$) in a bow-tie optical cavity has been directly measured [169]. Secondly, large cross-Kerr nonlinearities have been demonstrated in recent years [156]. For example, phase shifts of ≈ 1.04 ($\pi/3$) rad per photon in atomic ensembles [170], ≈ 0.35 ($\pi/9$) rad per photon in artificial atoms [171] and ≈ 0.28 ($\pi/11$) rad per photon in CQED [172] has been experimentally observed.

Apart from optical quantum computers, this approach can be extended to a wide range of areas where strong cross-Kerr nonlinearity is required [173–176]. Another

very similar approach of amplifying phase shifts in Kerr media via quadrature squeezing has been proposed in [177]. The major difference we observe between ours and their method is that they obtain an extra phase shift in b mode that may lead to a residual error, which is restrained in our case due to Trotterization. We further notice that if DA is implemented for both modes a and b, with the overall composition $\mathcal{M}_{DA,b}(\mathcal{M}_{DA,a}(H_{ck}))$ the Hamiltonian H_{ck} is amplified to a factor of $\cosh^2(2r)$. Notably, larger amplification is achieved in comparison to single-mode amplification for a given squeezing parameter.

It should be noted that the amplification of system dynamics also enhances the system-environment interactions which speed-up the decoherence of our system. This is also evident in the experiments conducted by Burd et al. [127] (see Fig. 4). However, with an appropriate composition of DD and DA, desired components in the system can be amplified and unwanted interactions can be decoupled in the same cycle of operations [9]. We wish to investigate the feasibility of DD and DA for the amplification of cross-Kerr phase shifts in our future work.

Chapter 5

CONCLUSIONS

In this thesis, we have studied two open-loop quantum protocols that share a similar framework, but achieve completely opposite transformations for the system of interest. The first technique is DD, which aims to suppress decoherence-causing components in the system. We began by studying the decoherence caused by the unavoidable interaction of a quantum system with its environment. In particular, we discussed simple mathematical models of decoherence in a single qubit system. We showed that in an open quantum system, the ability of a quantum system to exist in a superposition state is limited by the coherence time, which in general is very small for large-scale computations.

In order to suppress decoherence in a qubit system, we investigated the scheme of DD and derived the necessary conditions for effective decoupling of the system and environment in Chapter 3. Specifically, we saw that DD can successfully decouple the system from the environment without any knowledge about the strength of system-environment coupling. Then, we demonstrated the feasibility of decoupling conditions by numerically simulating single-qubit systems. From a general description of continuous-time controls, we obtained discrete-time bang-bang controls, which, when applied instantaneously fast, yielded the complete removal of decoherence-causing components in the system. At the end of Chapter 3, we analytically studied the mathematical model in [8, 63] to conclude that the evolution of system-environment interactions governed by any finite traceless operator can be completely eliminated with appropriately designed, sufficiently fast bang-bang controls.

The scope of this thesis was limited to the application of DD to finite-dimensional

systems; however, recent proposals suggest that decoherence in a certain class of infinite-dimensional systems can be suppressed via DD [79, 96]. A thorough study of these proposals might open up a promising direction to find a control sequence that could extend coherence time in quantum technologies that work with continuous variable systems [178–180].

Based on the framework described in DD, we investigated DA, which is aimed at amplifying system components instead of suppressing them. Through this scheme, a speed-up in the evolution of infinite-dimensional systems is achieved, which results in the amplification of interactions in harmonic oscillators. We began Chapter 4 by studying squeezed operations and reviewing protocols that aim to amplify the displacement of coherent states through reversible squeezing. Then, we showed that by squeezing and anti-squeezing harmonic oscillators in a Trotter-type sequence, an amplification factor can be achieved in the system dynamics without full knowledge of the system. Other than a single mode of quantum harmonic oscillator, we investigated DA for interacting oscillators and for a general quadratic Hamiltonian. We briefly reviewed the potential areas where this scheme can render an advantage, and finally, we proposed the application of DA in the amplification of the cross-Kerr phase shift to obtain a speed-up in the implementation of the controlled-phase gate. Our numerical results show that large amplification in cross-Kerr phase shifts can be achieved with sufficient squeezing resources. Using state-dependent Trotter error bound [159] we upper-bounded the error between a CZ gate and amplified cross-Kerr phase shifts. Furthermore, our results show that for large amplifications, the gate error becomes constant and does not increase with the amplification factor. Thus, with this scheme, a large amplification in the speed of controlled phase gates can be achieved without scaling the error.

We recognize that there are several open questions that haven't been explored in

this work. Firstly, the effect of amplification on the decoherence of the system has not been investigated here. Experience shows that, in general, the amplification of a quantum system results in the strengthening of system-environment interactions [9, 127]. Arenz et al. [9] showed that in a particular form of harmonic oscillators, the desired interactions can be amplified and unwanted system-environment interactions can be suppressed through a selectively arranged sequence of controls in a cycle of operations. A similar framework for the amplification of the cross-Kerr phase shift will be investigated in our future work.

Secondly, in section 4.5.2 we concentrated only on the cross-Kerr phase shift in the Kerr medium and neglected the self-Kerr effect. This leaves us with the open question of what the impact of amplification might be on self-Kerr components. How is the cross-Kerr phase shift affected by the amplified self-Kerr components? An approach to analyzing these effects might be to squeeze the states of harmonic oscillators in directions other than along X and P quadratures. Certainly, investigating this will be a key focus of our future efforts.

REFERENCES

[1] Paul Adrien Maurice Dirac. On the theory of quantum mechanics. *Proceedings of the Royal Society of London. Series A, Containing Papers of a Mathematical and Physical Character*, 112(762):661–677, 1926.

[2] Salvatore Capozziello and Wladimir-Georges Boskoff. *A mathematical journey to quantum mechanics*. Springer, 2021.

[3] Thaddeus D Ladd, Fedor Jelezko, Raymond Laflamme, Yasunobu Nakamura, Christopher Monroe, and Jeremy Lloyd O'Brien. Quantum computers. *nature*, 464(7285):45–53, 2010.

[4] Sukhpal Singh Gill, Adarsh Kumar, Harvinder Singh, Manmeet Singh, Kamalpreet Kaur, Muhammad Usman, and Rajkumar Buyya. Quantum computing: A taxonomy, systematic review and future directions. *Software: Practice and Experience*, 52(1):66–114, 2022.

[5] Daniel A Lidar and Todd A Brun. *Quantum error correction*. Cambridge university press, 2013.

[6] Maximilian A Schlosshauer. *Decoherence: and the quantum-to-classical transition*. Springer Science & Business Media, 2007.

[7] Heinz-Peter Breuer, Francesco Petruccione, et al. *The theory of open quantum systems*. Oxford University Press on Demand, 2002.

[8] Lorenza Viola and Seth Lloyd. Dynamical suppression of decoherence in two-state quantum systems. *Physical Review A*, 58(4):2733, 1998.

[9] Christian Arenz, Denys I Bondar, Daniel Burgarth, Cecilia Cormick, and Herschel Rabitz. Amplification of quadratic hamiltonians. *Quantum*, 4:271, 2020.

[10] Jun John Sakurai and Eugene D Commins. Modern quantum mechanics, revised edition, 1995.

[11] Wolfgang Rueckner and Joseph Peidle. Young's double-slit experiment with single photons and quantum eraser. *American Journal of Physics*, 81(12):951–958, 2013.

[12] Alberto Galindo and Miguel Angelo Martin-Delgado. Information and computation: Classical and quantum aspects. *Reviews of Modern Physics*, 74(2):347, 2002.

[13] Mark Hillery. Coherence as a resource in decision problems: The deutsch-jozsa algorithm and a variation. *Physical Review A*, 93(1):012111, 2016.

[14] Alfred V Aho. Ubiquity symposium: Computation and computational thinking. *Ubiquity*, 2011(January), 2011.

[15] Fernando GSL Brandao, Michał Horodecki, Jonathan Oppenheim, Joseph M Renes, and Robert W Spekkens. Resource theory of quantum states out of thermal equilibrium. *Physical review letters*, 111(25):250404, 2013.

[16] John Goold, Marcus Huber, Arnau Riera, Lídia Del Rio, and Paul Skrzypczyk. The role of quantum information in thermodynamics—a topical review. *Journal of Physics A: Mathematical and Theoretical*, 49(14):143001, 2016.

[17] Christian L Degen, Friedemann Reinhard, and Paola Cappellaro. Quantum sensing. *Reviews of modern physics*, 89(3):035002, 2017.

[18] Samuel L Braunstein and Carlton M Caves. Statistical distance and the geometry of quantum states. *Physical Review Letters*, 72(22):3439, 1994.

[19] Alexander Streltsov, Gerardo Adesso, and Martin B Plenio. Colloquium: Quantum coherence as a resource. *Reviews of Modern Physics*, 89(4):041003, 2017.

[20] Gregory S Engel, Tessa R Calhoun, Elizabeth L Read, Tae-Kyu Ahn, Tomáš Mančal, Yuan-Chung Cheng, Robert E Blankenship, and Graham R Fleming. Evidence for wavelike energy transfer through quantum coherence in photosynthetic systems. *Nature*, 446(7137):782–786, 2007.

[21] Elisabetta Collini, Cathy Y Wong, Krystyna E Wilk, Paul MG Curmi, Paul Brumer, and Gregory D Scholes. Coherently wired light-harvesting in photosynthetic marine algae at ambient temperature. *Nature*, 463(7281):644–647, 2010.

[22] AL Malvezzi, 1 G Karpat, B Çakmak, FF Fanchini, T Debarba, and RO Vianna. Quantum correlations and coherence in spin-1 heisenberg chains. *Physical Review B*, 93(18):184428, 2016.

[23] Barış Çakmak, Göktuğ Karpat, and Felipe F Fanchini. Factorization and criticality in the anisotropic xy chain via correlations. *Entropy*, 17(2):790–817, 2015.

[24] Ashley Montanaro. Quantum algorithms: an overview. *npj Quantum Information*, 2(1):1–8, 2016.

[25] Peter W Shor. Polynomial-time algorithms for prime factorization and discrete logarithms on a quantum computer. *SIAM review*, 41(2):303–332, 1999.

[26] Jau Tang and ZB Hu. Analysis of single-photon self-interference in young's double-slit experiments. *Results in Optics*, 9:100281, 2022.

[27] Max Born and Emil Wolf. *Principles of optics: electromagnetic theory of propagation, interference and diffraction of light*. Elsevier, 2013.

[28] Elise M Crull. *Quantum decoherence and interlevel relations*. PhD thesis, 2011.

[29] Karl Blum. *Density matrix theory and applications*, volume 64. Springer Science & Business Media, 2012.

[30] Göran Wendin and VS Shumeiko. Quantum bits with josephson junctions. *Low Temperature Physics*, 33(9):724–744, 2007.

[31] Jarryd J Pla, Kuan Y Tan, Juan P Dehollain, Wee H Lim, John JL Morton, David N Jamieson, Andrew S Dzurak, and Andrea Morello. A single-atom electron spin qubit in silicon. *Nature*, 489(7417):541–545, 2012.

[32] Chenlu Wang, Xuegang Li, Huikai Xu, Zhiyuan Li, Junhua Wang, Zhen Yang, Zhenyu Mi, Xuehui Liang, Tang Su, Chuhong Yang, et al. Towards practical quantum computers: Transmon qubit with a lifetime approaching 0.5 milliseconds. *npj Quantum Information*, 8(1):3, 2022.

[33] Alexander PM Place, Lila VH Rodgers, Pranav Mundada, Basil M Smitham, Mattias Fitzpatrick, Zhaoqi Leng, Anjali Premkumar, Jacob Bryon, Andrei Vrajitoarea, Sara Sussman, et al. New material platform for superconducting transmon qubits with coherence times exceeding 0.3 milliseconds. *Nature communications*, 12(1):1779, 2021.

[34] Richard Phillips Feynman and FL Vernon Jr. The theory of a general quantum system interacting with a linear dissipative system. *Annals of physics*, 281(1-2): 547–607, 2000.

[35] Wojciech Hubert Zurek. Decoherence, einselection, and the quantum origins of the classical. *Reviews of modern physics*, 75(3):715, 2003.

[36] Wojciech Hubert Zurek. Decoherence and the transition from quantum to classical—revisited. In *Quantum Decoherence: Poincaré Seminar 2005*, pages 1–31. Springer, 2007.

[37] Satish Ramakrishna. A microscopic model of wave-function dephasing and decoherence in the double-slit experiment. *Scientific Reports*, 11(1):20986, 2021.

[38] Łukasz Cywiński, Wayne M Witzel, and S Das Sarma. Electron spin dephasing due to hyperfine interactions with a nuclear spin bath. *Physical review letters*, 102(5):057601, 2009.

[39] G Massimo Palma, Kalle-Antti Suominen, and Artur Ekert. Quantum computers and dissipation. *Proceedings of the Royal Society of London. Series A: Mathematical, Physical and Engineering Sciences*, 452(1946):567–584, 1996.

[40] MOSM Hillery, Robert F O'Connell, Marlan O Scully, and Eugene P Wigner. Distribution functions in physics: Fundamentals. *Physics reports*, 106(3):121–167, 1984.

[41] Fedor Jelezko, T Gaebel, I Popa, M Domhan, A Gruber, and Jorg Wrachtrup. Observation of coherent oscillation of a single nuclear spin and realization of a two-qubit conditional quantum gate. *Physical Review Letters*, 93(13):130501, 2004.

[42] Dohun Kim, Zhan Shi, CB Simmons, DR Ward, JR Prance, Teck Seng Koh, John King Gamble, DE Savage, MG Lagally, Mark Friesen, et al. Quantum control and process tomography of a semiconductor quantum dot hybrid qubit. *Nature*, 511(7507):70–74, 2014.

[43] Jarryd J Pla, Kuan Y Tan, Juan P Dehollain, Wee H Lim, John JL Morton, Floris A Zwanenburg, David N Jamieson, Andrew S Dzurak, and Andrea Morello. High-fidelity readout and control of a nuclear spin qubit in silicon. *Nature*, 496(7445):334–338, 2013.

[44] Matthias F Brandl. A quantum von neumann architecture for large-scale quantum computing. *arXiv preprint arXiv:1702.02583*, 2017.

[45] Kosuke Fukui and Shuntaro Takeda. Building a large-scale quantum computer with continuous-variable optical technologies. *Journal of Physics B: Atomic, Molecular and Optical Physics*, 55(1):012001, 2022.

[46] Osamu Hirota, Aleksandr Semenovich Holevo, and CM Caves. *Quantum Communication, Computing, and Measurement*. Springer Science & Business Media, 2012.

[47] Sajeev Damodarakurup, Marco Lucamarini, Giovanni Di Giuseppe, David Vitali, and Paolo Tombesi. Experimental inhibition of decoherence on flying qubits via "bang-bang" control. *Physical review letters*, 103(4):040502, 2009.

[48] Michael J Biercuk, Hermann Uys, Aaron P VanDevender, Nobuyasu Shiga, Wayne M Itano, and John J Bollinger. Optimized dynamical decoupling in a model quantum memory. *Nature*, 458(7241):996–1000, 2009.

[49] Ronald Hanson, Leo P Kouwenhoven, Jason R Petta, Seigo Tarucha, and Lieven MK Vandersypen. Spins in few-electron quantum dots. *Reviews of modern physics*, 79(4):1217, 2007.

[50] Vaibhav N Prakash and Aranya Bhuti Bhattacherjee. Decoherence control of a single-photon optomechanical system in phase-sensitive reservoirs. *arXiv preprint arXiv:2111.05554*, 2021.

[51] Simon J Devitt, William J Munro, and Kae Nemoto. Quantum error correction for beginners. *Reports on Progress in Physics*, 76(7):076001, 2013.

[52] David P DiVincenzo and Peter W Shor. Fault-tolerant error correction with efficient quantum codes. *Physical review letters*, 77(15):3260, 1996.

[53] Joschka Roffe. Quantum error correction: an introductory guide. *Contemporary Physics*, 60(3):226–245, 2019.

[54] David G Cory, MD Price, W Maas, Emanuel Knill, Raymond Laflamme, Wojciech H Zurek, Timothy F Havel, and Shyamal S Somaroo. Experimental quantum error correction. *Physical Review Letters*, 81(10):2152, 1998.

[55] Debbie Leung, Lieven Vandersypen, Xinlan Zhou, Mark Sherwood, Constantino Yannoni, Mark Kubinec, and Isaac Chuang. Experimental realization of a two-bit phase damping quantum code. *Physical Review A*, 60(3):1924, 1999.

[56] Suppressing quantum errors by scaling a surface code logical qubit. *Nature*, 614 (7949):676–681, 2023.

[57] Daniel A Lidar, Isaac L Chuang, and K Birgitta Whaley. Decoherence-free subspaces for quantum computation. *Physical Review Letters*, 81(12):2594, 1998.

[58] Michael Freedman, Alexei Kitaev, Michael Larsen, and Zhenghan Wang. Topological quantum computation. *Bulletin of the American Mathematical Society*, 40(1):31–38, 2003.

[59] Sankar Das Sarma, Michael Freedman, and Chetan Nayak. Topological quantum computation. *Physics today*, 59(7):32–38, 2006.

[60] Ali Ahmed and Mustafa Ahmed. *Dynamical decoupling using NMR for quantum computing*. PhD thesis, 2013.

[61] Ulrich Haeberlen and John S Waugh. Coherent averaging effects in magnetic resonance. *Physical Review*, 175(2):453, 1968.

[62] Lieven MK Vandersypen and Isaac L Chuang. Nmr techniques for quantum control and computation. *Reviews of modern physics*, 76(4):1037, 2005.

[63] Lorenza Viola, Emanuel Knill, and Seth Lloyd. Dynamical decoupling of open quantum systems. *Physical Review Letters*, 82(12):2417, 1999.

[64] Lorenza Viola, Seth Lloyd, and Emanuel Knill. Universal control of decoupled quantum systems. *Physical Review Letters*, 83(23):4888, 1999.

[65] Jiangfeng Du, Xing Rong, Nan Zhao, Ya Wang, Jiahui Yang, and RB Liu. Preserving electron spin coherence in solids by optimal dynamical decoupling. *Nature*, 461(7268):1265–1268, 2009.

[66] Alexandre M Souza, Gonzalo A Alvarez, and Dieter Suter. Robust dynamical decoupling for quantum computing and quantum memory. *Physical review letters*, 106(24):240501, 2011.

[67] Zhi-Hui Wang and VV Dobrovitski. Aperiodic dynamical decoupling sequences in the presence of pulse errors. *Journal of Physics B: Atomic, Molecular and Optical Physics*, 44(15):154004, 2011.

[68] Jacob R West, Daniel A Lidar, Bryan H Fong, and Mark F Gyure. High fidelity quantum gates via dynamical decoupling. *Physical review letters*, 105 (23):230503, 2010.

[69] Wenzheng Dong, FA Calderon-Vargas, and Sophia E Economou. Precise high-fidelity electron–nuclear spin entangling gates in nv centers via hybrid dynamical decoupling sequences. *New Journal of Physics*, 22(7):073059, 2020.

[70] VJ Martínez-Lahuerta, L Pelzer, K Dietze, L Krinner, PO Schmidt, and K Hammerer. Quadrupole transitions and quantum gates protected by continuous dynamic decoupling. *arXiv preprint arXiv:2301.07974*, 2023.

[71] Piotr Szańkowski, Guy Ramon, Jan Krzywda, Damian Kwiatkowski, et al. Environmental noise spectroscopy with qubits subjected to dynamical decoupling. *Journal of Physics: Condensed Matter*, 29(33):333001, 2017.

[72] Shlomi Kotler, Nitzan Akerman, Yinnon Glickman, Anna Keselman, and Roee Ozeri. Single-ion quantum lock-in amplifier. *Nature*, 473(7345):61–65, 2011.

[73] Jonas Bylander, Simon Gustavsson, Fei Yan, Fumiki Yoshihara, Khalil Harrabi, George Fitch, David G Cory, Yasunobu Nakamura, Jaw-Shen Tsai, and William D Oliver. Noise spectroscopy through dynamical decoupling with a superconducting flux qubit. *Nature Physics*, 7(7):565–570, 2011.

[74] Tobias Staudacher, Fazhan Shi, S Pezzagna, Jan Meijer, Jiangfeng Du, Carlos A Meriles, Friedemann Reinhard, and Joerg Wrachtrup. Nuclear magnetic resonance spectroscopy on a (5-nanometer) 3 sample volume. *Science*, 339(6119): 561–563, 2013.

[75] Erwin L Hahn. Spin echoes. *Physical review*, 80(4):580, 1950.

[76] Herman Y Carr and Edward M Purcell. Effects of diffusion on free precession in nuclear magnetic resonance experiments. *Physical review*, 94(3):630, 1954.

[77] Wayne Martin Witzel. *Decoherence and dynamical decoupling in solid-state spin qubits*. University of Maryland, College Park, 2007.

[78] Stefan Putz. *Circuit Cavity QED with Macroscopic Solid-State Spin Ensembles*. Springer, 2017.

[79] Christian Arenz. *Control of open quantum systems*. PhD thesis, Aberystwyth University, 2016.

[80] Jeeva Anandan and Jun Suzuki. Quantum mechanics in a rotating frame. *Relativity in rotating frames: relativistic physics in rotating reference frames*, pages 361–370, 2004.

[81] Wilhelm Magnus. On the exponential solution of differential equations for a linear operator. *Communications on pure and applied mathematics*, 7(4):649–673, 1954.

[82] Nico M Temme. *Special functions: An introduction to the classical functions of mathematical physics*. John Wiley & Sons, 1996.

[83] Frank Bowman. *Introduction to Bessel functions*. Courier Corporation, 2012.

[84] Alan V Oppenheim, Alan S Willsky, Syed Hamid Nawab, and Jian-Jiun Ding. *Signals and systems*, volume 2. Prentice hall Upper Saddle River, NJ, 1997.

[85] Michael A Nielsen and Isaac Chuang. Quantum computation and quantum information, 2002.

[86] Hans J Weber and George B Arfken. *Essential mathematical methods for physicists, ISE*. Elsevier, 2003.

[87] David Vitali and Paolo Tombesi. Using parity kicks for decoherence control. *Physical Review A*, 59(6):4178, 1999.

[88] Joel E Cohen, Shmuel Friedland, Tosio Kato, and Frank P Kelly. Eigenvalue inequalities for products of matrix exponentials. *Linear Algebra and its Applications*, 45:55–95, 1982.

[89] Daniel Lidar. Dynamical decoupling a tutorial. University of Southern California (USC), 2011. URL `https://doi.org/10.5446/35300`. https://doi.org/10.5446/35300.

[90] Wan-Jung Kuo and Daniel A Lidar. Quadratic dynamical decoupling: Universality proof and error analysis. *Physical Review A*, 84(4):042329, 2011.

[91] Lorenza Viola and Emanuel Knill. Random decoupling schemes for quantum dynamical control and error suppression. *Physical review letters*, 94(6):060502, 2005.

[92] Kaveh Khodjasteh and Daniel A Lidar. Fault-tolerant quantum dynamical decoupling. *Physical review letters*, 95(18):180501, 2005.

[93] Genko T Genov, Nati Aharon, Fedor Jelezko, and Alex Retzker. Mixed dynamical decoupling. *Quantum Science and Technology*, 4(3):035010, 2019.

[94] Poulami Das, Swamit Tannu, Siddharth Dangwal, and Moinuddin Qureshi. Adapt: Mitigating idling errors in qubits via adaptive dynamical decoupling. In *MICRO-54: 54th Annual IEEE/ACM International Symposium on Microarchitecture*, pages 950–962, 2021.

[95] Gregory Quiroz and Daniel A Lidar. Optimized dynamical decoupling via genetic algorithms. *Physical Review A*, 88(5):052306, 2013.

[96] Christian Arenz, Daniel Burgarth, Paolo Facchi, and Robin Hillier. Dynamical decoupling of unbounded hamiltonians. *Journal of Mathematical Physics*, 59 (3):032203, 2018.

[97] John D Teufel, Dale Li, MS Allman, K Cicak, AJ Sirois, JD Whittaker, and RW Simmonds. Circuit cavity electromechanics in the strong-coupling regime. *Nature*, 471(7337):204–208, 2011.

[98] Florian Marquardt, Joe P Chen, Aashish A Clerk, and SM Girvin. Quantum theory of cavity-assisted sideband cooling of mechanical motion. *Physical review letters*, 99(9):093902, 2007.

[99] Ignacio Wilson-Rae, Nima Nooshi, W Zwerger, and Tobias J Kippenberg. Theory of ground state cooling of a mechanical oscillator using dynamical backaction. *Physical review letters*, 99(9):093901, 2007.

[100] Alexander Bilmes, Serhii Volosheniuk, Jan David Brehm, Alexey V Ustinov, and Jürgen Lisenfeld. Quantum sensors for microscopic tunneling systems. *npj Quantum Information*, 7(1):27, 2021.

[101] Shimon Kolkowitz, Ania C Bleszynski Jayich, Quirin P Unterreithmeier, Steven D Bennett, Peter Rabl, JGE Harris, and Mikhail D Lukin. Coherent sensing of a mechanical resonator with a single-spin qubit. *Science*, 335 (6076):1603–1606, 2012.

[102] A Bermudez, T Schaetz, and Martin B Plenio. Dissipation-assisted quantum information processing with trapped ions. *Physical review letters*, 110(11):110502, 2013.

[103] Andrew M Steane and David M Lucas. Quantum computing with trapped ions, atoms and light. *Fortschritte der Physik: Progress of Physics*, 48(9-11):839–858, 2000.

[104] Mahdi Sameti, Jake Lishman, and Florian Mintert. Strong-coupling quantum logic of trapped ions. *Physical Review A*, 103(5):052603, 2021.

[105] Daniel Burgarth and Koji Maruyama. Indirect hamiltonian identification through a small gateway. *New Journal of Physics*, 11(10):103019, 2009.

[106] Sonia G Schirmer and Daniel KL Oi. Two-qubit hamiltonian tomography by bayesian analysis of noisy data. *Physical Review A*, 80(2):022333, 2009.

[107] Roger A Horn and Charles R Johnson. *Matrix analysis*. Cambridge university press, 2012.

[108] Christopher Gerry, Peter Knight, and Peter L Knight. *Introductory quantum optics*. Cambridge university press, 2005.

[109] M Moshinsky and O Novaro. Harmonic oscillator in atomic and molecular physics. *The Journal of Chemical Physics*, 48(9):4162–4180, 1968.

[110] Franz Mandl and Graham Shaw. *Quantum field theory*. John Wiley & Sons, 2010.

[111] Chan Roh, Geunhee Gwak, and Young-Sik Ra. Robust squeezed light against mode mismatch using a self imaging optical parametric oscillator. *Scientific Reports*, 11(1):18991, 2021.

[112] Benjamin J Lawrie, Paul D Lett, Alberto M Marino, and Raphael C Pooser. Quantum sensing with squeezed light. *Acs Photonics*, 6(6):1307–1318, 2019.

[113] C Leroux, LCG Govia, and AA Clerk. Enhancing cavity quantum electrodynamics via antisqueezing: Synthetic ultrastrong coupling. *Physical review letters*, 120(9):093602, 2018.

[114] Shinya Kato and Takao Aoki. Strong coupling between a trapped single atom and an all-fiber cavity. *Physical review letters*, 115(9):093603, 2015.

[115] Wei Qin, Adam Miranowicz, Peng-Bo Li, Xin-You Lü, Jian-Qiang You, and Franco Nori. Exponentially enhanced light-matter interaction, cooperativities, and steady-state entanglement using parametric amplification. *Physical Review Letters*, 120(9):093601, 2018.

[116] Xin-You Lü, Ying Wu, JR Johansson, Hui Jing, Jing Zhang, and Franco Nori. Squeezed optomechanics with phase-matched amplification and dissipation. *Physical review letters*, 114(9):093602, 2015.

[117] Marc-Antoine Lemonde, Nicolas Didier, and Aashish A Clerk. Enhanced nonlinear interactions in quantum optomechanics via mechanical amplification. *Nature communications*, 7(1):11338, 2016.

[118] Mingjie Xin, Wui Seng Leong, Zilong Chen, Yu Wang, and Shau-Yu Lan. Rapid quantum squeezing by jumping the harmonic oscillator frequency. *Physical Review Letters*, 127(18):183602, 2021.

[119] M Malnou, DA Palken, BM Brubaker, Leila R Vale, Gene C Hilton, and KW Lehnert. Squeezed vacuum used to accelerate the search for a weak classical signal. *Physical Review X*, 9(2):021023, 2019.

[120] Andrew Eddins, Sydney Schreppler, David M Toyli, Leigh S Martin, Shay Hacohen-Gourgy, Luke CG Govia, Hugo Ribeiro, Aashish A Clerk, and Irfan Siddiqi. Stroboscopic qubit measurement with squeezed illumination. *Physical review letters*, 120(4):040505, 2018.

[121] Peng-Bo Li, Yuan Zhou, Wei-Bo Gao, and Franco Nori. Enhancing spin-phonon and spin-spin interactions using linear resources in a hybrid quantum system. *Physical Review Letters*, 125(15):153602, 2020.

[122] SC Burd, R Srinivas, JJ Bollinger, AC Wilson, DJ Wineland, D Leibfried, DH Slichter, and DTC Allcock. Quantum amplification of mechanical oscillator motion. *Science*, 364(6446):1163–1165, 2019.

[123] Mehrtash Babadi, Michael Knap, Ivar Martin, Gil Refael, and Eugene Demler. Theory of parametrically amplified electron-phonon superconductivity. *Physical Review B*, 96(1):014512, 2017.

[124] Roman Schnabel. Squeezed states of light and their applications in laser interferometers. *Physics Reports*, 684:1–51, 2017.

[125] Carlton M Caves, Kip S Thorne, Ronald WP Drever, Vernon D Sandberg, and Mark Zimmermann. On the measurement of a weak classical force coupled to a quantum-mechanical oscillator. i. issues of principle. *Reviews of Modern Physics*, 52(2):341, 1980.

[126] Katherine C McCormick, Jonas Keller, Shaun C Burd, David J Wineland, Andrew C Wilson, and Dietrich Leibfried. Quantum-enhanced sensing of a single-ion mechanical oscillator. *Nature*, 572(7767):86–90, 2019.

[127] SC Burd, HM Knaack, R Srinivas, C Arenz, AL Collopy, LJ Stephenson, AC Wilson, DJ Wineland, D Leibfried, JJ Bollinger, et al. Experimental speedup of quantum dynamics through squeezing. *arXiv preprint arXiv:2304.05529*, 2023.

[128] Christian Arenz, Denys I Bondar, Daniel Burgarth, Cecilia Cormick, and Herschel Rabitz. Hamiltonian amplification. *arXiv preprint arXiv:1806.00444*, 1, 2018.

[129] Gianfranco Cariolaro and Gianfranco Pierobon. From hamiltonians to complex symplectic transformations. *arXiv preprint arXiv:1704.02008*, 2017.

[130] Alessio Serafini. *Quantum continuous variables: a primer of theoretical methods*. CRC press, 2017.

[131] Arshag Danageozian. Recovery with incomplete knowledge: Fundamental bounds on real-time quantum memories. *arXiv preprint arXiv:2208.04427*, 2022.

[132] Ye-Hong Chen, Wei Qin, Xin Wang, Adam Miranowicz, and Franco Nori. Shortcuts to adiabaticity for the quantum rabi model: Efficient generation of giant entangled cat states via parametric amplification. *Physical Review Letters*, 126 (2):023602, 2021.

[133] Hoi-Kwan Lau and Aashish A Clerk. High-fidelity bosonic quantum state transfer using imperfect transducers and interference. *npj Quantum Information*, 5 (1):31, 2019.

[134] Wenchao Ge. Hamiltonian amplification: Another application of parametric amplification. *Quantum Views*, 4:41, 2020.

[135] Juan Ignacio Cirac, Peter Zoller, H Jeff Kimble, and Hideo Mabuchi. Quantum state transfer and entanglement distribution among distant nodes in a quantum network. *Physical Review Letters*, 78(16):3221, 1997.

[136] K Lake, S Weidt, J Randall, ED Standing, SC Webster, and WK Hensinger. Generation of spin-motion entanglement in a trapped ion using long-wavelength radiation. *Physical Review A*, 91(1):012319, 2015.

[137] H Pino, J Prat-Camps, K Sinha, B Prasanna Venkatesh, and O Romero-Isart. On-chip quantum interference of a superconducting microsphere. *Quantum Science and Technology*, 3(2):025001, 2018.

[138] Juan I Cirac and Peter Zoller. Quantum computations with cold trapped ions. *Physical review letters*, 74(20):4091, 1995.

[139] Jonathan A Jones. Quantum computing with nmr. *arXiv preprint arXiv:1011.1382*, 2010.

[140] Christoph Kloeffel and Daniel Loss. Prospects for spin-based quantum computing in quantum dots. *Annu. Rev. Condens. Matter Phys.*, 4(1):51–81, 2013.

[141] Jeremy L O'brien. Optical quantum computing. *Science*, 318(5856):1567–1570, 2007.

[142] Ady Stern and Netanel H Lindner. Topological quantum computation—from basic concepts to first experiments. *Science*, 339(6124):1179–1184, 2013.

[143] Elizabeth Gibney. Inside microsoft's quest for a topological quantum computer. *Nature*, 2016.

[144] Tim C Ralph and Geoff J Pryde. Optical quantum computation. In *Progress in optics*, volume 54, pages 209–269. Elsevier, 2010.

[145] Peter Rabl, P Cappellaro, MV Gurudev Dutt, Liang Jiang, JR Maze, and Mikhail D Lukin. Strong magnetic coupling between an electronic spin qubit and a mechanical resonator. *Physical Review B*, 79(4):041302, 2009.

[146] KS Kim, RH Stolen, WA Reed, and KW Quoi. Measurement of the nonlinear index of silica-core and dispersion-shifted fibers. *Optics letters*, 19(4):257–259, 1994.

[147] Jean-Louis Coutaz and Martin Kull. Saturation of the nonlinear index of refraction in semiconductor-doped glass. *JOSA B*, 8(1):95–98, 1991.

[148] Hiroo Azuma. Quantum computation with kerr-nonlinear photonic crystals. *Journal of Physics D: Applied Physics*, 41(2):025102, 2007.

[149] Vivek Venkataraman, Kasturi Saha, and Alexander L Gaeta. Phase modulation at the few-photon level for weak-nonlinearity-based quantum computing. *Nature Photonics*, 7(2):138–141, 2013.

[150] Emanuel Knill, Raymond Laflamme, and Gerald J Milburn. A scheme for efficient quantum computation with linear optics. *nature*, 409(6816):46–52, 2001.

[151] Daniel J Brod and Joshua Combes. Passive cphase gate via cross-kerr nonlinearities. *Physical review letters*, 117(8):080502, 2016.

[152] Nicolas C Menicucci. Fault-tolerant measurement-based quantum computing with continuous-variable cluster states. *Physical review letters*, 112(12):120504, 2014.

[153] Mark S Tame, Bryn A Bell, Carlo Di Franco, William J Wadsworth, and John G Rarity. Experimental realization of a one-way quantum computer algorithm solving simon's problem. *Physical Review Letters*, 113(20):200501, 2014.

[154] Sebastien GR Louis, Kae Nemoto, WJ Munro, and TP Spiller. The efficiencies of generating cluster states with weak nonlinearities. *New Journal of Physics*, 9(6):193, 2007.

[155] Kae Nemoto and William J Munro. Nearly deterministic linear optical controlled-not gate. *Physical review letters*, 93(25):250502, 2004.

[156] Daniel J Brod, Joshua Combes, and Julio Gea-Banacloche. Two photons co- and counterpropagating through n cross-kerr sites. *Physical Review A*, 94(2): 023833, 2016.

[157] GD Hutchinson and GJ Milburn. Nonlinear quantum optical computing via measurement. *Journal of Modern Optics*, 51(8):1211–1222, 2004.

[158] WJ Munro, Kae Nemoto, Timothy P Spiller, Sean D Barrett, Pieter Kok, and Raymond G Beausoleil. Efficient optical quantum information processing. *Journal of Optics B: Quantum and Semiclassical Optics*, 7(7):S135, 2005.

[159] Daniel Burgarth, Niklas Galke, Alexander Hahn, and Lauritz van Luijk. State-dependent trotter limits and their approximations. *Physical Review A*, 107(4): L040201, 2023.

[160] Jeffrey H Shapiro. Single-photon kerr nonlinearities do not help quantum computation. *Physical Review A*, 73(6):062305, 2006.

[161] Julio Gea-Banacloche. Impossibility of large phase shifts via the giant kerr effect with single-photon wave packets. *Physical Review A*, 81(4):043823, 2010.

[162] Giuseppe Calajó, Philipp K Jenke, Lee A Rozema, Philip Walther, Darrick E Chang, and Joel D Cox. Nonlinear quantum logic with colliding graphene plasmons. *Physical Review Research*, 5(1):013188, 2023.

[163] Keyu Xia, Mattias Johnsson, Peter L Knight, Jason Twamley, et al. Cavity-free scheme for nondestructive detection of a single optical photon. *Physical review letters*, 116(2):023601, 2016.

[164] Balakrishnan Viswanathan and Julio Gea-Banacloche. Analytical results for a conditional phase shift between single-photon pulses in a nonlocal nonlinear medium. *Physical Review A*, 97(3):032314, 2018.

[165] Christopher Chudzicki, Isaac L Chuang, and Jeffrey H Shapiro. Deterministic and cascadable conditional phase gate for photonic qubits. *Physical Review A*, 87(4):042325, 2013.

[166] Henning Vahlbruch, Moritz Mehmet, Simon Chelkowski, Boris Hage, Alexander Franzen, Nico Lastzka, Stefan Gossler, Karsten Danzmann, and Roman Schnabel. Observation of squeezed light with 10-db quantum-noise reduction. *Physical review letters*, 100(3):033602, 2008.

[167] Moritz Mehmet, Stefan Ast, Tobias Eberle, Sebastian Steinlechner, Henning Vahlbruch, and Roman Schnabel. Squeezed light at 1550 nm with a quantum noise reduction of 12.3 db. *Optics express*, 19(25):25763–25772, 2011.

[168] Henning Vahlbruch, Moritz Mehmet, Karsten Danzmann, and Roman Schnabel. Detection of 15 db squeezed states of light and their application for the absolute calibration of photoelectric quantum efficiency. *Physical review letters*, 117(11): 110801, 2016.

[169] Biveen Shajilal, Oliver Thearle, Aaron Tranter, Yuerui Lu, Elanor Huntington, Syed Assad, Ping Koy Lam, and Jiri Janousek. 12.6 db squeezed light at 1550 nm from a bow-tie cavity for long-term high duty cycle operation. *Optics Express*, 30(21):37213–37223, 2022.

[170] Kristin M Beck, Mahdi Hosseini, Yiheng Duan, and Vladan Vuletić. Large conditional single-photon cross-phase modulation. *Proceedings of the National Academy of Sciences*, 113(35):9740–9744, 2016.

[171] Io-Chun Hoi, Anton F Kockum, Tauno Palomaki, Thomas M Stace, Bixuan Fan, Lars Tornberg, Sankar R Sathyamoorthy, Göran Johansson, Per Delsing, and CM Wilson. Giant cross–kerr effect for propagating microwaves induced by an artificial atom. *Physical review letters*, 111(5):053601, 2013.

[172] Quentin A Turchette, Christina J Hood, Wolfgang Lange, HJKH Mabuchi, and H Jerey Kimble. Measurement of conditional phase shifts for quantum logic. *Physical Review Letters*, 75(25):4710, 1995.

[173] TJ Quinn, S Leschiutta, and P Tavella. Quantum metrology with entangled photons.

[174] RF Haglund, Li Yang, RH Magruder, JE Wittig, K Becker, and RA Zuhr. Picosecond nonlinear optical response of a cu: silica nanocluster composite. *Optics letters*, 18(5):373–375, 1993.

[175] J Ph Poizat and Philippe Grangier. Experimental realization of a quantum optical tap. *Physical review letters*, 70(3):271, 1993.

[176] Hai Wang, David Goorskey, and Min Xiao. Controlling light by light with three-level atoms inside an optical cavity. *Optics letters*, 27(15):1354–1356, 2002.

[177] Monika Bartkowiak, Lian-Ao Wu, and Adam Miranowicz. Quantum circuits for amplification of kerr nonlinearity via quadrature squeezing. *Journal of Physics B: Atomic, Molecular and Optical Physics*, 47(14):145501, 2014.

[178] Fabian Laudenbach, Christoph Pacher, Chi-Hang Fred Fung, Andreas Poppe, Momtchil Peev, Bernhard Schrenk, Michael Hentschel, Philip Walther, and Hannes Hübel. Continuous-variable quantum key distribution with gaussian modulation—the theory of practical implementations. *Advanced Quantum Technologies*, 1(1):1800011, 2018.

[179] Craig S Hamilton, Regina Kruse, Linda Sansoni, Sonja Barkhofen, Christine Silberhorn, and Igor Jex. Gaussian boson sampling. *Physical review letters*, 119 (17):170501, 2017.

[180] Olivier Pfister. Continuous-variable quantum computing in the quantum optical frequency comb. *Journal of Physics B: Atomic, Molecular and Optical Physics*, 53(1):012001, 2019.

[181] Daniel A Lidar, Paolo Zanardi, and Kaveh Khodjasteh. Distance bounds on quantum dynamics. *Physical Review A*, 78(1):012308, 2008.

[182] Robert C Thompson. Proof of a conjectured exponential formula. *Linear and Multilinear Algebra*, 19(2):187–197, 1986.

[183] Masuo Suzuki. Decomposition formulas of exponential operators and lie exponentials with some applications to quantum mechanics and statistical physics. *Journal of mathematical physics*, 26(4):601–612, 1985.

APPENDIX A

QUANTUM MECHANICS REFERENCES

A.1 Pauli Operators

The Pauli operators are given by

$$\sigma_x = \begin{pmatrix} 0 & 1 \\ 1 & 0 \end{pmatrix}, \tag{A.1}$$

$$\sigma_y = \begin{pmatrix} 0 & -i \\ i & 0 \end{pmatrix}, \tag{A.2}$$

$$\sigma_z = \begin{pmatrix} 1 & 0 \\ 0 & -1 \end{pmatrix}. \tag{A.3}$$

A.2 Properties of Pauli Opertors

The Pauli operators follow these multiplication properties

$$\begin{gathered} \sigma_i^2 = \mathbb{1}, \text{ where } i \in \{x, y, z\} \text{ and} \\ \sigma_{ij} = -\sigma_{ji} = i\sigma_k, \text{ where } i, j, k = x, y, z \text{ respectively.} \end{gathered} \tag{A.4}$$

The Pauli operators follow the commutation and anticommutation relation as

$$\begin{aligned} [\sigma_i, \sigma_j] &= 2i\varepsilon_{ijk}\sigma_k, \\ \{\sigma_i, \sigma_j\} &= 2\delta_{ij}\mathbb{1}. \end{aligned} \tag{A.5}$$

where ε_{ijk} is the Levi-Civita symbol which describes the cyclic permutation of Pauli matrices and δ_{ij} is the Kronecker delta function.

A.3 Properties of Density Operator

The density operator ρ follow these fundamental properties

1. ρ is Hermitian

$$\rho^\dagger = \rho. \tag{A.6}$$

2. ρ is positive semidefinite

$$\rho \geq 0. \tag{A.7}$$

3. ρ is a projector

$$\rho^2 = \rho. \tag{A.8}$$

4. Trace of ρ is normalized

$$\mathrm{Tr}(\rho) = 1. \tag{A.9}$$

5. if ρ represent a mixed ensemble

$$0 < \mathrm{Tr}(\rho^2) < 1. \tag{A.10}$$

A.4 Partial Trace

For two sub-systems A and B, if the states in the combined system are described by composite density operator ρ_{AB} then, the partial trace over the system B is denoted by Tr_B such that

$$\mathrm{Tr}_B\{\rho_{AB}\} = \sum_r (\mathbb{1}_A \otimes \langle\phi_r|)\rho_{AB}(\mathbb{1}_A \otimes |\phi_r\rangle), \tag{A.11}$$

where $\{|\phi_r\rangle\}$ is an orthonormal basis for the Hilbert space of system B. Similarly the partial trace over the system A is given by

$$\mathrm{Tr}_A\{\rho_{AB}\} = \sum_r (\langle\varphi_r| \otimes \mathbb{1}_B)\rho_{AB}(|\varphi_r\rangle \otimes \mathbb{1}_B), \tag{A.12}$$

where $\{|\varphi_r\rangle\}$ is an orthonormal basis for the Hilbert space of system A.

A.5 Rotating Frame

The concept of the rotating frame is invoked to simplify the dynamics of the composite system by moving into a frame where the dynamics of a subsystem is absent. Let us consider we have a time-independent Hamiltonian H_0 driven by a time-dependent Hamiltonian $V(t)$ such that the combined Hamiltonian is

$$H(t) = H_0 + V(t). \tag{A.13}$$

In Schrödinger picture, the evolution of state $|\psi(t)\rangle$ for the given Hamiltonian will be

$$i\frac{\partial |\psi(t)\rangle}{\partial t} = H(t)\,|\psi(t)\rangle\,. \tag{A.14}$$

We can define a state in a rotating frame such that

$$|\phi(t)\rangle = R(t)\,|\psi(t)\rangle\,. \tag{A.15}$$

To obtain the equation of motion for the state $|\phi(t)\rangle$ we differentiate it and multiply by i s.t.

$$\begin{aligned} i\frac{\partial |\phi(t)\rangle}{\partial t} &= i\frac{\partial R(t)}{\partial t}\ |\psi(t)\rangle + R(t)\, i\frac{\partial |\psi(t)\rangle}{\partial t} \\ &= i\,\frac{\partial R(t)}{\partial t}R^\dagger(t)\,|\phi(t)\rangle + R(t)H(t)R^\dagger(t)\,|\phi(t)\rangle \\ &= \left(i\frac{\partial R(t)}{\partial t}R^\dagger(t) + R(t)H(t)R^\dagger(t)\right)|\phi(t)\rangle\,. \end{aligned} \tag{A.16}$$

Here, one can choose $R(t)$ to move into a frame where the dynamics are defined by the subsystem of our interest. For example, if the system of interest is H_0 we move into a frame defined by $R(t) = U_V^\dagger(t)$ where $U_V(t) = \mathcal{T}\exp\Big(-i\int_0^t du V(u)\Big)$, such that in the above expression

$$\frac{\partial R(t)}{\partial t} = \frac{\partial U_V^\dagger(t)}{\partial t} = iU_V^\dagger(t)V(t). \tag{A.17}$$

Hence, (A.16) can be written as

$$i\frac{\partial |\phi(t)\rangle}{\partial t} = \Big(-U_V^\dagger(t)V(t)U_V(t) + U_V^\dagger(t)H(t)U_V(t)\Big)\,|\phi(t)\rangle\,. \tag{A.18}$$

From (A.13) the terms defining dynamics of $V(t)$ are cancelled in the above equation and the remaining evolution is given by

$$i\frac{\partial |\phi(t)\rangle}{\partial t} = \widetilde{H}(t)\,|\phi(t)\rangle\,, \tag{A.19}$$

where $\widetilde{H}(t) = U_V^\dagger(t)H_0U_V(t)$ is the Hamiltonian in the reference frame rotated about the control propagator $U_V(t)$. The interaction picture is a case of rotating frame

where the system itself is split into free Hamiltonian and interacting Hamiltonian i.e.

$$H(t) = H_0 + H_I(t), \tag{A.20}$$

where the subsystem of interest is the interaction part. Thus, we move to a reference frame rotating about the evolution governed by the free Hamiltonian such that the state $|\phi(t)\rangle$ is given by

$$|\phi(t)\rangle = U_0^\dagger(t)\,|\psi(t)\rangle\,, \tag{A.21}$$

and the Hamiltonian in the interaction picture is

$$\widetilde{H}(t) = U_0^\dagger(t) H_I(t) U_0(t). \tag{A.22}$$

A.6 Baker-Campbell-Hausdorff Formulae

For the product of the exponentials of two operators A and B, the BCH formula is

$$e^A e^B = e^{A+B+\frac{1}{2}[A,B]+\frac{1}{12}[A,[A,B]]-\frac{1}{12}[B,[A,B]]+\ldots}. \tag{A.23}$$

An useful lemma of BCH formulae is

$$e^A B e^{-A} = B + [A,B] + \frac{1}{2}[A,[A,B]] + \frac{1}{3!}[A,[A,[A,B]]] + \ldots \tag{A.24}$$

APPENDIX B

DERIVATIONS FOR DECOHERENCE IN QUBIT-BOSON MODEL

This model for decoherence in qubit-boson model has been thoroughly studied in [7, 8, 39]. The key elements of that work will be briefly reviewed here. For the combined Hamiltonian described in (2.26) the interaction Hamiltonian $\widetilde{H}_{SB}(t)$ is given by

$$\begin{aligned}\widetilde{H}_{SB}(t) =& e^{i(\omega_0\sigma_z+\sum_k \omega_k b_k^\dagger b_k)\Delta t}\Big[\sum_k \hbar\sigma_z(g_k b_k^\dagger + g_k^* b_k)\Big]e^{-i(\omega_0\sigma_z+\sum_k \omega_k b_k^\dagger b_k)\Delta t} \\ =& \hbar\sigma_z\sum_k (g_k e^{i(\omega_k b_k^\dagger b_k)\Delta t} b_k^\dagger e^{-i(\omega_k b_k^\dagger b_k)\Delta t} + g_k^* e^{i(\omega_k b_k^\dagger b_k)\Delta t} b_k e^{-i(\omega_k b_k^\dagger b_k)\Delta t}).\end{aligned} \tag{B.1}$$

Using BCH lemma (A.24) the above expression is simplified to

$$\widetilde{H}_{SB}(t) = \sum_k \hbar\sigma_z(g_k b_k^\dagger e^{i\omega_k t} + g_k^* b_k e^{-i\omega_k t}). \tag{B.2}$$

Now, the time evolution of $\widetilde{H}_{SB}(t)$ is given by a time-ordered unitary operator

$$\widetilde{U}_{tot}(t,t_0) = \mathcal{T}\exp\bigg(-i\int_{t_0}^t ds\sum_k \sigma_z(g_k b_k^\dagger e^{i\omega_k s} + g_k^* b_k e^{-i\omega_k s})\bigg). \tag{B.3}$$

Let us now consider that ρ_{tot} is the density operator that describes the states in the combined system-environment Hilbert space. We wish to focus on the evolution governed by system-environment interaction and for that purpose, it is convenient to move into the interaction picture to obtain $\widetilde{\rho}_{tot}(t)$ as

$$\widetilde{\rho}_{tot}(t) = e^{i(H_S+H_B)(t-t_0)}\rho_{tot}(t)e^{-i(H_S+H_B)(t-t_0)}. \tag{B.4}$$

The time evolution of $\widetilde{H}_{SB}(t)$ is given by a time-ordered unitary operator

$$\widetilde{U}_{tot}(t,t_0) = \mathcal{T}\exp\bigg(-i\int_{t_0}^t ds\sum_k \sigma_z(g_k b_k^\dagger e^{i\omega_k s} + g_k^* b_k e^{-i\omega_k s})\bigg). \tag{B.5}$$

We know that in the evolution of a system, the time order can be omitted if the Hamiltonians commute to a complex scalar at different times [5]. In our case

$$[\widetilde{H}_{SB}(t'), \widetilde{H}_{SB}(t'')] = -2i\sum_k |g_k|^2 \sin\omega_k(t'-t''), \tag{B.6}$$

which is simply a complex number. Thus we can simply integrate $\widetilde{H}_{SB}(t)$ over time without worrying about the order to find

$$\widetilde{U}_{tot}(t,t_0) = \exp\bigg\{\frac{\sigma_z}{2}\sum_k (b_k^\dagger e^{i\omega_k t_0}\xi_k(t-t_0)) + (b_k e^{-i\omega_k t_0}\xi_k^*(t-t_0))\bigg\}, \tag{B.7}$$

where

$$\xi_k(t-t_0) = \xi_k(\Delta t) = \frac{2g_k}{\omega_k}(1 - e^{i\omega_k \Delta t}). \tag{B.8}$$

For the eigenstate of σ_z and a pure bath state $|\Phi\rangle$ the time evolution $\widetilde{U}_{tot}(t,t_0)$ is defined by

$$\begin{aligned}
\widetilde{U}_{tot}(t,t_0)\,|0\rangle\,|\Phi\rangle &= |0\rangle \prod_k D(e^{i\omega_k t_0}\frac{1}{2}\xi_k(\Delta t))\,|\Phi\rangle\,, \\
\widetilde{U}_{tot}(t,t_0)\,|1\rangle\,|\Phi\rangle &= |1\rangle \prod_k D(-e^{i\omega_k t_0}\frac{1}{2}\xi_k(\Delta t))\,|\Phi\rangle\,,
\end{aligned} \tag{B.9}$$

where $D(\xi_k)$ is a displacement operator given by

$$D(\xi_k) = e^{(b_k^\dagger \xi_k - b_k \xi_k^*)}. \tag{B.10}$$

Hence, the unitary operator $\widetilde{U}_{tot}(t,t_0)$ can be described by a displacement operator $D(\xi_k)$, where the direction of the displacement of a bath state depends on the logical state of the qubit [39]. To observe the effect of this entanglement we compute the elements of reduced density matrix $\widetilde{\rho}_S(t)$ given by

$$\langle i|\,\widetilde{\rho}_S(t)\,|j\rangle = \widetilde{\rho}_{ij}(t) = \langle i|\,\mathrm{Tr}_B\{\widetilde{U}_{tot}(t,t_0)\widetilde{\rho}_{tot}(t_0)\widetilde{U}_{tot}^\dagger(t,t_0)\}\,|j\rangle\,. \tag{B.11}$$

This can be solved by invoking two standard assumptions from [8]:

(i) qubit and bath are initially uncorrelated:

$$\widetilde{\rho}_{tot}(t_0) = \rho_S(t_0) \otimes \rho_B(t_0); \tag{B.12}$$

(ii) at temperature T the bath is in thermal equilibrium, s.t. for given k modes

$$\rho_{tot}(t_0) = \prod_k \rho_{B,k}(T) = \prod_k (1 - e^{\beta\hbar\omega_k}) \sum_{n=0}^{\infty} e^{-n\beta\hbar\omega_k}\,|n\rangle\,\langle n|\,. \tag{B.13}$$

where $\beta = 1/k_B T$, where T is temperature and k_B is the Boltzmann constant. For simplicity, we assume $k_B = 1$. From (B.9) and (B.11) we see that $\widetilde{\rho}_{00}(t) = \rho_{00}(t_0)$ and $\widetilde{\rho}_{11}(t) = \rho_{11}(t_0)$ whereas for the off-diagonal elements we obtain

$$\begin{aligned}
\widetilde{\rho}_{01}(t) &= \langle 0|\,\mathrm{Tr}_B\{\widetilde{U}_{tot}(t,t_0)\widetilde{\rho}_{tot}(t_0)\widetilde{U}_{tot}^\dagger(t,t_0)\}\,|1\rangle \\
&= \rho_{01}(t_0) \prod_k \mathrm{Tr}_k\{\rho_{B,k}(t_0) D(e^{i\omega_k t_0}\xi_k(t-t_0))\}.
\end{aligned} \tag{B.14}$$

From [40] we know that (B.14) is the symmetric order generating function for a

harmonic oscillator in thermal equilibrium. Then, one can simply rewrite the above expression in the form

$$\widetilde{\rho}_{01}(t) = \rho_{01}(t_0)e^{-\Gamma(t-t_0)}, \tag{B.15}$$

where

$$\Gamma(t-t_0) = \Gamma(\Delta t) = \sum_k \frac{|\xi_k(\Delta t)|^2}{2} \coth\left(\frac{\omega_k}{2T}\right). \tag{B.16}$$

APPENDIX C

DD FOR TRACELESS OPERATORS

For an arbitrary finite-dimensional traceless operator given by the combination

$$S_a = \lambda^x \sigma_x + \lambda^y \sigma_y + \lambda^z \sigma_z, \tag{C.1}$$

where λ^x, λ^y and λ^z are coefficients associated with Pauli-X,Y and Z operators respectively, if we implement bang-bang DD through the decoupling set $\mathcal{G} = \{\sigma_x, \sigma_y, \sigma_z, \mathbb{1}\}$ in the sequence as described in (3.39) we obtain

$$\begin{aligned} \mathcal{M}_{DD}(S_a) =& \frac{1}{|\mathcal{G}|} \sum_{g_k \in \mathcal{G}} g_k^\dagger S_a g_k. \\ =& \frac{1}{4}\Big(\sigma_x^\dagger S_a \sigma_x + \sigma_y^\dagger S_a \sigma_y + \sigma_z^\dagger S_a \sigma_z + \mathbb{1} S_a \mathbb{1}\Big), \end{aligned} \tag{C.2}$$

where

$$\begin{aligned} \sigma_x^\dagger S_a \sigma_x =& \lambda^x(\sigma_x^\dagger \sigma_x \sigma_x) + \lambda^y(\sigma_x^\dagger \sigma_y \sigma_x) + \lambda^z(\sigma_z^\dagger \sigma_x \sigma_x) \\ =& \lambda^x \sigma_x - \lambda^y \sigma_y - \lambda^z \sigma_z. \end{aligned} \tag{C.3}$$

Similarly, the other terms are

$$\begin{aligned} \sigma_y^\dagger S_a \sigma_y =& -\lambda^x \sigma_x + \lambda^y \sigma_y - \lambda^z \sigma_z, \\ \sigma_z^\dagger S_a \sigma_z =& -\lambda^x \sigma_x + \lambda^y \sigma_y + \lambda^z \sigma_z. \end{aligned} \tag{C.4}$$

Thus, (C.2) is simply

$$\begin{aligned} \mathcal{M}_{DD}(S_a) &= \frac{1}{4}\Big(-2\lambda^x \sigma_x - 2\lambda^y \sigma_y - 2\lambda^z \sigma_z + 2\lambda^x \sigma_x + 2\lambda^y \sigma_y + 2\lambda^z \sigma_z\Big) \\ &= 0. \end{aligned} \tag{C.5}$$

APPENDIX D

DERIVATIONS FOR DD IN QUBIT-BOSON MODEL

We analyze bang-bang decoupling in the qubit-boson model from (2.26), by applying controls through the control Hamiltonian $H_c(t)$ which induces spin-flip transitions to the system. As demonstrated in [8] we implement the controls with the Hamiltonian

$$H_c(t) = \sum_{k=1}^{n_p} \frac{\pi}{2}\sigma_x \delta(t - t_{P_k}). \tag{D.1}$$

From (3.2) we know that the unitary operator of a π pulse is simply

$$U_c(t_{P_k}) = \exp\Big(-i\frac{\pi}{2}\sigma_x\Big). \tag{D.2}$$

To easily analyze the contribution of the pulses to system-bath interaction we move into the interaction picture. The Hamiltonian in the interaction picture is rewritten as

$$\widetilde{H}(t) = \widetilde{H}_c(t) + \widetilde{H}_{SB}(t), \tag{D.3}$$

where $\widetilde{H}_{SB}(t)$ is calculated in (B.2) and $\widetilde{H}_c(t)$ can be easily calculated to obtain

$$\widetilde{H}_c(t) = \frac{\pi}{2}\sum_{k=1}^{n_p} e^{i\omega_0\sigma_z t_{P_k}}\sigma_x e^{-i\omega_0\sigma_z t_{P_k}}. \tag{D.4}$$

Now, the time evolution of $\widetilde{H}_c(t)$ for kth pulse is described by

$$\widetilde{U}_c(t_{P_k}) = \exp\Big(-i\frac{\pi}{2}e^{i\omega_0\sigma_z t_{P_k}}\sigma_x e^{-i\omega_0\sigma_z t_{P_k}}\Big). \tag{D.5}$$

For simplicity lets call $\widetilde{U}_c(t_{P_k}) = P_k$. We implement the sequence for $n_p = 2$, in the order as schematically shown in Fig 3.6. The pulses are kept equally spaced in time. Let's consider the time taken to implement one cycle as T_c; $T_c = 2\Delta t$. The cycle is said to be complete at time t_1, where $t_1 = t_0 + 2\Delta t$. For the considered zero width pulses, $t_{P_2} = t_1$. The joint propagator for one cycle of application of control pulses is given by

$$\widetilde{U}(t_1, t_0) = P_2 P_1 \times [P_1^\dagger \widetilde{U}_{tot}(t_{P_2}, t_{P_1}) P_1] \times \widetilde{U}_{tot}(t_{P_1}, t_0). \tag{D.6}$$

To keep it simple we divide the task of finding $\widetilde{U}(t_1, t_0)$ into three simpler calculations: (i) calculate $\widetilde{U}_{tot}(t_{P_1}, t_0)$; (ii) calculate pulses P_2P_1 and (iii) calculate $P_1^\dagger \widetilde{U}_{tot}(t_{P_2}, t_{P_1})P_1$.

We earlier derived the unitary operator $\widetilde{U}_{tot}(t,t_0)$ in (B.7) which in turn describes the evolutions in the absence of control fields. P_2P_1 can be easily calculated from (D.5) as

$$\begin{aligned} P_2P_1 &= e^{i\omega_0\sigma_z t_{P_2}}\sigma_x e^{-i\omega_0\sigma_z t_{P_2}} e^{i\omega_0\sigma_z t_{P_1}}\sigma_x e^{-i\omega_0\sigma_z t_{P_1}} \\ &= e^{i\omega_0\sigma_z 2\Delta t}. \end{aligned} \tag{D.7}$$

Hence, now our goal is to find the (iii) term which is

$$\begin{aligned} P_1^\dagger \widetilde{U}_{tot}(t_{P_2},t_{P_1})P_1 = \\ \exp\Bigg\{ P_1^\dagger \frac{\sigma_z}{2} P_1 \sum_k (b_k^\dagger e^{i\omega_k t_{P_1}}\xi_k(t_{P_2}-t_{P_1}) + b_k e^{-i\omega_k t_{P_1}}\xi_k^*(t_{P_2}-t_{P_1}))\Bigg\}. \end{aligned} \tag{D.8}$$

From the properties of Pauli matrices; $e^{i\omega_0\sigma_z t_k}\sigma_z e^{-i\omega_0\sigma_z t_k} = -\sigma_z$, therefore

$$P_1^\dagger \widetilde{U}_{tot}(t_{P_2},t_{P_1})P_1 = \exp\Bigg\{ -\frac{\sigma_z}{2}\sum_k (b_k^\dagger e^{i\omega_k t_{P_1}}\xi_k(\Delta t) + b_k e^{-i\omega_k t_{P_1}}\xi_k^*(\Delta t))\Bigg\}. \tag{D.9}$$

and henceforth we can write the complete evolution over a cycle by finding the product of unitary operators from (D.6) to get

$$\begin{aligned} \widetilde{U}(t_1,t_0) = \exp\Bigg\{ & i\omega_0\sigma_z(t_1-t_0) - \frac{\sigma_z}{2}\sum_k (b_k^\dagger e^{i\omega_k t_{P_1}}\xi_k(\Delta t) + b_k e^{-i\omega_k t_{P_1}}\xi_k^*(\Delta t)) \\ & + \frac{\sigma_z}{2}\sum_k (b_k^\dagger e^{i\omega_k t_0}\xi_k(\Delta t) + b_k e^{-i\omega_k t_0}\xi_k^*(\Delta t))\Bigg\}. \end{aligned} \tag{D.10}$$

Notice that for the derivation of the unitary operator, we have omitted the time ordering operator owing to the fact that the evolution due to commutators of Hamiltonian is a global phase. In order to compare the evolution (D.10) with the one described in absence of pulses (B.7) we replace $t_{P_1} \to t_0 + \Delta t$ to obtain

$$\widetilde{U}(t_1,t_0) = \exp\Bigg\{ i\omega_0\sigma_z(t_1-t_0) + \frac{\sigma_z}{2}\sum_k (b_k^\dagger e^{i\omega_k t_0}\mu_k(\Delta t) + b_k e^{-i\omega_k t_0}\mu_k^*(\Delta t))\Bigg\}, \tag{D.11}$$

where,

$$\mu_k(\Delta t) = \xi_k(\Delta t)(e^{i\omega_k\Delta t}-1) = -\frac{2g_k}{\omega_k}(1-e^{i\omega_k\Delta t})^2. \tag{D.12}$$

We wish to observe the effects of the pulse sequence after its implementation for N cycles. The total duration t_n to execute n cycles is given by

$$t_n = 2n\Delta t + t_0, \quad n = 1,2,3\ldots,N \tag{D.13}$$

From (D.11) the time evolution for nth cycle is

$$\widetilde{U}(t_n, t_{n-1}) = \exp\Big\{ i\omega_0\sigma_z(t_n - t_{n-1}) + \frac{\sigma_z}{2}\sum_k (b_k^\dagger e^{i\omega_k t_{n-1}}\mu_k(\Delta t) + b_k e^{-i\omega_k t_{n-1}}\mu_k^*(\Delta t)) \Big\}. \tag{D.14}$$

The total evolution after N cycles is determined by the time-ordered product of the evolutions during each cycle, s.t.

$$\widetilde{U}(t_N, t_0) = \widetilde{U}(t_N, t_{N-1}) \ldots \widetilde{U}(t_2, t_1)\widetilde{U}(t_1, t_0). \tag{D.15}$$

A simple approach to obtain $\widetilde{U}(t_N, t_0)$ is through calculating any two consecutive terms in (D.15) and then generalizing the solution for N cycles. Hence, let's try to find the product

$$\begin{aligned}\widetilde{U}(t_{j+1}, t_j)\widetilde{U}(t_j, t_{j-1}) = \exp\Big\{ & i\omega_0\sigma_z(t_{j+1} - t_j) + \frac{\sigma_z}{2}\sum_k (b_k^\dagger e^{i\omega_k t_j}\mu_k(\Delta t) \\ & + b_k e^{-i\omega_k t_j}\mu_k^*(\Delta t)) \Big\} \times \exp\Big\{ i\omega_0\sigma_z(t_j - t_{j-1}) \\ & + \frac{\sigma_z}{2}\sum_k (b_k^\dagger e^{i\omega_k t_{j-1}}\mu_k(\Delta t) + b_k e^{-i\omega_k t_{j-1}}\mu_k^*(\Delta t)) \Big\}.\end{aligned} \tag{D.16}$$

Since, the Hamiltonians in the above expression commute, we can write the product as exponential of the sum of the operators. Moreover, from (D.13) we know that for jth cycle $t_j = 2j\Delta t + t_0$, thus we simplify (D.16) to

$$\begin{aligned}\widetilde{U}(t_{j+1}, t_j)\widetilde{U}(t_j, t_{j-1}) &= \exp\Big\{ i\omega_0\sigma_z 2\Delta t + \frac{\sigma_z}{2}\sum_k (b_k^\dagger e^{i\omega_k t_0}\mu_k(\Delta t)[e^{i\omega_k(2j\Delta t)} + \\ & e^{i\omega_k 2(j-1)\Delta t)}] + b_k e^{-i\omega_k t_0}\mu_k^*(\Delta t)[e^{-i\omega_k(2j\Delta t)} + e^{-i\omega_k 2(j-1)\Delta t)}]) \Big\} \\ &= \exp\Big\{ i\omega_0\sigma_z 2\Delta t + \frac{\sigma_z}{2}\sum_k (b_k^\dagger e^{i\omega_k t_0}\mu_k(j+1, \Delta t) \\ & + b_k e^{-i\omega_k t_0}\mu_k^*(j+1, \Delta t)) \Big\}.\end{aligned} \tag{D.17}$$

The product of unitary operators which describe the overall evolution for N cycles is given by

$$\widetilde{U}(t_N,t_0)=\exp\Big\{i\omega_0\sigma_z(t_N-t_0)+\frac{\sigma_z}{2}\sum_k(b_k^\dagger e^{i\omega_k t_0}\mu_k(N,\Delta t)+b_k e^{-i\omega_k t_0}\mu_k^*(N,\Delta t))\Big\}, \tag{D.18}$$

where

$$\mu_k(N,\Delta t)=\xi_k(\Delta t)(e^{i\omega_k\Delta t}-1)\sum_{n=1}^{N}e^{i\omega_k 2(n-1)\Delta t}. \tag{D.19}$$

If we calculate $\xi_k(\Delta t)$ for N cycles we get

$$\begin{aligned}\xi_k(t_N-t_0)=\xi_k(2N\Delta t)&=\frac{2g_k}{\omega_k}(1-e^{i\omega_k 2N\Delta t})\\&=\frac{2g_k}{\omega_k}(1-e^{i\omega_k 2\Delta t})\frac{(1-e^{i\omega_k 2N\Delta t})}{(1-e^{i\omega_k 2\Delta t})}\\&=\xi_k(2\Delta t)\sum_{n=1}^{N}e^{i\omega_k 2(n-1)\Delta t},\end{aligned} \tag{D.20}$$

where

$$\xi(2\Delta t)=\xi(\Delta t)(1+e^{i\omega_k\Delta t}). \tag{D.21}$$

While considering a single mode, with (D.19) and (D.20) we can calculate the ratio

$$\frac{|\mu(N,\Delta t)|^2}{|\xi(t_N-t_0)|^2}=\frac{\left|e^{i\omega\Delta t}+1\right|^2}{\left|e^{i\omega\Delta t}-1\right|^2}=\tan^2\left(\frac{\omega\Delta t}{2}\right). \tag{D.22}$$

In order to find an ideal case of decoupling we evaluate the limit in (3.53). With the assumption that $\Delta t\to 0$, we exploit (D.19), (D.20) and (D.21) to calculate the limiting case

$$\begin{aligned}\lim_{\substack{\Delta t\to 0\\N\to\infty}}\mu_k(N,\Delta t)&=\lim_{\Delta t\to 0}\xi(2N\Delta t)-\lim_{\Delta t\to 0}2\xi(\Delta t)\sum_{n=1}^{N}e^{i\omega_k 2(n-1)\Delta t}\\&=\xi(2N\Delta t)\left\{1-\lim_{\Delta t\to 0}2\frac{\xi(\Delta t)}{\xi(2N\Delta t)}\sum_{n-1=0}^{N}e^{i\omega_k t_{n-1}}e^{-i\omega_k t_0}\right\}\\&=\xi(2N\Delta t)\left\{1-\frac{e^{-i\omega_k t_0}}{1-e^{i\omega_k(t_N-t_0)}}\lim_{\Delta t\to 0}\frac{1-e^{i\omega_k\Delta t}}{\Delta t}\sum_{n-1=0}^{N}2\Delta t e^{i\omega_k t_{n-1}}\right\}\\&=\xi(2N\Delta t)\left\{1-\frac{e^{-i\omega_k t_0}}{1-e^{i\omega_k(t_N-t_0)}}\lim_{\Delta t\to 0}\frac{1-e^{i\omega_k\Delta t}}{\Delta t}\int_{t_0}^{t_N}ds e^{i\omega_k s}\right\}\\&=\xi(2N\Delta t)\left\{1-\lim_{\Delta t\to 0}\frac{e^{i\omega_k\Delta t}-1}{i\omega_k\Delta t}\right\}=0.\end{aligned} \tag{D.23}$$

APPENDIX E

DYNAMICAL AMPLIFICATION REFERENCES

E.1 Non-applicability of DA on Finite Hamitlonians

The general proof that the dynamics of a finite-dimensional system cannot be amplified is concisely explained in the Appendix of [9]. We go through the details of the work by following the results from [181]. Let's consider a finite-dimensional quantum system H_0, which is controlled through Hamiltonian $H_c(t)$ which aims to speed-up its dynamics. As we did with DD, we move into a reference frame rotating about the control propagator $U_c(t) = \mathcal{T}\exp\Big(-i\int_0^t dsH_c(s)\Big)$ to obtain the total evolution

$$U(t) = U_c(t)\widetilde{U}(t), \tag{E.1}$$

where

$$\widetilde{U}(t) = \mathcal{T}\exp\left(-i\int_0^t ds\widetilde{H}(s)\right), \tag{E.2}$$

and, where $\widetilde{H}(t)$ is Hamiltonian in rotating frame. The time-ordered evolution $\widetilde{U}(t)$ can be written as an infinite, ordered product

$$\widetilde{U}(t) = \lim_{n\to\infty}\prod_{j=0}^{n}\exp\left[-i\frac{t}{n}\widetilde{H}\left(\frac{jt}{n}\right)\right]. \tag{E.3}$$

From Thompson's theorem [182], for a given pair of operators A and B, there exist unitary operators V and W which satisfies the relation

$$e^A e^B = e^{VAV^\dagger + WBW^\dagger}. \tag{E.4}$$

Thus, for given Hermitian operators $\{A_j\}_{j=1}^n$ there exists unitary operators $\{W_j\}_{j=1}^n$ such that

$$\prod_{j=0}^{n}\exp(-iA_j) = \exp\left[\sum_{j=0}^{n}(-iW_jA_jW_j^\dagger)\right]. \tag{E.5}$$

Applying these results in (E.3) we obtain

$$\begin{aligned}\widetilde{U}(t) &= \lim_{n\to\infty}\exp\left[-i\frac{t}{n}\sum_{j=0}^{n}W_j\widetilde{H}\left(\frac{jt}{n}\right)W_j^\dagger\right] \\ &= \mathcal{T}\exp\left[-i\int_0^t dsW_j(s)\widetilde{H}(s)W_j^\dagger(s)\right].\end{aligned} \tag{E.6}$$

We calculate the Frobenius norm of the Hamiltonian operator governing the evolution $\widetilde{U}(t)$ and use triangle inequality for integrals of a norm to find

$$\begin{aligned}\left\|\int_0^t ds W_j(s)\widetilde{H}(s)W_j^\dagger(s)\right\| &\leq \int_0^t ds \left\|W_j(s)\widetilde{H}(s)W_j^\dagger(s)\right\| \\ &\leq \int_0^t ds \left\|W_j(s)U_c^\dagger(s)H_0U_c(s)W_j^\dagger(s)\right\|.\end{aligned} \tag{E.7}$$

Since the Frobenius norm is unitarily invariant, we obtain

$$\left\|\int_0^t ds\widetilde{H}(s)\right\| \leq t\left\|H_0\right\|. \tag{E.8}$$

Hence, the dynamics of a finite-dimensional Hamiltonian is upper bounded. Therefore a finite system cannot be amplified with any admissible controls. This reasoning also applies to Schrödinger's picture where the bound is

$$\left\|\int_0^t ds(H_0 + H_c(s))\right\| \leq t\left\|H_0 + H_c(t)\right\|. \tag{E.9}$$

E.2 DA for N Interacting Quantum Harmonic Oscillators

With the resources to implement squeezing operations $V = \{\mathcal{S}_\pi, \mathcal{S}_0\}$ where $\mathcal{S}_\beta = \prod_{i=1}^N S_{(i)\beta}(r)$, DA executed on (4.46) yields

$$\begin{aligned}\mathcal{M}_{DA}(H_0) =&\mathcal{M}_{DA}\left(\sum_{j=1}^N \omega_j a_j^\dagger a_j\right) + \mathcal{M}_{DA}\left(\sum_{i=1}^N \omega_i a_i^\dagger a_i\right) + \mathcal{M}_{DA}\left(\sum_{i,j=1}^N h_{ij}[a_i^\dagger a_j + a_i a_j^\dagger]\right) \\ &+ \mathcal{M}_{DA}\left(\sum_{i,j=1}^N g_{ij}[a_i^\dagger a_j^\dagger + a_i a_j]\right).\end{aligned} \tag{E.10}$$

From (4.45) we know

$$\mathcal{M}_{DA}\left(\sum_{j=1}^N \omega_j a_j^\dagger a_j\right) = \cosh(2r)\sum_{j=1}^N \omega_j a_j^\dagger a_j, \tag{E.11}$$

$$\mathcal{M}_{DA}\left(\sum_{i=1}^N \omega_i a_i^\dagger a_i\right) = \cosh(2r)\sum_{i=1}^N \omega_i a_i^\dagger a_i. \tag{E.12}$$

For the third term

$$\begin{aligned}\mathcal{M}_{DA}\left(\sum_{i,j=1}^{N} h_{ij}[a_i^\dagger a_j + a_i a_j^\dagger]\right) =& \frac{1}{2}\Bigg[\Bigg(\sum_{i,j=1}^{N} h_{ij}[S^\dagger_{(i)\pi}(r)a_i^\dagger S_{(i)\pi}S^\dagger_{(j)\pi}a_j S_{(j)\pi} \\ &+ S^\dagger_{(i)\pi}a_i S_{(i)\pi}S^\dagger_{(j)\pi}a_j^\dagger S_{(j)\pi}]\Bigg) + \Bigg(\sum_{i,j=1}^{N} h_{ij}[S^\dagger_{(i)0}(r)a_i^\dagger S_{(i)0} \\ & S^\dagger_{(j)0}a_j S_{(j)0} + S^\dagger_{(i)0}a_i S_{(i)0}S^\dagger_{(j)0}a_j^\dagger S_{(j)0}]\Bigg)\Bigg] \\ =& \frac{1}{2}\Bigg[\Bigg(\sum_{i,j=1}^{N} h_{ij}[S^\dagger_{(i)\pi}(r)a_i^\dagger S_{(i)\pi}S^\dagger_{(j)\pi}a_j S_{(j)\pi} \\ &+ S^\dagger_{(i)0}(r)a_i^\dagger S_{(i)0}S^\dagger_{(j)0}a_j S_{(j)0}]\Bigg) + \Bigg(\sum_{i,j=1}^{N} h_{ij}[S^\dagger_{(i)\pi}a_i S_{(i)\pi} \\ & S^\dagger_{(j)\pi}a_j^\dagger S_{(j)\pi} + S^\dagger_{(i)0}a_i S_{(i)0}S^\dagger_{(j)0}a_j^\dagger S_{(j)0}]\Bigg)\Bigg],\end{aligned} \tag{E.13}$$

we invoke the relations from (4.26) to obtain

$$S^\dagger_{(i)\pi}(r)a_i^\dagger S_{(i)\pi}S^\dagger_{(j)\pi}a_j S_{(j)\pi} + S^\dagger_{(i)0}a_i^\dagger S_{(i)0}S^\dagger_{(j)0}a_j S_{(j)0} = 2\cosh(2r)a_i^\dagger a_j. \tag{E.14}$$

Similarly,

$$S^\dagger_{(i)\pi}(r)a_i S_{(i)\pi}S^\dagger_{(j)\pi}a_j^\dagger S_{(j)\pi} + S^\dagger_{(i)0}a_i S_{(i)0}S^\dagger_{(j)0}a_j^\dagger S_{(j)0} = 2\cosh(2r)a_i a_j^\dagger. \tag{E.15}$$

As a result

$$\mathcal{M}_{DA}\left(\sum_{i,j=1}^{N} h_{ij}[a_i^\dagger a_j + a_i a_j^\dagger]\right) = \cosh(2r)\sum_{i,j=1}^{N} h_{ij}[a_i^\dagger a_j + a_i a_j^\dagger]. \tag{E.16}$$

In a similar manner, the last term in (E.10) is

$$\mathcal{M}_{DA}\left(\sum_{i,j=1}^{N} g_{ij}[a_i^\dagger a_j^\dagger + a_i a_j]\right) = \cosh(2r)\sum_{i,j=1}^{N} g_{ij}[a_i^\dagger a_j^\dagger + a_i a_j]. \tag{E.17}$$

Hence, (E.10) is transformed as

$$\mathcal{M}_{DA}(H_0) = \cosh(2r)H_0. \tag{E.18}$$

E.3 Error for DA of Cross-Kerr Phase Shift

In order to derive the upper bound for the error in (4.60), consider the Trotter sequence

$$\left(U_+\left(\frac{t}{2k}\right)U_-\left(\frac{t}{2k}\right)\right)^k, \tag{E.19}$$

where k is Trotter steps and $U_\pm(t) = e^{-iH_\pm(t)}$, where $H_\pm$ from (4.61) is

$$H_\pm = \chi\left[\cosh(2r)a^\dagger a \mp \frac{\sinh(2r)}{2}(a^\dagger a^\dagger + aa)\right]b^\dagger b, \tag{E.20}$$

For simplicity, in the expression, the tensor product between the two modes is shown by simple multiplication. For the given operators, we can develop an error estimate similar to the error obtained in [183], given by

$$\|P\Lambda_k P\| \leq \sup\|\Lambda_k \left|n_1 n_2\right\rangle\|, \tag{E.21}$$

where $\Lambda_k = \left(\left[U_+\left(\frac{t}{2k}\right)U_-\left(\frac{t}{2k}\right)\right]^k - U_p(t)\right)$ and states $\left|n_1 n_2\right\rangle \in \{\left|00\right\rangle, \left|01\right\rangle, \left|10\right\rangle, \left|11\right\rangle\}$. The projection of transformations through Λ_k onto the space defined by bases $\left|n_1 n_2\right\rangle$ is given by the projection matrix P and $U_p(t)$ describes the CZ gate configuration such that

$$U_p(t) = \left|00\right\rangle\left\langle 00\right| + \left|01\right\rangle\left\langle 01\right| + \left|10\right\rangle\left\langle 10\right| - \left|11\right\rangle\left\langle 11\right|, \tag{E.22}$$

and

$$P = U_p(t) + 2\left|11\right\rangle\left\langle 11\right|. \tag{E.23}$$

In the computational bases $\left|n_1 n_2\right\rangle$, the expression in (E.21) is upper bounded by

$$\|P\Lambda_k P\| \leq \sup\|\Lambda_k \left|n_1 n_2\right\rangle\| \leq \sum_{\left|n_1 n_2\right\rangle} \|\Lambda_k \left|n_1 n_2\right\rangle\|. \tag{E.24}$$

This can be solved by following the result from [159] by calculating the eigenstate of $(\hat{H}_+ + \hat{H}_-)$, through eigenvalue equation

$$(H_+ + H_-)\left|n_1 n_2\right\rangle = n_1 n_2 \chi \cosh(2r)\left|n_1 n_2\right\rangle. \tag{E.25}$$

If we assume $h = n_1 n_2 \chi \cosh(2r)$, then the Trotter error will be bounded as

$$\|([U_+(t/2k)U_-(t/2k)]^k - U_p(t))\,|n_1 n_2\rangle\| \leq \frac{2t}{k}\max\left(\left\|\left[H_+ - \frac{h}{2}\right]^2 |n_1 n_2\rangle\right\|, \left\|\left[H_- - \frac{h}{2}\right]^2 |n_1 n_2\rangle\right\|\right), \tag{E.26}$$

where for the given computational bases,

$$\left[H_\pm - \frac{h}{2}\right]^2 |n_1 n_2\rangle = \left(\frac{\pm\chi n_2 \sinh(2r)}{4}\right)^2 \{\ \sqrt{n_1+4}\sqrt{n_1+3}\sqrt{n_1+2}\ \sqrt{n_1+1}\,|n_1+4, n_2\rangle\}\ . \tag{E.27}$$

With this expression, we can calculate the operator norm in (E.26). For states $\{|00\rangle, |10\rangle\}$ the norms are given by

$$\left\|\left(\left[\hat{H}_\pm - \frac{h}{2}\right]^2 |00\rangle\right)\right\| = \left\|\left(\left[\hat{H}_\pm - \frac{h}{2}\right]^2 |10\rangle\right)\right\| = 0. \tag{E.28}$$

Now for the remaining states, we obtain the norms

$$\begin{aligned}\left\|\left(\left[\hat{H}_\pm - \frac{h}{2}\right]^2 |01\rangle\right)\right\| &= \left\|\left(\frac{\pm\chi\sinh(2r)}{4}\right)^2 \sqrt{24}\,|4,1\rangle\right\| \\ &= \left(\frac{\chi\sinh(2r)}{4}\right)^2 \sqrt{24}.\end{aligned} \tag{E.29}$$

Similarly,

$$\begin{aligned}\left\|\left(\left[\hat{H}_\pm - \frac{h}{2}\right]^2 |11\rangle\right)\right\| &= \left\|\left(\frac{\pm\chi\sinh(2r)}{4}\right)^2 \sqrt{120}\,|5,1\rangle\right\| \\ &= \left(\frac{\chi\sinh(2r)}{4}\right)^2 \sqrt{120}.\end{aligned} \tag{E.30}$$

Hence, by adding up all the norms we obtain the error in (4.60) as

$$\|P([U_+(t/2k)U_-(t/2k)]^k - U_p(t))P\| \leq \left(\frac{\chi^2\sinh^2(2r)}{4}\right)\frac{t}{k}\sqrt{6}(1+\sqrt{5}). \tag{E.31}$$